

1-1-2011

Laser-induced breakdown spectroscopy (libs): an innovative tool for studying bacteria

Qassem I. Mohaidat
Wayne State University,

Follow this and additional works at: http://digitalcommons.wayne.edu/oa_dissertations

 Part of the [Microbiology Commons](#), and the [Physics Commons](#)

Recommended Citation

Mohaidat, Qassem I., "Laser-induced breakdown spectroscopy (libs): an innovative tool for studying bacteria" (2011). *Wayne State University Dissertations*. Paper 322.

This Open Access Dissertation is brought to you for free and open access by DigitalCommons@WayneState. It has been accepted for inclusion in Wayne State University Dissertations by an authorized administrator of DigitalCommons@WayneState.

**LASER-INDUCED BREAKDOWN SPECTROSCOPY (LIBS): AN
INNOVATIVE TOOL FOR STUDYING BACTERIA**

by

QASSEM I. MOHAIDAT

DISSERTATION

Submitted to the Graduate School

of Wayne State University,

Detroit, Michigan

in partial fulfillment of the requirements

for the degree of

DOCTOR OF PHILOSOPHY

2011

MAJOR: PHYSICS

Approved by:

Advisor

Date

DEDICATION

I would like to dedicate my dissertation to my wife, my children Amr, Sarah and Muhammad, my mother, my Father, and my brothers and sisters, for their love, patience, and support.

ACKNOWLEDGMENTS

First and foremost I would like to gratefully and sincerely thank my advisor Dr. Steven Rehse for his guidance, understanding, and patience from the very early stage of this research as well as giving me extraordinary experiences throughout the work. I would like also to thank my committee members Dr. Sunil Palchadhuri, Dr. Jogindra Wadehra, and Dr. Peter Hoffmann for their encouraging words and guidance over the years. Special thanks to Dr. Ratna Naik for her endless support and keeping an eye on me through my graduate study.

I would like to also extend my gratitude to Dr. Hossein Salimnia for helpful conversations concerning bacterial pathogenesis and bacterial strain selection and Dr. Robert Mitchell for providing *E. coli* specimens and bacterial preparation guidance. I would like to take this opportunity to thank Dr. Choong-Min Kang (Wayne State University, Department of Biological Sciences) for the preparation of the *M. smegmatis* samples.

My graduate studies would not have been the same without the social and academic challenges and diversions provided by all my student-colleagues in our department. I am particularly thankful to my friends Caleb Ryder, Eldar Kurtovic, and Emir Kurtovic. My enormous debt of gratitude can hardly be repaid to my wife Khozima Hamasha, who not only proof-read multiple versions of all the chapters of this dissertation, but also provided many stylistic suggestions to help me improve my presentation and clarify my arguments.

TABLE OF CONTENTS

Dedication	ii
Acknowledgments	iii
List of Tables	viii
List of Figures	ix
CHAPTER 1 “INTRODUCTION”	1
1.1 The Identification of Bacteria in Clinical Samples	2
1.2 LIBS Technique Comparison with Other Techniques	6
1.3 Objectives of This Work	13
References	19
CHAPTER 2 “PRINCIPLES OF LIBS, BACTERIAL PHYSIOLOGY, AND CHEMOMETRIC ANALYSIS”	22
2.1 Principles of LIBS	22
2.1.1 Energy Source	22
2.1.2 Spatial Intensity Distribution	24
2.2 Fundamental Ablation Processes	25
2.2.1 Ablation and Plasma Creation	25
2.2.2 Plasma Breakdown	27
2.2.3 Spectral Emission from Plasma	31
2.2.4 Temperature and Spectral Lines Intensities	33
2.3 Bacteria Physiology	36
2.3.1 Cell Wall Structure of the Gram-Negative Bacteria	38
2.3.2 Cell Wall Structure of the Gram-Positive Bacteria	40
2.4 Selection of Bacterial Species for LIBS Study	41

2.5 Discriminant Function Analysis (DFA)	43
2.5.1 Definition	43
2.5.2 How Discriminant Analysis Works	43
2.5.3 The Approach	43
2.5.4 The Linear Discriminant Model	44
References	46

CHAPTER 3 “INSTRUMENTATION AND STANDARD METHODS”.....50

3.1 Laser System	50
3.1.1 Laser Delivery Optics	51
3.1.2 Optical Collection	57
3.2 Bacterial Culture and Growth	61
3.2.1 Media Preparation	61
3.2.2 Liquid Culture	62
3.2.3 Inoculating and Dilution on Solid Culture	63
3.2.4 Preparation of Bacterial Targets	64
3.3 Experimental Parameters	67
References	72

CHAPTER 4 “THE EFFECT OF SEQUENTIAL DUAL-GAS TESTING ON LIBS-BASED DISCRIMINATION: APPLICATION TO BRASS SAMPLES AND BACTERIAL STRAINS”73

4.1 Introduction	73
4.2 Experimental	74
4.3 Results and Discussion	77

4.3.1 Brass Samples	77
4.3.2 Bacterial Samples	86
4.4 Conclusions	90
4.5 Summary	91
References	93
CHAPTER 5 “THE EFFECT OF MIXED CULTURES AND SAMPLE DILUTION ON BACTERIAL IDENTIFICATION”	95
5.1 Introduction	95
5.2 Experiment	96
5.2.1 LIBS Experiment	96
5.2.2 Bacterial Sample Preparation	97
5.2.3 Mixed Samples	98
5.3 Results and Discussion	99
5.3.1 Mixing Experiment	99
5.4 Sample Dilution	103
5.4.1 Dilution Experiment	103
5.5 Bacterial Discrimination and Library	108
5.6 Conclusions / Summary	110
References	112
Chapter 6 “THE EFFECT OF BACTERIAL ENVIRONMENTAL AND METABOLIC STRESSES ON A LIBS-BASED IDENTIFICATION OF <i>E. COLI</i> AND <i>S. VIRIDANS</i>”	113
6.1 Introduction	113
6.2 LIBS Instrumentation	114

6.3 Nutrition Medium Environment: Effect on <i>E. coli</i> Strain Discrimination	116
6.4 LIBS Identification of Live and Dead Bacteria	117
6.5 LIBS Identification of Pathogenic and Non-Pathogenic Bacteria under Nutrient Deprivation Conditions.....	123
6.6 Conclusions.....	126
6.7 Summary	128
References	129
CHAPTER 7 TOWARD THE IDENTIFICATION OF BACTERIA IN CLINICAL SAMPLES.....	131
7.1 Introduction	131
7.2 Experiment	132
7.2.1 Bacterial Sample Preparation	132
7.2.2 LIBS Experiment	133
7.3 The Identification of <i>S. epidermidis</i> Bacteria in A Sterile Urine Suspension	134
7.4 Identification of Bacteria in Mixed Clinical Samples	137
7.5 The Detection of Bacteria on a Membrane Filtration Method	138
7.6 Summary	142
References	144
CHAPTER 8 CONCLUSIONS AND FUTURE WORK	146
Abstract.....	151
Autobiographical Statement.....	153

LIST OF TABLES

Table 2.1: The Gram-staining process of bacterial identification	37
Table 4.1: The composition of the four brass alloys used in this study	77
Table 4.2: The strongest emission lines observed in brass LIBS plasmas acquired in argon and helium	79
Table 4.3: The structure matrix for the DFA of four brass alloys ablated in an argon atmosphere	82
Table 5.1: Classification results from the discriminant function analysis of <i>M. smegmatis</i> / <i>E. coli</i> mixed samples	102
Table 5.2: Classification results from the discriminant function analysis of 10 different bacteria	109
Table 6.1: The LIBS classification accuracies of the three tests described in this article	125
Table 8.1: A list of some bacteria which need to be analyzed by LIBS	148

LIST OF FIGURES

1.1	Diagram of a typical LIBS experiment	7
2.1	Schematic energy levels of an Nd:YAG laser	23
2.2	Cylindrical transverse mode patterns TEM_{nm}	25
2.3	Illustration of plasma shielding effect	27
2.4	Ionization by multiphoton absorption	28
2.5	Examples of plasmas as a function of temperature and electron density	29
2.6	All the main LIBS processes	31
2.7	Energy levels and electron transitions	32
2.8	The cellular structure of a typical bacterial cell	36
2.9	The schematic drawing of the outer membrane of the Gram-negative bacterium	39
2.10	The schematic drawing of the Gram-positive bacterium.....	40
3.1	Diagram of a typical LIBS set-up	50
3.2	High-Power Nanosecond Laser System (Spectra-Physics Lab-150-10)	51
3.3	A schematic diagram of the energy attenuation optics	52
3.4	A picture of the energy attenuation optics	52
3.5	A schematic diagram of the telescope	53
3.6	A picture diagram of the telescope	54
3.7	The schematic side view of the periscope	55
3.8	A picture side view of the periscope	56
3.9	A schematic diagram of the purge chamber	57
3.10	The geometry of an échelle grating	58
3.11	Operation principal of an échelle spectrograph	59

3.12 Arrangement of the échelle-Spectrograph (ESA 3000)	60
3.13 Different turbidity due to the growth of bacterial cells	62
3.14 Inoculating and employing streak plate techniques to isolate individual bacterial colonies on a solid medium	63
3.15 <i>E. coli</i> pellet after centrifugation with the supernatant removed	64
3.16 The bacterial mounting procedure used in this study.	66
3.17 Three bacterial pads deposited on the agar surface	66
3.18 The control menu of the ESAWIN software which controlled the timing of the laser and spectrometer	67
3.19 Temporal history of LIBS plasma	68
3.20 A LIBS spectrum of <i>E. coli</i> bacteria ablated on agar	69
3.21 Arrangement of orders in the focal plane of an échelle spectrograph	70
3.22 The ROI view of the spectrum shown in figure 3.11	71
4.1 LIBS emission spectra for one of the brass samples in argon and helium	78
4.2 A DFA plot showing the first two discriminant function scores of LIBS spectra obtained from four brass samples in argon	81
4.3 A DFA plot showing the first two discriminant function scores of LIBS spectra obtained from four brass samples in helium	84
4.4 A DFA plot of brass samples tested in both gases sequentially.	85
4.5 A DFA plot of LIBS spectra from bacterial specimens of two strains of <i>E. coli</i> (Nino C and HF4714) and <i>Streptococcus mutans</i> ablated in argon and helium	88
4.6 A DFA plot of three bacterial samples tested sequentially in both argon and helium.	89
5.1 The first three discriminant function scores from a DFA of the LIBS spectra from pure samples of three different bacteria	100

5.2	DFA plot showing the first two discriminant function scores for the spectra obtained from pure samples of two bacteria: a wild-type strain of <i>M. smegmatis</i> and a strain of <i>E. coli</i> (C) and four mixtures of those two bacteria at various mixing fraction	101
5.3	A DFA plot showing the first two DF scores for three different concentrations of <i>M. smegmatis</i> (WT)	104
5.4	A typical LIBS spectrum from the lowest concentration of <i>M. smegmatis</i> (WT) tested in this study.....	106
5.5	The total spectral power associated with each of the five elements observed in the LIBS spectrum of <i>M. smegmatis</i> (WT) ablated in argon as a function of bacterial cell number.	107
5.6	A DFA plot showing the first two DF scores for LIBS spectra from two species of <i>Staphylococcus</i> (<i>aureus</i> and <i>saprophyticus</i>), two species of <i>Streptococcus</i> (<i>viridans</i> and <i>mutans</i>), two conditional mutants of <i>M. smegmatis</i> (WT and TE) and four strains of <i>E. coli</i> (enterohemorrhagic <i>E. coli</i> O157:H7, C, HF4714, and HfrK12)	109
6.1	Optical micrographs of the bacterial bed mounted on an agar substrate.	115
6.2	A DFA plot of the LIBS spectra from four <i>E. coli</i> strains.....	117
6.3	A DFA of three specimens of <i>E. coli</i> strain C, one specimen of <i>E. coli</i> strain ATCC 25922, and one specimen of <i>M. smegmatis</i>	120
6.4	A DFA of three specimens of <i>S. viridans</i> , one specimen of <i>E. coli</i> strain ATCC 25922, and one specimen of <i>M. smegmatis</i>	122
6.5	A DFA plot of the spectra from many different bacterial specimens: starved <i>S. viridans</i> , autoclaved <i>S. viridans</i> , UV-irradiated <i>S. viridans</i> , starved <i>E. coli</i> C, autoclaved <i>E. coli</i> C, UV-irradiated <i>E. coli</i> C, and <i>M. smegmatis</i>	124
7.1	<i>E. coli</i> C bacteria deposited on a membrane filter with 0.45 μm pore size	134
7.2	A DFA plot of the LIBS spectra from <i>E. coli</i> C, <i>S. epidermidis</i> harvested from both urine and water, and <i>S. viridans</i>	135
7.3	A DFA plot of the LIBS spectra from <i>S. epidermidis</i> harvested from a urine sample and water, <i>S. aureus</i> and <i>S. saprophyticus</i>	136
7.4	DFA plot showing the first two discriminant function scores for the spectra obtained from pure samples of two bacteria.....	137

7.5 A typical LIBS spectrum from the Millipore cellulose membrane filter in this study.....139

7.6 A typical LIBS spectrum from *E. coli* bacteria ablated on the cellulose membrane filter in an argon atmosphere140

7.7 DFA plot showing the first two discriminant function scores for the spectra obtained from, *E. coli* ATCC 25922, *M. smegmatis*, *E. coli* C, and filter142

Chapter 1

Introduction

Bacteria, both pathogenic and non-pathogenic, are the omnipresent companions to human existence. They live all around us and within us. In fact, it was found that the number of bacterial cells that exist in an average healthy adult is estimated to outnumber human cells 10 to 1.¹ Due to their impact on so many aspects of human health and safety, different approaches have been investigated in order to develop biosensing technologies that can be used as robust and rugged tools for the positive identification of bacteria in real-time.²

Such technology is urgently needed to identify bacteria in clinical samples at the time when a clinical sample of blood, urine or sputum is obtained, particularly if this could be done with little or no sample preparation. Currently, no such technology exists to fill this role. This ability to identify the bacteria rapidly and onsite would allow doctors to successfully diagnose the disease and then initiate the proper treatment without waiting for offsite lab results to be returned. In addition to that, the integration of new technology could play an important role in the epidemiology of outbreaks of illness such as tuberculosis (TB),³ not only in the treatment of patients, but also in the tracking of the TB bacteria to help identify the source of infection and to keep the infections from spreading. An accurate rapid identification of bacteria could also minimize the use and overuse of broad spectrum antibiotics. The consequences of such overuse and abuse of broad spectrum antibiotics include not only excessive costs of billions of dollars, but also has led to the ever-increasing emergence of drug resistant bacteria.

This type of new technology would be important not only clinically, but could provide an immediate identification of dangerous pathogens in certain types of foods such as meats,

vegetables, and dairy products at a relatively low cost. As an example, recent outbreaks of *salmonella* and *Escherichia coli* (*E. coli*) infections have occurred in several nations. Some *E. coli* strains can be deadly if consumed via contaminated food.

A rapid and definitive bacterial identification is important not only for many areas of industry and health and human safety, but also for the correct diagnosis of disease and the subsequent treatment of infection. This rapid identification could help hospitals and physicians improve patient outcomes, lower costs, and reduce the worldwide impact of antibiotic resistant microbes.

Nowadays, medical microbiologists still depend heavily on a century-old technique, which is the broad classification of bacteria by Gram-staining. This involves, streaking a unknown bacteria on a microbiological selective media, staining with colored dyes, and immunological methods for the initial identification of pathogenic bacteria. This is described in more detail in chapter 2.

1.1 The Identification of Bacteria in Clinical Samples

Currently, medical microbiologists mostly still use traditional or old-fashioned methods in order to identify bacteria in clinical samples. All methods of bacterial identification fall into three main categories: phenotypic (morphology), immunological (serological), and genotypic methods.^{4,5} Morphological methods depend on many factors including, cell size, shape, and Gram-stain.* This type of bacterial identification not only requires starting with a pure culture (which means that only one type of bacterium is present), but it is also a slow process. For

* The Gram stain is a protocol which uses a series of dyes that leaves some bacteria purple (Gram-positive) and others pink (Gram-negative). The specific stain reaction of a bacterium results from the structure of its cell wall. This classification will be used to categorize bacteria later in this dissertation.

example, while *E. coli* bacteria require 24 hours to grow, many other bacteria like *Mycobacterium tuberculosis* (TB) can take weeks to be cultured.⁶ Problems can occur when more than one type of bacteria is present in a sample. In cases of mixed bacterial samples, cultures need to be streaked onto an appropriate agar plate to isolate the bacteria for accurate identification later. In all cases, this type of identification of bacteria requires expertise in microbiology and is time-consuming, expensive (requiring large stocks of consumable supplies), and labor-intensive.

On the other hand, serological methods involve the interaction of a microbial antigen (a substance or molecule that elicits an immune response and is then capable of binding to the subsequently produced antibodies) with a complementary antibody (produced by the host immune system). For example, enzyme-linked immunosorbent assay (ELISA) is a simple and sensitive biological method that can detect less than 10 ng of antigenic protein from bacterial culture.⁷ In this method, a single bacterium cell can be identified by utilizing the right antibody which can bind with the bacterial antigen. One disadvantage of this method is the specificity of antibodies, which make any test only sensitive to one specific bacterium.

Finally, genotypic methods involve testing the genetic material of the microorganisms. Polymerase chain reaction (PCR) is a genotypic technique that is widely used for the rapid detection of microbial pathogens in clinical specimens including blood, urine, sputum, and cerebrospinal fluid (CSF). In this technique, a specific segment of deoxyribonucleic acid (DNA) is amplified to produce millions of copies to be adequately tested.⁸ However, to perform a PCR reaction we need pure DNA that has been extracted from a bacterial cell. Moreover, the application of PCR to clinical samples has many potential pitfalls such as the difficulty of

detection of specific target bacteria in a mixture sample. In this case, additional steps are required such as culturing followed by isolation and detection of the target bacteria DNA. The previous processes not only need an expert microbiologist, but also require *a priori* knowledge of conserved nucleic acid sequences.

Fluorescent in situ hybridization (FISH) is another molecular technique used to identify microbes based on the presence or absence of specific DNA sequences. In this technique, the hybridization probe, a fragment of DNA, and a fluorescent tag are applied to the sample of interest (i.e. bacteria) under conditions that allow probe-target base pairing due to the complementary sequence between the probe and target. After that a fluorescent microscope is used for testing. Measuring the amount of fluorescence can allow us to determine if the patient is infected with a specific pathogen or not, and if so, how many bacteria are present in a sample. But there are some disadvantages of using FISH in clinical applications due to the difficulty of preparing probes and the difficulty of counting the total number of probe-target base pairings.⁹

Matrix assisted laser desorption/ionization time-of-flight mass spectrometry (MALDI-TOF-MS) is another fast and reliable technique that can be used for the rapid identification of microorganisms.¹⁰ In this technique, a laser is used to ablate bacteria to generate ions of high molecular weight (i.e. proteins) as a result of the relatively large amount of absorbed energy. After that, the ions are accelerated by an electric field in a flight tube towards a detector. An analyzer is used to measure the time of flight (TOF) for ions to reach the detector (smaller ions arrive at the detector in a shorter amount of time compared to the larger ions). At the end, separated ion fractions are detected by a recorder that generates a signal upon the impact of each ion group which will be used as a mass-spectrum fingerprint for the organism. Although it

requires a small amount of biological material with easy sample preparation and can yield highly reproducible measurements, it must still be considered an expensive high-vacuum mass-spectrometry technique that must be situated in a laboratory and staffed by mass spectrometry experts.

Raman spectroscopy is a molecular technique that has been widely used for identification of bacteria.^{11,12} In this technique, a laser beam is incident on a bacterial target and the inelastically scattered light is carefully dispersed. Shifts in the scattered photon energy corresponding to vibrational, rotational, and other low-frequency modes in the molecules of the target are then measured to determine molecular composition.¹³ This optical spectrum can be used as a “spectral fingerprint” or a “whole-organism fingerprint.”¹⁴

To sum up, one might ask is it possible to create a new technology for the rapid identification of bacteria which does not require any prior information about nucleic acid sequences or antibodies against known bacterial antigens? Could such a new technology identify pathogens in test samples at “time zero”, require little or no sample preparation, give robust and reproducible data, be inexpensive, and not require culturing bacteria for one or more days?

To address the previous mentioned points, I propose to develop a promising technology known as “laser-induced breakdown spectroscopy” (LIBS) that can rapidly (within minutes) identify bacteria based on their unique atomic compositions. The goal of my dissertation is to prove that this type of atomic composition-based identification is possible, to explore its ultimate specificity and sensitivity, and to carefully investigate the microbiological diversity that may naturally occur in any biological system which could impede or prevent accurate bacterial identification.

In the following section I will give a brief introduction to the principles of LIBS (the theory of LIBS will be discussed in detail in chapter 2), I will compare the LIBS technique with the other mentioned techniques, and give a chronological recounting of the short history of the use of LIBS in bacterial systems.

1.2 LIBS Technique Comparison with Other Techniques

Laser-induced breakdown spectroscopy (LIBS) is a spectrochemical technique which uses an intense laser pulse to determine the elemental composition of a sample and the relative quantities of the target's constituent elements. LIBS employs a low-energy pulsed laser in the order of tens to hundreds of mJ per pulse and focusing optics, i.e. a lens, in order to generate a plasma that vaporizes a small amount of target material.^{15,16} The generated plasma contains the excited atoms and ions that were present in the target and sometimes molecules formed by recombination of those atoms. As the plasma cools, the atoms, ions, and molecules lose energy via the spontaneous emission of optical wavelength photons. A spectroscopic analysis of the plasma light will thus yield the elements that are present in the target material. The positive identification of many elemental lines including both the wavelength and the intensity within the emission spectrum will form a unique spectral fingerprint of the target such as bacteria. A typical LIBS experiment consists of a pulsed laser (i.e. nanosecond or femtosecond laser), optics for focusing the laser beam onto the sample surface (i.e. pure bacteria or a bacteria-containing liquid), some optical method of collecting the light produced during the LIBS process (i.e. lenses, mirrors, or an optical fiber), and a spectrometer for the dispersion of light as shown in

Figure 1.1. In chapter 3 I will describe the specific experimental set-up we use with a detailed description of the instruments and the optics used.

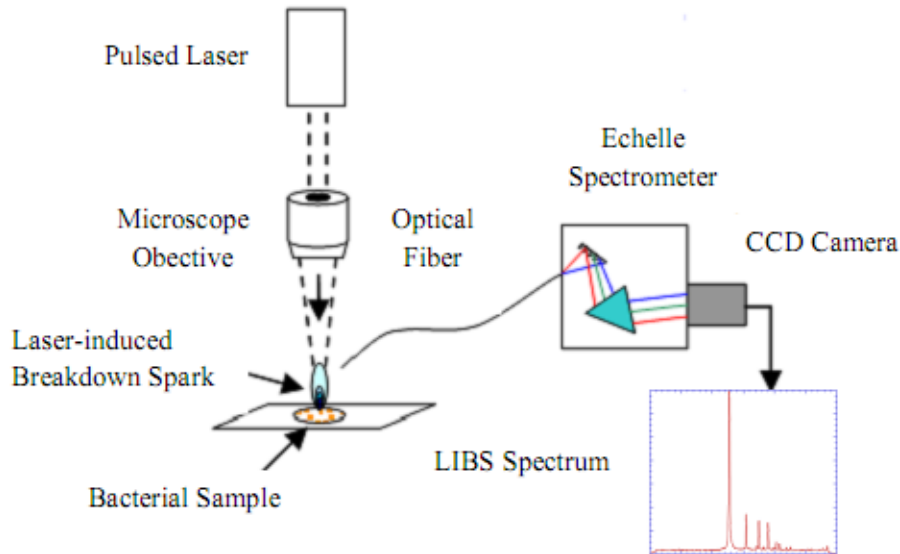


Figure 1.1: Diagram of a typical LIBS experiment.

LIBS has numerous advantages compared to the other techniques. This technique does not require any special sample preparation, and requires only a small volume or mass of material to be tested. It has a high spatial resolution on the target material, typically less than 100 μm , which is limited by the size of the focused laser being used. In addition, it is relatively simple to implement, not very expensive, yields a real-time response, and can be performed by non-experts.¹⁷

The history of LIBS dates back to the early 1960s when the first ruby laser was developed.¹⁸ In 1963, Q-switched pulsed lasers were invented which led to the “birth” of the LIBS technique.¹⁶ Following this, and specifically in 1972, Felske et al. studied the analysis of steel by means of a Q-switched ruby laser.¹⁹ During the 1980’s, the Nd:YAG crystal laser

became the most common laser system used in most LIBS applications since it has the capability of producing well-focused high energy single pulses in a short time for reliable laser plasma generation.²⁰ After that, a number of portable LIBS units were developed for field measurements during the 1990's.²¹ In 2001, people became interested in LIBS as a promising portable technology for the detection of hazardous materials after the attacks of September 11th and the subsequent lethal attacks utilizing *Bacillus anthracis* (anthrax) transmitted through the U.S. mail.²²

It is only in the last decade that it has begun to be recognized that LIBS can be used for rapid bacterial identification. This is due to several modern technological advances. One is the use of advanced computerized chemometric methods to analyze LIBS spectra. Another is the development of high resolution broadband Echelle spectrometers combined with sensitive CCD and ICCD detectors. Yet another is the availability of light-weight inexpensive high-powered lasers. By utilizing all these advances, LIBS has recently begun to be used for characterizing biological samples such as microorganisms (i.e. bacteria) and tissues. It offers a potentially faster, more reliable, and more robust platform than other methods to perform rapid measurements which are useful for the detection and identification of harmful pathogens in real-time.

In 2003 Morel et al. investigated the detection of six bacterial samples in addition to two pollens using LIBS. In this paper, all bio-samples were compressed to form dry pellets in order to achieve a strong high signal to noise ratio (SNR). At that time, relative line intensities of inorganic elements such as magnesium, sodium, iron, phosphorus, potassium, and calcium, and organic elements like carbon and nitrogen were used for the LIBS- based discrimination between

the eight species. This paper raised the idea that LIBS may be considered a good tool to detect the presence of biomaterials.²³

Also in 2003, Samuels et al. used nanosecond laser-induced breakdown spectroscopy to study bacterial spores, molds, pollens, and proteins. In this study, all bio-samples were deposited on a 0.45 μm average pore size silver membrane filter. LIBS spectra from single laser pulses were analyzed by principal component analysis (PCA), a chemometric technique, which successfully categorized the bio- samples in three distinct clusters.²⁴

At the same time Hybl et al. were using *Q*-switched Nd:YAG laser pulse with 1064 nm wavelength for detection and discrimination of various types of bioaerosols. A compact Ocean Optics HR2000 spectrometer was used to collect LIBS spectra. In their study, the discrimination was based on the atomic emission strength of inorganic elements such as Ca, Mg, and Na present at different concentrations in the microorganism. PCA was again used to analyze the LIBS spectra. The authors concluded that PCA can readily discriminate between bioaerosol classes and they suggested using sensitive Echelle spectrometers coupled with intensified CCD cameras for better discrimination.²⁵

Kim et al. have carried out laser-induced breakdown spectroscopy for discriminating between five nonpathogenic bacterial strains, *Bacillus thuringiensis* T34, *Escherichia coli* IHII/pHT315, *Bacillus subtilis* 168, *Bacillus megaterium* QM B1551, and *Bacillus megaterium* PV361. A pulsed *Q*-switched Nd:YAG laser with 532 nm pulses was used for the plasma generation. In their study, they measured the elements such as calcium, iron, manganese, zinc, sodium, potassium and sulfur. The final discrimination was accomplished by creating maps of the ratios of two calcium lines to the ratios of two phosphate lines for each bacilli species.²⁶

In 2004, Leone et al. used time-resolved laser induced breakdown spectroscopy (TRELIBS) to discriminate between six bacteria samples. In their study, the cumulative intensity ratios (CIR) of ten laser shots for P (253.560 nm) and C (247.856 nm) were measured. The CIR ratios of P/C showed a good discrimination among different bacteria. In this study, no advanced chemometric methods were used, but they suggested using a better spectrometer (they used Czerny-Turner spectrometer) such as the Echelle spectrometer for a better discrimination.²⁷

DeLucia et al. reported the use of a new man-portable LIBS system, developed in part both by the U.S. Army Research Laboratory and Ocean Optics, for the rapid identification and discrimination between potentially hazardous biomaterials.²⁸ They also commented on the use of the same instrument for sensitive chemical agent threat detection. Expanding on this work, Gottfried et al. at the Army Research Laboratory used LIBS for the standoff detection of chemical and biological threats at distances of up to 20 m.²⁹ The ability to identify threats while the operator remains 10's of meters away from the material being tested is a safety advantage of LIBS that none of the other techniques described (other than Raman spectroscopy) can match. The same group also investigated the use of partial least squares – discriminant analysis (PLS-DA) for the discrimination between explosives and nonexplosives materials.³⁰

Some of the most significant LIBS work on bacteria was performed at the Laboratoire de Spectrométrie Ionique et Moléculaire, Université Claude Bernard-Lyon, Cedex, France. There, Baudelet et al. used femto-second laser-induced breakdown spectroscopy for the identification of biological samples.³¹ In 2006 they used LIBS in order to analyze five microbiological samples. In their study, six elements, Na, Mg, P, K, Ca and Fe were detected. The discrimination between the bacteria spectra depended on three elements, Ca, K and Na. The analysis was carried out and

they found that the Gram-negative bacteria such as *Escherichia coli* have more Ca compared to Gram-positive bacteria (*Bacillus subtilis*) which is due to the fact that divalent cations maintain the cohesion of proteins present in the outer membrane of the Gram-negative bacterium cell.³² They also compared the LIBS spectra of bacterial samples (*Escherichia coli* and *Bacillus subtilis*) obtained by the use of femtosecond and nanosecond lasers. In this study, they found that the femtosecond regime has a lower plasma temperature compared to the nanosecond one. Based on this result, the trace mineral elements (i.e. potassium) can be detected from bacteria with a higher contrast which may provide valuable information resulting in better discrimination of biological samples.³³

In our own laboratory, *E. coli* identification and strain discrimination were studied by using nanosecond laser-induced breakdown spectroscopy. In this study, three different strains of *E. coli*, one strain of environmental mold, and one strain of *Candida albicans* yeast were studied to determine if bacteria were easily differentiable from common background biological contaminants. All the spectra were dominated by singly ionized and neutral Mg and Ca, which is due, in some part, to the presence of Mg^{+2} and Ca^{+2} in the outer membrane of the bacteria cell. In this paper discriminant function analysis (DFA), another chemometric technique, was used for the first time to classify LIBS spectra. DFA is a type of chemometric analysis that reduces the entire LIBS spectrum to a much lower dimensional vector characterized by coordinates called discriminant function scores. The mathematics of DFA will be discussed extensively in chapter 2. The DFA ,showed a significant variance between the spectra obtained from different strains and biotypes. All the group memberships were predicted with a 100% confidence.³⁴

Recently, our own group (Diedrich, et al.) have applied LIBS to analyze a pathogenic strain, *enterohemorrhagic E. coli* (EHEC) in order to compare it with nonpathogenic strains of *E. coli* such as C and K-12 (AB). According to their analysis, they showed that LIBS can be used as a powerful tool in order to identify and discriminate between a pathogenic strain and a nonpathogenic one. The DFA analysis showed that the discrimination between those different strains is based primarily on the concentration of both Ca and Mg.³⁵

The same research group investigated the technique's potential for detecting and discriminating *Pseudomonas aeruginosa* grown on different nutrient media: a trypticase soy agar (TSA) plate, blood agar plate, and a MacConkey agar plate containing bile salts. The DFA showed no difference between *P. aeruginosa* grown on the TS agar and the one that was grown on the blood plate. On the other hand, the bacteria grown on a MacConkey plate was different from the other two which could be related to the additional calcium concentration that came from the bile salts during culturing.³⁶

Our group also studied the effect of growing two bacterial species in three different nutrient media: a standard TS agar, a MacConkey agar containing a 0.01% concentration of bile salts, and a TS agar with a higher 0.4% concentration of deoxycholate. LIBS spectra for both *Pseudomonas aeruginosa* and *E. coli* C grown in the 0.01% concentration of bile salts were altered in a highly reproducible way. This could be related to an excess of divalent cations around the bacteria by the formation of an extracellular polysaccharide capsule. On the other hand, LIBS spectra for bacteria cultured in 0.4% medium were also altered. This could be related to the disruption of the bacterial outer membrane due to the change of the concentrations of the divalent cations.³⁷

In a very recent development, Multari et al. showed that LIBS can specifically discriminate with 100% accuracy between strains of methicillin-resistant *Staphylococcus aureus* (MRSA) in a blind test. In their study, all the LIBS spectra were dominated by the presence of organic and inorganic elements, specifically, Na, K, Mg, C, Mg, Si, H, and N. Interestingly, even though it is believed that calcium (Ca) is responsible for the stability of the bacterial cell wall and is a dominant emission feature in our LIBS spectrum, no Ca lines were observed in the LIBS spectra of the MRSA strains. LIBS spectra for all bacteria were collected from lyophilized samples, which took three days to prepare, while in our laboratory LIBS spectra will be collected from live bacteria (the entire process from the time the sample is obtained until pathogen diagnosis should take no more than 15 minutes). Moreover, the authors used the raw (unprocessed) LIBS spectrum in their analysis, but without mentioning any information about the benefits of using the entire spectral range (in their case, from 205.42 to 850 nm) or using the most relevant lines that may exist in the LIBS spectrum.³⁸ The appropriateness of using the entire LIBS spectrum or only portions of it (“down-selected variables”) is still an open question within this field.

1.3 Objectives of This Work

In all previous papers, LIBS was performed as “proof-of-concept” experiments in highly idealized, but not very realistic conditions on a limited number of bacterial species. In this work, I performed several new experiments that may allow us to develop a new robust technology that can be used easily for the best bacterial identifications in real-world samples. To accomplish this goal, different experiments need to be conducted (as described below) that will allow the identification of the most medically important and relevant pathogens. Importantly, the

influence of natural environmental and biological factors that may alter bacterial compositions, thus ruining a LIBS-based identification, have never been investigated. It is one of the goals of this work to investigate these “real-world” conditions that clinically relevant pathogens may encounter to determine if they will limit the applicability of the LIBS method.

In Chapter 2 and 3 I will discuss the physics behind the main principles of LIBS and the mathematics of the chemometric analysis in addition to describing the experimental apparatus used to conduct the LIBS experiments.

Several studies have been performed in order to investigate the effect of various buffer gases such as argon, neon, helium, nitrogen, and air on the plasma formation during LIBS. The results showed that both argon and helium have the ability to enhance the intensities of the plasma emission lines, particularly of phosphorus and carbon. In chapter 4, I will describe my experiments to investigate the effect that sequential testing in two ambient gas environments at atmospheric pressure would have on the ability to identify or discriminate between highly similar samples of bacteria and less-similar samples of brass based on their LIBS spectra. In both the brass alloy and the bacterial system, sequential LIBS spectra in argon and helium were collected and analyzed with DFA. After that, I will investigate the effect of using the two ambient gases on the overall accuracy of identification.

In chapter 5, I will begin to compile a reference library of atomic emission fingerprints for a wide variety of clinically relevant species (Gram-negative and Gram-positive bacteria). To do this, LIBS spectra of bacterial specimens and strains prepared over numerous weeks were acquired. The saved LIBS spectra were analyzed by a computerized discrimination algorithm. The resultant library is essential for performing an immediate diagnosis of an unknown specimen

statistically and without user bias. The selectivity of this type of test (the classification accuracy) was studied.

I will show that the intensity of the LIBS spectrum is linearly dependent on cell number. This is important, as it indicates that LIBS spectra obtained from specimens with a much lower titer will be identified accurately by the reference library spectra that I propose to construct from specimens of a much higher titer. Therefore, I will investigate the sensitivity or the “limit of identification” (which is NOT the “limit of detection”) of the LIBS test for bacterial strain identification and discrimination. In this experiment, serial dilutions of bacterial aliquots were prepared to determine the minimum number of bacteria which are required for an effective identification and discrimination. The question of the required number of bacteria is a crucial parameter that has not been measured by anyone. The results will be shown in chapter 5.

At the end of chapter 5, I will investigate the impact on the LIBS-based bacterial identification when other types of bacteria are present (mixed cultures). Specifically, the effect of mixing bacterial samples will be studied by creating mixtures of known titer. Specimens of distinct bacteria in different ratios, including but not limited to *Mycobacterium smegmatis* and *E. coli* bacteria, were created for this purpose. The reduction in the ability to identify the bacterial constituents as a function of mixing ratio will be presented.

In chapter 6, I will also study in much more detail the effect of the growth medium on the LIBS-based bacterial identification. A non-pathogenic strain of *Escherichia coli* was cultured in two different nutrient media: a trypticase soy agar and a MacConkey agar with a 0.01% concentration of deoxycholate to perform these studies.

I also investigated the effect that the state of growth of the bacteria had on bacterial identification. LIBS spectra were collected from specimens of a non-pathogenic *E. coli* strain and an avirulent derivative of the pathogen *Streptococcus viridans* in four different metabolic situations: live bacteria, bacteria exposed to ultra-violet irradiation, bacteria killed via autoclaving, and bacteria that were deprived of nutrition for a period of time ranging from one day to nine days by deposition on an abiotic surface at room temperature. In this experiment, I intended to prove that the LIBS spectrum is independent of any of these conditions. In proving this last statement, LIBS can be considered a powerful tool to handle dangerous bacteria safely (since they can be killed prior to testing), which will increase the safety for public health care workers.

In chapter 7, I will also investigate the possibility of identifying bacteria in “dirty” clinical samples (sterile urine) without washing. This test was a very realistic simulation of a test on a real clinical sample. Surrogates of clinical samples were used to control bacterial titer and to provide a guaranteed known identity. Specifically, LIBS spectra of *Staphylococcus epidermidis* bacteria that were prepared via our usual protocol were compared with other spectra obtained from the same bacteria that were “spiked” into a sterile urine specimen at appropriate titers and recovered without washing.

In addition, membrane micro-filters were used to isolate and concentrate the bacteria from liquid samples in an effort to simplify the sample preparation steps and to make the technique more widely applicable to more situations. After that, I tested the ability to identify bacteria by analyzing the LIBS spectra from bacteria tested directly on the filter using an appropriate chemometric analysis.

REFERENCES

-
- ¹ R. Sleator, “The human superorganism – of microbes and men,” *Medical Hypotheses* **74**, 214–215 (2010).
- ² A.L. Truant, *Manual of Commercial Methods in Clinical microbiology*, (ASM Press) 2002.
- ³ R.H. George, P.R. Gully, N. Gill, J.A. Inness, S.S. Bakhshig, and M. Connolly, “An outbreak of tuberculosis in a children’s hospital,” *Journal of Hospital Infection* **8**, 129-142 (1986).
- ⁴ P. Singleton, *Bacteria in Biology, Biotechnology and Medicine*, (John Wiley & Sons, Ltd.) 1999.
- ⁵ M. Madigan, J. Martinko and J. Parker, *Brock Biology of Microorganisms*, 9th Edition, (Prentice Hall College Div) 1996.
- ⁶ K. Kaneko, O. Qndera, T. Miyatake, and S. Tsuji, “Rapid diagnosis of tuberculous meningitis by polymerase chain reaction (PCR),” *Neurology* **40**, 1617-1618 (1990).
- ⁷ W.A. Pryor, *Bio-Assays for Oxidative Stress Status (BOSS)*, (Elsevier Science B.V.) 2001.
- ⁸ J.S. Santo Domingo and M.J. Sadowsky, eds., *Microbial Source Tracking* (ASM Press) 2007.
- ⁹ Q. Hoshino, L.S. Yilmaz, D.R. Noguera, H. Daims, and M. Wagner, “Quantification of target molecules need to detect microorganisms by fluorescence in situ hybridization (FISH) and catalyzed reporter deposition-FISH,” *Applied and Environmental Microbiology* **74**, 5068-5077 (2008).
- ¹⁰ J.O. Lay, “MALDI-TOF mass spectrometry of bacteria,” *Mass Spectrometry Reviews* **20**, 172-94 (2001).

-
- ¹¹ R. Petry, M. Schmitt, and J. Popp, "Raman spectroscopy - a prospective tool in the life sciences," *European Journal of Chemical Physics and Physical Chemistry* **4**, 14-30 (2003).
- ¹² D. Pappas, B.W. Smith, and J.D. Winefordner, "Raman spectroscopy in bioanalysis," *Talanta* **51**, 131-144 (2000).
- ¹³ K. Maquelin, C. Kirschner, L.-P. Choo-Smith, N. Van den Braak, H. Ph. Endtz, D. Naumann, and G.J. Puppels, "Identification of medically relevant microorganisms by vibrational spectroscopy," *Journal of Microbiological Methods* **51**, 255-271 (2002).
- ¹⁴ R. Goodacre, E. M. Timmins, R. Burton, N. Kaderbhai, A. Woodward, D. B. Kell, and P. J. Rooney, "Rapid identification of urinary tract infection bacteria using hyperspectral, whole organism fingerprinting and artificial neural networks," *Microbiology* **144**, 1157-1170 (1998).
- ¹⁵ D. Cremers and L. Radziemski, *Handbook of Laser-Induced Breakdown Spectroscopy*, (John Wiley & Sons Ltd.) 2006.
- ¹⁶ A.W. Miziolek, V. Palleschi, and I. Schechter, *Laser Induced Breakdown Spectroscopy*, 1st ed. (Cambridge University Press, Cambridge) 2006.
- ¹⁷ J.P. Singh and S. N. Thakur, Eds., *Laser-Induced Breakdown Spectroscopy*, (Elsevier, Amsterdam) 2007.
- ¹⁸ T.H. Maiman, "Stimulated optical emission in ruby," *Nature* **187**, 493-494 (1960).
- ¹⁹ A. Felske, W.D. Hagenah, K. Laqua, "Über einige Erfahrungen bei der Makrospektroskopie mit Laserlichtquellen: I Durchschnittsanalyse metallischer Proben," *Spectrochimica Acta Part B* **27**, 1-16 (1972).

-
- ²⁰ C. Pasquini, J. Cortez, L.MC Silva, and Fabiano B. Gonzaga, "Laser Induced Breakdown Spectroscopy," *Journal of the Brazilian Chemical Society* **18**, 463-512 (2007).
- ²¹ K.Y. Yamamoto, D.A. Cremers, M.J. Ferris, and L.E. Foster, "Detection of Metals in the Environment Using a Portable Laser-Induced Breakdown Spectroscopy Instrument," *Applied Spectroscopy* **50**, 222 (1996).
- ²² R.T. Wainner, R.S. Harmon, A.W. Miziolek, K.L. McNesby, and P.D. French, "Analysis of environmental lead contamination: comparison of LIBS field and laboratory instruments," *Spectrochimica Acta Part B*, **56**, 777-793 (2001).
- ²³ S. Morel, M. Leone, P. Adam, and J. Amouroux., "Detection of bacteria by time-resolved laser-induced breakdown spectroscopy," *Applied Optics* **42**, 6184-6191(2003).
- ²⁴ A. Samuels, F. DeLucia, Jr., K. McNesby, and A. Miziolek, "Laser-induced breakdown spectroscopy of bacterial spores, molds, pollens, and protein: initial studies of discrimination potential," *Applied Optics* **42**, 6205-6209 (2003).
- ²⁵ J.D. Hybl, G.A. Lithgow, and S.G. Buckley, "Laser-induced breakdown spectroscopy detection and classification of biological aerosols," *Applied Spectroscopy* **57**, 1207-1215 (2003).
- ²⁶ T. Kim, Z. Specht, P. Vary, and C. Lin, "Spectral fingerprints of bacterial strains by laser-induced breakdown spectroscopy," *The Journal of Physical Chemistry B* **108**, 5477-5482 (2004).
- ²⁷ N. Leone, G. D'Arthur, P. Adam, and J. Amouroux, "Detection of bacterial deposits and bioaerosals by time-resolved laser-induced breakdown spectroscopy (TRELIBS)," *High Technology Plasma Processes* **8**, 1-22 (2004).

-
- ²⁸ F.C. DeLucia, Jr., A.C. Samuels, R.S. Harmon, R.A. Walter, K.L. McNesby, A. LaPointe, R.J. Winkel, Jr., and A.W. Miziolek, "Laser-induced breakdown spectroscopy (LIBS): a promising versatile chemical sensor technology for hazardous material detection," *IEEE Sensors Journal* **50**, 681-689 (2005).
- ²⁹ J.L. Gottfried, F.C. De Lucia, C.A. Munson, and A.W. Miziolek, "Standoff Detection of Chemical and Biological Threats Using Laser-Induced Breakdown Spectroscopy," *Appl. Spectrosc.* **62**, 353-363 (2008).
- ³⁰ F.C. De Lucia Jr., J.L. Gottfried, C.A. Munson, and A.W. Miziolek, "Multivariate analysis of standoff laser-induced breakdown spectroscopy spectra for classification of explosive-containing residues," *Applied Optics* **47**, 112–121 (2008).
- ³¹ M. Baudelet, L. Guyon, J. Yu, J. P. Wolf, T. Amodeo, E. Frejafon, and P. Laloi, "Spectral signature of native CN bonds for bacterium detection and identification using femtosecond laser-induced breakdown spectroscopy," *Applied Physics Letters* **88**, 06391 1-3 (2006).
- ³² M. Baudelet, J. Yu, M. Bossu, J. Jovelet, J. Wolf, T. Amodeo, E. Fréjafon, and P. Laloi, "Discrimination of microbiological samples using femtosecond laser-induced breakdown spectroscopy," *Applied Physics Letters* **89**, 163903 (2006).
- ³³ M. Baudelet, L. Guyon, J. Yu, J.-P. Wolf, T. Amodeo, E. Frejafon, and P. Laloi, "Femtosecond time-resolved laser-induced breakdown spectroscopy for detection and identification of bacteria: A comparison to the nanosecond regime," *Journal of Applied Physics* **99**, 084701 1-9 (2006).

-
- ³⁴ J. Diedrich, S.J. Rehse, and S. Palchaudhuri, “*Escherichia coli* identification and strain discrimination using nanosecond laser-induced breakdown spectroscopy,” *Applied Physics Letters* **90**, 163901-1-3 (2007).
- ³⁵ J. Diedrich, S.J. Rehse, and S. Palchaudhuri, “Pathogenic *Escherichia coli* strain discrimination using laser-induced breakdown spectroscopy,” *Journal of Applied Physics* **102**, 014702 (2007).
- ³⁶ S.J. Rehse, J. Diedrich, and S. Palchaudhuri, “Identification and discrimination of *Pseudomonas aeruginosa* bacteria grown in blood and bile by laser-induced breakdown spectroscopy,” *Spectrochimica Acta Part B* **62**, 1169–1176 (2007).
- ³⁷ S.J. Rehse, N. Jeyasingham, J. Diedrich, and S. Palchaudhuri, “A membrane basis for bacterial identification and discrimination using laser-induced breakdown spectroscopy,” *Journal of Applied Physics* **105**, 102034 (2009).
- ³⁸ R. Multari, D.A. Cremers, J.M. Dupre, and J.E. Gustafson, “The use of laser-induced breakdown spectroscopy for distinguishing between bacterial pathogen species and strains,” *Applied Spectroscopy*. **64**, 750-759 (2010).

Chapter 2

Principles of LIBS, Bacterial Physiology, and Chemometric Analysis

2.1 Principles of LIBS

The overall processes that occur during nanosecond LIBS can be summarized in the following basic steps (which will be explained in much more detail below):

1. A short laser pulse is incident on a target material.
2. The incident energy is deposited in the sample and as a result it will vaporize a small amount of the sample. The incoming laser pulse will also interact with the vapor plume to create a high-temperature plasma.
3. An optic (lens or optical fiber) is used to collect light and a spectrometer dispersing element (typically a grating) is used to disperse the light. The light originates from the spontaneous emission of hot atoms and/or ions in the plasma.
4. The resulting atomic emission peaks are analyzed to determine the elemental constituents of the sample and their relative concentrations.

In the following sections I will discuss the previous four steps in detail to show all the physical processes that occur.

2.1.1 Energy Source

Many LIBS applications use an Nd:YAG (neodymium-doped yttrium aluminum garnet) pulsed laser with an infrared wavelength of 1064 nm. This laser is the most common type of solid-state laser and is widely used because it is reliable, easy to use, and because of its high peak pulse energies. In an Nd:YAG laser, neodymium ions doped into the amorphous YAG glass act

as the gain medium. Nd^{3+} energy levels create a 4-level laser system and its energy schematic is shown in Figure 2.1. The two main pump bands of Nd:YAG take place at wavelengths shorter than 900 nm, specifically at ~ 730 and 800 nm. These bands are coupled by a fast nonradiative transition (decay) to the ${}^4F_{3/2}$ energy level. At this point, the metastable (long life) ${}^4F_{3/2}$ level will be occupied and as a result a population inversion is achieved. After that, the laser emission is generated by the transition from ${}^4F_{3/2}$ to ${}^4I_{11/2}$ at $\lambda = 1064$ nm. Furthermore, the level ${}^4I_{11/2}$ is also coupled by a fast nonradiative decay to the ${}^4I_{9/2}$ ground state energy level.¹

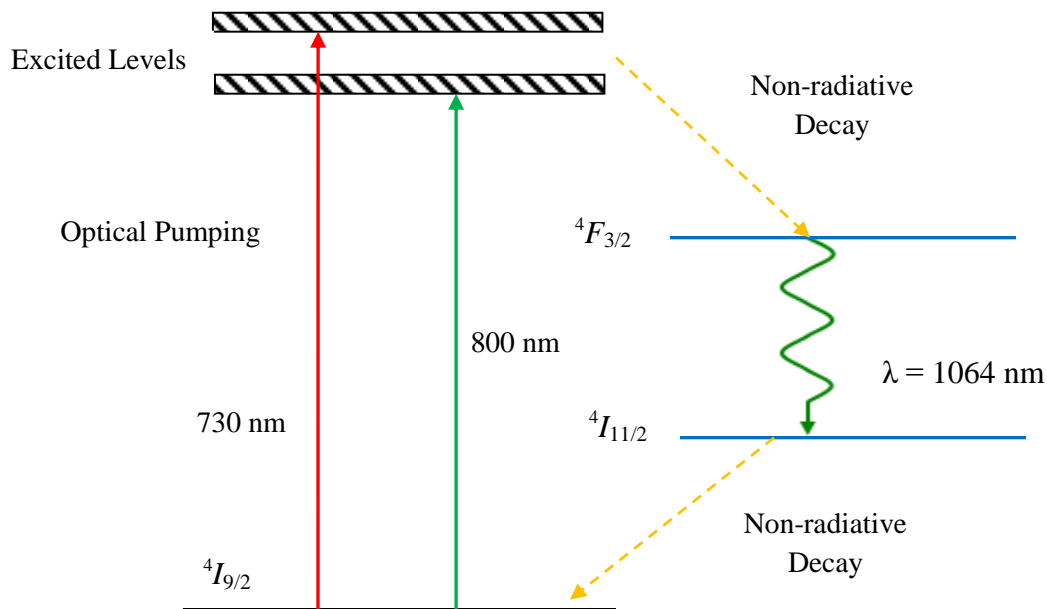


Figure 2.1: Schematic energy levels of an Nd:YAG laser.

Nd:YAG lasers are also usable at the second and third harmonic wavelengths of $\lambda = 532$ nm (visible emission) and 355 nm (ultraviolet emission), respectively.² Those harmonics can be generated by inserting a non-linear optical crystal into the path of the 1064 nm laser beam. Moreover, these lasers can be operated in continuous wave (cw) or Q-switched mode (pulse mode). In the case of cw lasers, the energy flows smoothly and constantly with time. Q-

switched mode can be achieved by inserting an electro-optical device (i.e. polarizer) inside the laser cavity, specifically between the active medium and the rear mirror, to control when stimulated emission occurs. In this mode, the output of the laser occurs in a series of very short (nanosecond domain) energy pulses that are compressed into concentrated packages. On the other hand, recent LIBS experiments have also been carried out with femtosecond lasers.^{3,4}

2.1.2 Spatial Intensity Distribution

The irradiance of a laser beam is defined as the power carried by the beam across a unit area perpendicular to the beam (W/m^2). In a typical LIBS experiment, the capability of delivering the laser energy to a specific location on the target material is of great importance. To do this, it is necessary to know the spot size to which the beam can be focused and the energy that the laser pulse contains (typically tens to hundreds of mJ per pulse).⁵

The ability to focus the laser spot is affected by the mode of the laser beam, which is determined by the laser optical cavity. The optical cavity of a laser is determined by the configuration of the two end mirrors. The stationary patterns of the electromagnetic waves formed in this cavity are called modes. Lasers have longitudinal and transverse modes. A transverse mode of a laser beam is the mode which describes the distribution in space of the radiation field in a plane perpendicular to the direction of the laser beam propagation within the optical cavity.⁶

The TEM_{00} (transverse electromagnetic) mode is the lowest order transverse mode, and it has a Gaussian radial profile. It has also the minimum divergence and can be focused to the smallest possible spot size. For these reasons, it is often the most preferable mode for experimental applications (i.e. LIBS). Higher order modes are larger in diameter and therefore

suffer higher diffraction losses and cannot be focused as effectively. Figure 2.2 depicts various transverse intensity patterns as they would appear in the output beam of a laser.⁷

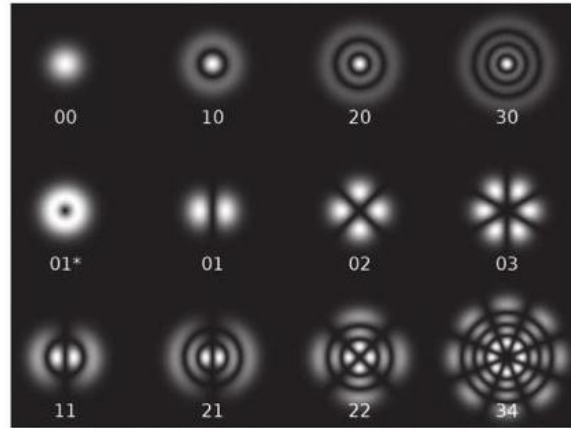


Figure 2.2: Cylindrical transverse mode patterns TEM_{nm} .

In our lab, our laser was designed to operate in a nearly TEM_{00} mode with a nearly-Gaussian profile. The quality of the mode improved with distance from the laser cavity, and “mode-cleaning” optics (described later) were used to improve the mode quality.

2.2 Fundamental Ablation Processes

The ablation events that can occur in a typical LIBS experiment will be divided into three main processes: primary laser-matter interaction (heating, evaporation, and bond breaking), plasma generation, and plasma expansion and cooling. In the following sections I will discuss those events in more detail.

2.2.1 Ablation and Plasma Creation

Initially a high-energy pulsed laser is typically focused to the smallest possible spot size, which depends on the beam’s quality as discussed earlier, onto the sample surface (i.e. bacteria). In our LIBS apparatus, the pulse duration is on the order of nano-seconds (termed ns-LIBS),

typically a 10 ns duration. Several LIBS experiments have been performed with either pico-second or femto-second pulsed lasers.^{8,9,10} The absorbed energy from the laser pulse is converted into heat resulting in the vaporization of a small amount of the sample (called ablation) and creating a high-pressure vapor plume above the sample's surface. The ablated mass is from hundreds of nano-grams to a few micro-grams. The maximum amount of ablated mass (M) that can be evaporated by a laser pulse can be calculated from the following equation,

$$M = \frac{E(1-R)}{C_p(T_b - T_0) + L_v} \quad (2.1)$$

where R is the surface reflectivity, C_p is the specific heat, T_b the boiling point (K), T_0 room temperature (K), E is the energy of the laser pulse, and L_v the latent heat of vaporization.³

The time scale for this process is shorter than the pulse duration in ns-LIBS. Therefore, the laser pulse will continue to illuminate the produced vapor plume which leads to further absorption within the vapor plume and the eventual formation of an ionized plasma. This plasma will shield the sample from further illumination and ablation, which will determine the ablated mass. The main process leading to plasma shielding is absorption of the laser energy by the electrons (inverse bremsstrahlung) and multiphoton ionization as will be discussed in the following section. As a result of the decoupling of the laser from the sample, there will be strong heating, ionization and plasma formation in this plume. This can be explained by the fact that absorption of the laser radiation occurs to a significant degree in the shielding process, which is maximized when the plasma frequency equals the laser frequency. This will result in a higher plasma temperature which can increase the degree of ionization and dissociate any tiny particle that has been ablated. This process is illustrated in Figure 2.3.^{3,5,6}

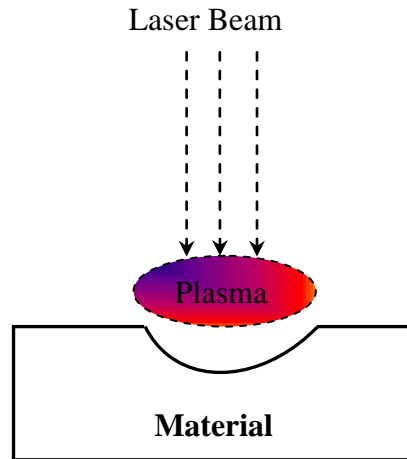
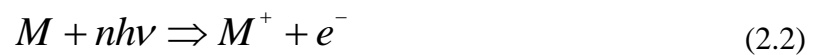


Figure 2.3: Illustration of plasma shielding effect.

2.2.2 Plasma Breakdown

There are two principal steps leading to the plasma breakdown event in the vapor plume. First of all, some free electrons must be present in the focal volume of the laser beam. This could be due to natural local radioactivity (e.g. cosmic rays).⁶ Secondly, an electron avalanche or electron cascade ionization occurs within the vapor in the focal region of the laser. A typical LIBS irradiance is on the order of $10^8 - 10^{10} \frac{W}{cm^2}$.³ At this range of irradiance, electron and ion densities are achieved via cascade ionization rather than the multiphoton production of electrons produced according to the following equation:



where n is the number of photons and M is the atom of interest.

In this process an atom can be ionized by the absorption of n photons from the laser field.¹¹ It was first observed by Voronov and Delone when they used a ruby laser to ionize xenon via the absorption of seven photons.¹² This happens when the intensity of radiation is

high enough and the photon energy is less than the atomic ionization energy (work function). From quantum mechanics there will be a probability that the atom will absorb several photons “simultaneously” and excite a bound-free transition. Consequently a free electron will be released. This process can be shown in Figure 2.4.

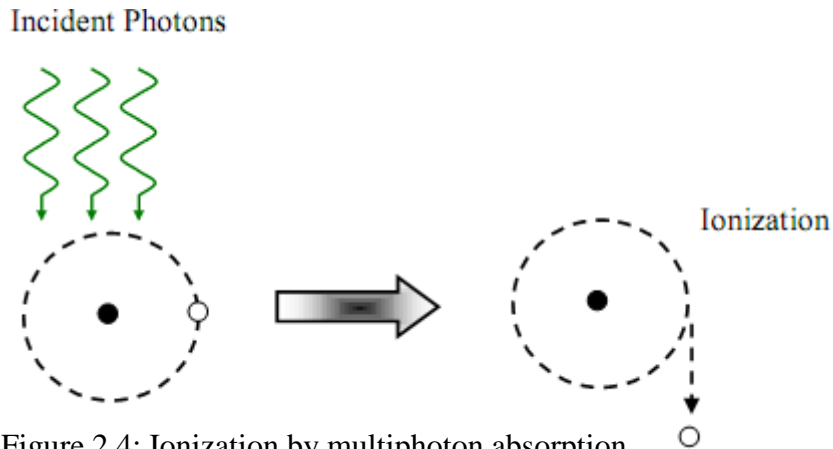


Figure 2.4: Ionization by multiphoton absorption.

As stated earlier, rather than multiphoton absorption, most of the electron generation occurs via an electron cascade. Classically, once free electrons are generated, they can be accelerated by the electric field in the optical pulse during the time period between collisions with neutral species via the inverse Bremsstrahlung process. As a result, the electrons will be thermalized quickly and they will gain sufficient energy in order to collisionally ionize an atom or molecule according to the following equation:



According to the above equation, more free electrons will be produced which will gain energy from the field again, which leads to more ionization during the laser pulse and an increase of the overall electron density. This is the process known as an “electron cascade” or an “electron avalanche.”^{3,6}

Eventually, enough free electrons and ions are generated to consider the vapor a plasma. Plasmas consist of atoms, ions and free electrons. Generally they contain equal numbers of positive and negative charges (in the form of ions and free electrons) making them electrically neutral. LIBS plasmas can be considered weakly ionized plasmas, in which the ratio of the electrons to other species is less than 10%. Figure 2.5 compares the LIBS plasma to other different plasmas plotted against electron density and temperature as all of these plasmas are a function of these two key parameters.¹³

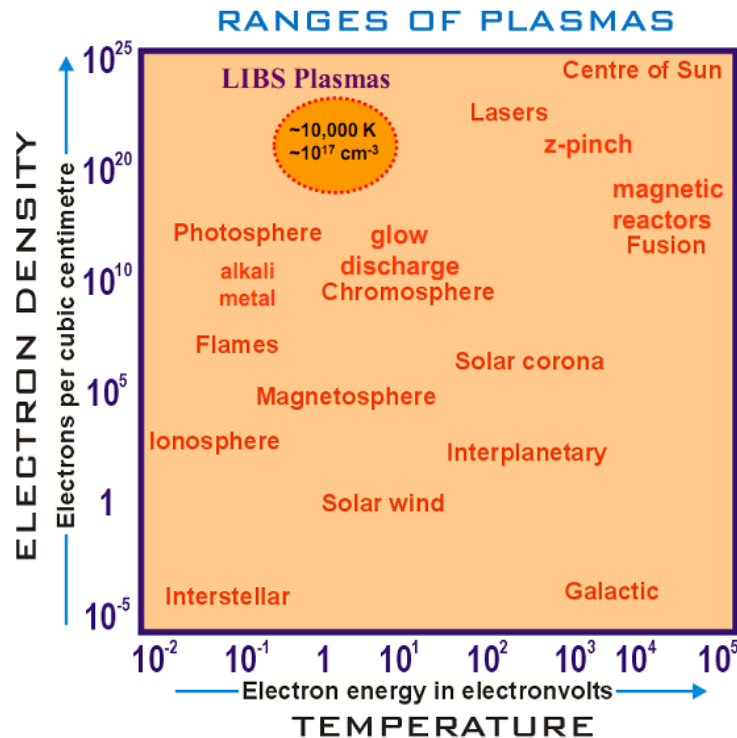


Figure 2.5: Examples of plasmas as a function of temperature and electron density.

After the exponential increase in the production of free electrons and ions by inverse bremsstrahlung in the electron avalanche process, the plasma will expand outward from the initial focal volume at a supersonic speed (a speed that is over the speed of sound) into the ambient gas. The produced high pressure plasma will compress the surrounding gas and as a

result a shock wave will be produced. In addition to that, a loud noise will be heard. The plasma can then evolve according to three different wave models depending on the incident irradiation intensity. These waves are (1) laser-supported combustion (LSC) waves, (2) laser-supported detonation (LSD) waves, and (3) laser-supported radiation (LSR) waves. LSC and LSD are the models that most closely represent typical LIBS experiments. In those models, the plasma and the surrounding atmosphere are transmissive enough to allow the incident laser energy to penetrate.

As we said before, the plasma will eventually become opaque when the plasma frequency equals the laser frequency. The previous condition can be achieved at a critical electron density

$$n_c \sim (10^{21} / \lambda^2) / \text{cm}^3 \quad (2.4)$$

where λ is the laser wavelength in microns.

For example, at 1064 nm $n_c \sim 10^{21} / \text{cm}^3$. After that, both the electron density and the plasma frequency will continue to increase and at some point the plasma frequency will be greater than laser frequency. In this case, the laser radiation will be reflected by the plasma and this signals the end of the plasma formation event and will lead to the plasma cooling.⁵ At some later time after significant expansion and cooling has occurred, light is collected from the plasma for LIBS analysis. In conclusion, all the main LIBS processes can be summarized in Figure 2.6 (next page).^{2,6,14}

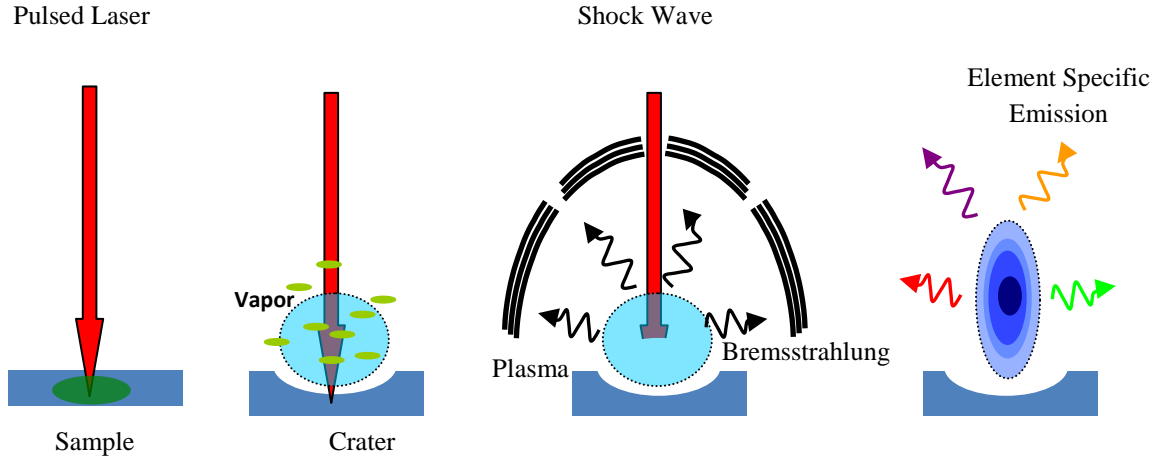
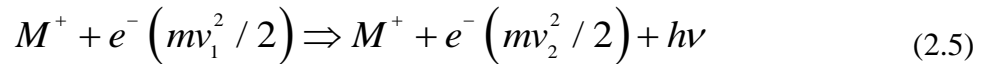


Figure 2.6: All the main LIBS processes.

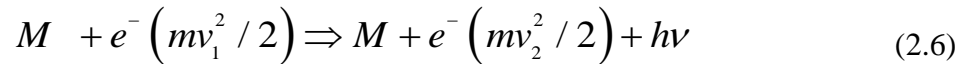
2.2.3 Spectral Emission from Plasma

The spectral composition of the plasma emission comes from two sources: characteristic line radiation from elemental emission as well as a broadband non-specific component (continuum emission). The continuum emission (radiation) is emitted by the plasma as a result of free-free and free-bound transitions. Free-free transitions occur when we have accelerated or decelerated electrons due to their interactions with the coulomb field of charged ions and neutral atoms. According to the classical theory of electricity and magnetism, they will radiate energy.³

The free-free transition in the field of an ion can be seen in the following reaction:



While the free-free transition in the field of an atom is given by the following reaction:

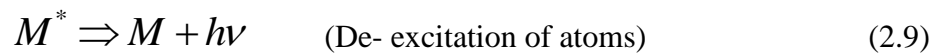


In the free-bound process (recombination radiation), a free electron is captured into an ionic (atomic) energy level and as a result the electron will give up its excess kinetic energy in the form of continuum radiation according to the following reaction:



The energy of the photon is equal to the difference between original energy of the electron and its new energy in whatever level of whatever atom it ends up in. Since this difference can have any value, the result of many free-bound transitions is a continuous spectrum.

Bound-bound transitions are responsible for the characteristic elemental radiation. When an atom or ion is found in the excited state, it will undergo a transition to a lower state through either spontaneous or stimulated emission. The energy of the emitted photon depends on the energy difference between the energy levels.⁶



All the above mentioned transitions can be shown in the Figure 2.7.

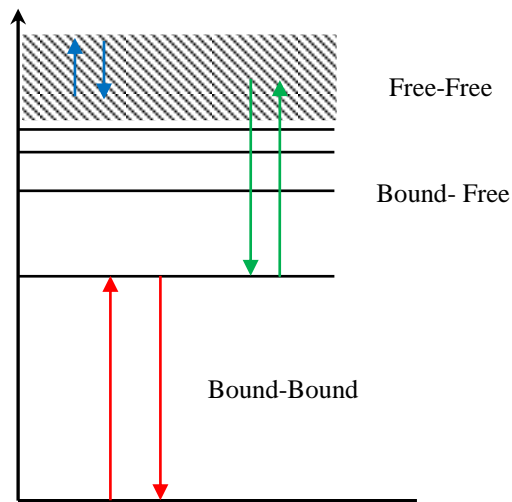


Figure 2.7: Energy levels and electron transitions.

2.2.4 Temperature and Spectral Lines Intensities

The determination of the elemental compositions of a sample using LIBS requires the measurement of the intensities of the characteristic spectral lines that are associated with the individual species that exist in the sample. The observed intensity of a spectral line from a plasma depends on two factors. The first factor can be related to the oscillator strength value. In quantum mechanics, the oscillator strength is used as a measure of the relative strength of the electronic transitions within atomic and molecular systems. The oscillator strength is a dimensionless number that describes the relative intensity of an optical transition whether it is absorption or emission. The second factor depends on the conditions of excitation, and specifically on the density of emitters within the plasma. For example, a plasma is “optically thin” when the radiation emitted from an atom travels through and escapes from the plasma without significant absorption or scattering by other atoms. In this case, not only more intense lines will be detected but better quantitative LIBS results will be achieved too.^{2,3,6}

The intensity of a spectral line for any atomic transition observed in the plasma is determined by the temperature of the plasma. The relative intensities of any two lines from a given atomic species can be related to each other and to the temperature by the Boltzmann and Saha equations. The Boltzmann equation can be used for lines originating from two transitions with two different upper state energies in one species, and is given by

$$\frac{I_1}{I_2} = \frac{g_1 A_1 \lambda_2}{g_2 A_2 \lambda_1} \exp \left[-\frac{E_2 - E_1}{K_B T} \right] \quad (2.10)$$

where A_1 and A_2 are the transition probabilities for the two transitions with wavelengths λ_1 and λ_2 , g_1 and g_2 are the statistical weights of the upper levels of the two transitions, E_1 and E_2 are the

energies of the upper states, and T is the plasma temperature at the time of observation. Frequently, this equation is used to calculate the plasma temperature by measuring the relative intensity of two or more easily observed lines.

Using the Boltzmann equation to generate a Boltzmann plot is another method used to find the plasma temperature. The intensity of a spectral line corresponding to the transition between the levels E_k and E_i of an atomic species s can be given by:

$$I = N_s g_k A_{ki} \frac{e^{-E_k/K_B T}}{U_s(T)} \quad (2.11)$$

where N_s is the number density (particle/cm³) for the corresponding species, A_{ki} is the transition probability, g_k is the degeneracy of the level k , and $U_s(T)$ is the partition function for the emitting species at the plasma temperature. In this method, we can rearrange this equation to define some scaled intensities ($I / g_k A_{ki}$) and we can then take the natural logarithm of both sides (equation 2.12).

$$\ln\left(\frac{I}{g_k A_{ki}}\right) = \frac{-E_k}{K_B T} + C \quad (2.12)$$

This is the equation of a straight line ($y = mx + b$). If we plot the rescaled intensities of many lines versus the upper state energy (E_k) and fit it to a straight line, the slope of the line will be $(-1/K_B T)$ and from this we can find the temperature.¹⁵ At no time do we need to know the other constants in the Boltzmann equation.

The Saha (Saha-Boltzmann) equation applies when one observed line is from a neutral atom and one from an ion (of the same species) and is given by

$$\frac{I_{\text{ion}}}{I_{\text{atom}}} = 2 \times \frac{(2\pi m_e kT)^{3/2}}{N_e h^3} \left(\frac{gA}{\lambda} \right)_{\text{ion}} \left(\frac{gA}{\lambda} \right)_{\text{atom}} \times \exp \left[-\frac{(V^+ + E_{\text{ion}} - E_{\text{atom}})}{K_B T} \right] \quad (2.13)$$

where I is the integrated emission intensity of the ion or atom, N_e is the electron density (cm^{-3}), gA is the product of the statistical weight and Einstein coefficient for spontaneous emission of the upper level (s^{-1}), λ is the wavelength (nm), V^+ is the ionization potential of the atom (J), E_{ion} is the excitation energy (upper level) of the ionic line (J), E_{atom} is the excitation energy (upper level) of the atomic line (J), K_B is the Boltzmann constant (J/K), h is Planck's constant (J s), and T is the plasma temperature.¹⁶

The previous equations were written assuming that the plasma is at thermodynamic equilibrium, $T_{\text{ion}} = T_{\text{electron}} = T$. The criterion for thermal equilibrium is that all processes in the plasma are collision-dominated which is unfortunately rarely achieved in such a complex dynamic plasma. However, the plasma is often described using a single temperature parameter. Moreover, to find the plasma temperature the electron density N_e (which is also a time-varying quantity) must first be known. The electron density can be extracted from the spectral line widths of hydrogen atoms and H-like ions that exhibit line broadening due to the linear Stark effect. For the linear Stark effect, the electron density and the line width are related by the following relation:

$$N_e = C(N_e, T) \Delta \lambda_{FWHM}^{3/2} \quad (2.14)$$

where $\Delta\lambda$ is the full width at half maximum (FWHM) and the parameter C is a constant used to calculate N_e which is tabulated in reference 17.¹⁷

2.3 Bacteria Physiology

Bacteria are very small microorganisms, typically on the order of a few micrometers ($10^{-6} m$) or less in length, which can be found everywhere. However, bacteria have different shapes such as rods, spheres and spirals as well as different sizes. The rod shape is called bacillus, while the spherical one is called coccus. Although some bacteria cause serious infectious diseases, some are important for non-harmful processes like making cheese, butter and yogurt.¹⁸

Bacteria are prokaryotes. Prokaryotes are single-celled organisms that usually lack a cell nucleus. In this case all the chromosomes are in contact with the cytoplasm and their structure is relatively simple as shown in a simple schematic in Figure 2.8. On the other hand, eukaryotes, including ourselves, plants, and animals, are multicellular organisms that have a membrane-bound nucleus. The cell wall of a bacterium plays an important role for identification and discrimination between them. Bacteria can be divided in two major groups, called Gram-positive and Gram-negative.

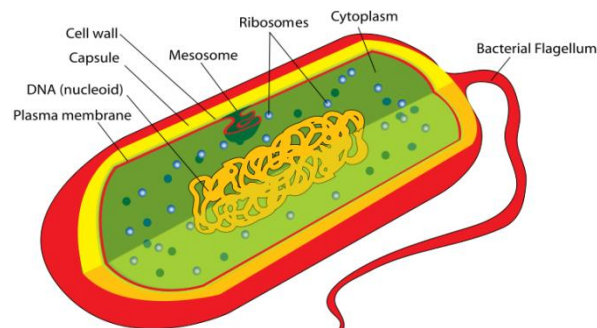










Figure 2.8: The cellular structure of a typical bacterial cell.¹⁹

Table 2.1: The Gram-staining process of bacterial identification.

Step	Microscopic Appearance of Cell	
	Gram -Positive	Gram-Negative
1. Crystal Violet		
2. Gram's Iodine		
3. Alcohol		
4. Safranin (Red Dye)		

Basically, this classification is based on a special staining procedure called the Gram stain. The Gram stain is one of the most important tools used for the identification of unknown bacteria, even today. This technique was developed in 1884 by Hans Christian Gram. This stain depends on the structure of the bacterial cell wall. The procedure requires four solutions: a basic dye (crystal violet), a mordant (Gram's iodine), a decolorizing agent (alcohol), and a counter stain (safranin; red dye). Table 2.1 explains the procedure of Gram staining in brief.^{20,21}

Firstly, bacterial cells, Gram-positive and Gram-negative, are transferred to glass slides. The purple dye (crystal violet) is then added to the cells. As a result, both Gram-positive and Gram-negative cells will retain the same purple color. Secondly, the cells are dipped into an iodine solution. Gram's iodine will penetrate the peptidoglycan layer of the cell. Because the peptidoglycan layer in Gram-positive cells is thicker than in Gram-negative cells, the entrapment of the dye is far more extensive in them than in Gram-negative cells. This allows the stain to be retained better by forming an insoluble crystal violet-iodine complex. Both Gram-positive and

Gram-negative bacteria remain purple after this step. In the third step, when alcohol (the decolorizing agent) is applied, it will dissolve the lipids in the outer membrane of the Gram-negative bacteria causing the dye to leave the cells. Therefore, Gram-negative cells appear colorless. On the other hand, the thick peptidoglycan layer in the Gram-positive bacteria will prevent the dye from leaving the cells. Consequently, the Gram-positive cells appear purple. Finally, the counter stain safranin is applied. Safranin will not disrupt the purple coloration in Gram-positive cells because it is lighter than the crystal violet. Thus, Gram-positive appear purple, and Gram-negative appear pink. For example, *Staphylococcus aureus* and *Streptococcus mutans* are Gram-positive bacteria while *Pseudomonas aeruginosa* is a Gram-negative bacterium.

2.3.1 Cell Wall Structure of the Gram-Negative Bacteria

The Gram-negative cell is 20-30 nm thick. The inner layer nearest to the cytoplasmic membrane is called peptidoglycan. This layer is rigid and it is responsible for the strength of the cell wall. The thickness of this layer is 15 nm which represents 1-10% of the dry weight of the cell.²⁰ The outer membrane is responsible for acting as the bacteria protective barrier. It is composed of phospholipids which represents the innermost layer of the outer membrane while lipopolysaccharide (LPS), which mainly contains polysaccharide and protein represents the outermost layer of outer membrane as shown in Figure 2.9 (next page).

There are three distinct components that can be identified in LPS: lipid A, the core polysaccharide, and O-specific polysaccharide. Lipid A is the innermost layer of LPS and consists of digluosamine sugar with attached acyl chains as well as phosphate groups.^{22,23,24} This layer is toxic to humans, causing septic shock. During this shock, the body tissues and organs do not get enough blood and oxygen. The core polysaccharide represents the middle layer in the

LPS. It consists of seven-carbon sugars called ketodeoxyoctonate (KDO) as well as phosphates and possesses an overall electronegative charge. Finally, the outermost layer of LPS is related to the O-specific polysaccharide which consists mainly of six-carbon sugars.²⁰

In addition to LPS, the outer membrane of the cell wall contains various proteins such as lipoprotein and porin. Porin is found in the outer membrane for both Gram-negative and Gram-positive bacteria. It allows hydrophilic low-molecular-weight substances to pass through it by diffusion. Lipoprotein plays a role as an anchor between the outer membrane and peptidoglycan.²⁰

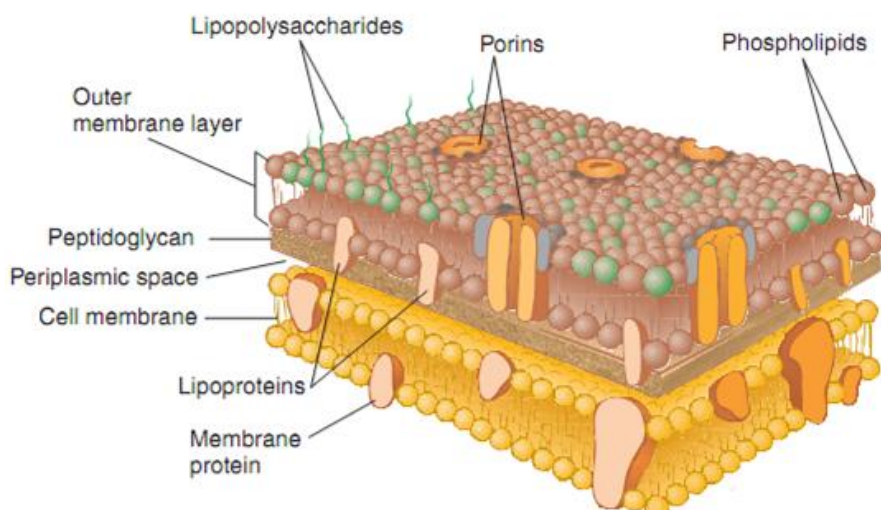


Figure 2.9: The schematic drawing of the outer membrane of the Gram-negative bacterium.

The components of the outer membrane have complicated molecular compositions, as shown. So one can ask how atomic spectroscopy such as LIBS gives any information about the function of such organisms? The answer for this question is based on the presence of inorganic elements such as Mg, P, Ca, and Na in the bacterial body, and perhaps specifically in the LPS

layer. More specifically, Ca^{2+} and Mg^{2+} play a crucial role in stabilizing the outer membrane by binding the adjacent LPS molecules.²⁵

It is believed that divalent cations such as Ca^{2+} and Mg^{2+} are important for stabilizing the outer membrane structure by forming metal ion bridges between the phosphate groups of phospholipids or LPS and the membrane proteins.²⁶ On the other hand, different studies suggest that these divalent cations play a significant role in neutralizing the electronegative charge of the KDO inner core region.^{27,28}

2.3.2 Cell Wall Structure of the Gram-Positive Bacteria

The Gram-positive cell wall is relatively thick (about 30-100 nm) in thickness. It is made of a tough, complex polymer, sheath of peptidoglycan (about 40-80% of the cell wall) in

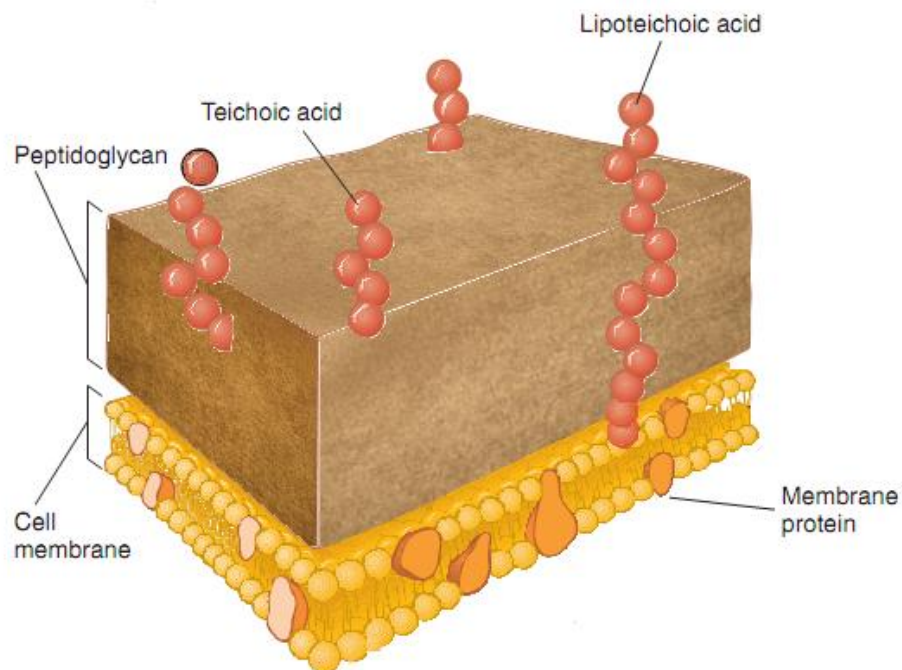


Figure 2.10: The schematic drawing of the Gram-positive bacterium.²¹

addition to teichoic and lipoteichoic acids as shown in Figure 2.10. Teichoic acid is a polymer of ribitol or glycerol and phosphate embedded in the peptidoglycan layer. It is also negatively charged and therefore contributes partially to the negative charge of the cell wall surface and functions to effect passage of divalent cations (positively charged) through the cell wall. On the other hand, lipoteichoic acid is similar in structure but is attached to the lipids in the plasma membrane.¹⁸

2.4 Selection of Bacterial Species for LIBS Study

This section summarizes all the bacterial samples that will be discussed in our study. These samples were chosen for several specific reasons, not only to prove that LIBS can be used for the detection and discrimination between different bio-samples (proof-of-concept) based on their elemental compositions, but also to show that LIBS may be broadly applicable to a wide class of either pathogenic or non-pathogenic bacteria.

The bacterium *Escherichia coli* is a Gram-negative rod with a wide variety of strains, some pathogenic some non-pathogenic. It is well known that *E. coli* is an important indicator of water contamination which may increase the risk of disease for people living in coastal areas.²⁹ *E. coli* was the first bacterium that I used initially in my project. Specifically, the strains (a strain is a subset of a bacterial species differing from other bacteria of the same species by some minor but identifiable difference) of *E. coli* I used were: *E. coli* K-12, *E. coli* C, *E. coli* HF4714, *E. coli* ATCC 25922, and *E. coli* O157:H7. As an example, *E. coli* O157:H7 is a highly pathogenic strain that produces toxin resulting in bloody diarrhea which may lead to the fatal hemolytic-uremic syndrome, whereas *E. coli* K-12 is a completely non-pathogenic strain whose genome is completely known.³⁰ All the *E. coli* strains I tested were grown in a normal bacteriological rich

broth or solid agar media in air in a 37 °C incubator or water bath with shaking. These strains are non-pathogenic and genetically well characterized. Since it is not difficult to test their genetic purity, we used them as a reference strain to begin LIBS studies.

Staphylococci are Gram-positive cocci (spherical shape) occurring in clusters and normally are not pathogenic. However, some of them are pathogens and some strains may be extremely virulent (*Staphylococci* are among the most frequent causal organisms in human bacterial infections). In our project we will study *S. aureus*, *S. epidermidis*, and *S. saprophyticus*, the three main species of staphylococci. For example, *S. aureus* can cause skin and soft tissue infections and bloodstream infections while *S. saprophyticus* is the second most common cause of urinary tract infections.³¹

Streptococcus is another genus of spherical Gram-positive bacteria, familiarly known as strep, which causes a multitude of diseases. The most important of these bacteria is a group of bacteria called *Streptococcus viridans* (which contains a variety of species, like *S. mutans*, *S. salivarius*, *S. sanguis*, and *S. mitis*). For example, *S. mutans* is responsible for tooth decay because when these bacteria encounter dietary sugars, they have the ability to convert the sugars into acids (like lactic acid).³² Consequently, the acid will lower the pH in that region, and the enamel starts to dissolve and as a result a tooth cavity may occur. In our study, LIBS spectra for both *S. mutans* and *S. viridans* will be collected for the construction of our LIBS-based bacterial library.

Finally two different mutants of *Mycobacterium smegmatis* (*M. smegmatis*) bacteria will be also tested in our study. *Mycobacterium smegmatis* is a Gram-positive bacterium with a rod shape. It is also a non-pathogenic bacterium that is widely used for the research analysis of other species in the genus *Mycobacteria* (i.e. *Mycobacterium tuberculosis*) in cell culture laboratories.

This organism was chosen because it is easy to culture and reproduces rapidly. It is also non-pathogenic to humans and other animals.³³

2.5 Discriminant Function Analysis (DFA)

2.5.1 Definition

DFA is a statistical technique (a chemometric technique) used for classifying a set of observations into mutually exclusive groups on the basis of a set of independent variables (predictors).³⁴ It will be used in this dissertation to classify an unknown bacterial target on the basis of its LIBS emission spectrum alone.

2.5.2 How Discriminant Analysis Works

The technique constructs a set of linear functions of the predictors that will discriminate between the groups in such a way that the misclassification error rates are minimized. It can be achieved by maximizing the ratio of the “between-group variance” to the “within-group variance.”

2.5.3 The approach

Consider a set of p variables X_1, X_2, \dots, X_p , from a set of n objects belonging to m known groups G_1, G_2, \dots, G_m . In this dissertation we will attempt to classify bacteria on the basis of their LIBS spectra (a typical bacterial spectrum will be discussed in Chapter 3). The intensity of observed emission lines in any given LIBS spectrum will be the set of predictor variables p for that spectrum. The number of spectra acquired from a specific type of bacterium is the set of n objects (typically 20-50 spectra could be acquired in a given experiment). While m will represent the number of different types (groups) of bacteria that I am trying to uniquely classify.

We denote by T the matrix of the total mean correlated sums-of-squares of cross-products (SSCP) for all observations, while W represents the within-groups sums-of-squares matrix. The matrix elements of T can be calculated from the following equation:

$$T_{rc} = \sum_{j=1}^m \sum_{i=1}^{n_j} (X_{ijr} - \bar{X}_r)(X_{ijc} - \bar{X}_c) \quad (2.15)$$

The matrix elements of W can be found from:

$$W_{rc} = \sum_{j=1}^m \sum_{i=1}^{n_j} (X_{ijr} - \bar{X}_{jr})(X_{ijc} - \bar{X}_{jc}) \quad (2.16)$$

Thus, the matrix of between-groups sums-of-squares can be found by the difference

$$B = T - W \quad (2.17)$$

2.5.4 The Linear Discriminant Model

For a set of p variables X_1, X_2, \dots, X_p , the dimensionality of this set can be reduced to i discriminant function scores Z_i . The general model is

$$Z_i = \sum_{j=1}^p b_{ij} X_j \quad (2.18)$$

where the X_j 's are the original variables and the b_{ij} 's are the discriminant function coefficients.

With respect to the linear composite $Z = \hat{b}' X$, the between-groups sums-of-squares are given by

$Z = \hat{b}' B \hat{b}$. Similarly, the within-groups sums-of-squares are $Z = \hat{b}' W \hat{b}$. Then we can define λ

as follows:

$$\hat{\lambda} = \frac{\hat{b}' B \hat{b}}{\hat{b}' W \hat{b}} \quad (2.19)$$

We wish to maximize λ with respect to b which will maximize the between-group variance, while minimizing the within-group variance. After some simplification we have

$$(B - \lambda W) \hat{b} = 0 \quad (2.20)$$

According to the previous equation, $\hat{\lambda}$ is called the eigenvalue and \hat{b} is the corresponding eigenvector. The number of eigenvalues gives an indication about the number of discriminant functions needed for discrimination. Moreover, the actual values for each eigenvalue can determine which discriminant axes capture the major sources of variation separating the groups.

In conclusion, the DFA will take the entire spectrum and reduces it to a data point (reduction of the dimension of the data) characterized by coordinates called discriminant function scores. These scores reflect specific, statistically significant, and quantifiable differences in atomic emission intensities which are related to differences in the elemental composition of the bacterial targets. In this way, all the information in a LIBS spectrum will be reduced to a few scalar discriminant function scores, which will be critical for rapid and autonomous classification of the LIBS spectra.

REFERENCES

-
- ¹ O. Svelto, *Principles of Lasers*, 5th Edition, (Springer) 2009.
- ² A.W. Miziolek, V. Palleschi, and I. Schechter, *Laser Induced Breakdown Spectroscopy*, 1st edition, (Cambridge University Press, Cambridge) 2006.
- ³ D. Cremers and L. Radziemski, *Handbook of Laser-Induced Breakdown Spectroscopy*, (John Wiley & Sons Ltd.) 2006.
- ⁴ S.L. Chin, *Femtosecond Laser Filamentation*, (Springer Series on Atomic, Optical, and Plasma Physics) 2009.
- ⁵ C. Pasquini, J. Cortez, L. Silva and F. Gonzaga, “Laser induced breakdown spectroscopy,” *Journal of the Brazilian Chemical Society* **18**, 463-512 (2007).
- ⁶ J.P. Singh and S.N. Thakur, Eds., *Laser-Induced Breakdown Spectroscopy*, (Elsevier, Amsterdam) 2007.
- ⁷ C. Raulin and S. Karsai, *Laser and IPL Technology in Dermatology and Aesthetic Medicine*, (Springer) 2011.
- ⁸ M. Baudalet, L. Guyon, J. Yu, J. P. Wolf, T. Amodeo, E. Frejafon, and P. Laloi, “Spectral signature of native CN bonds for bacterium detection and identification using femtosecond laser-induced breakdown spectroscopy,” *Applied Physics Letters* **88**, 06391 1-3 (2006).
- ⁹ M. Baudalet, J. Yu, M. Bossu, J. Jovelet, J. Wolf, T. Amodeo, E. Fréjafon, and P. Laloi, “Discrimination of microbiological samples using femtosecond laser-induced breakdown spectroscopy,” *Applied Physics Letters* **89**, 163903 (2006).

-
- ¹⁰ M. Baudelet, L. Guyon, J. Yu, J.-P. Wolf, T. Amodeo, E. Frejafon, and P. Laloi, “Femtosecond time-resolved laser-induced breakdown spectroscopy for detection and identification of bacteria: A comparison to the nanosecond regime,” *Journal of Applied Physics* **99**, 084701 1-9 (2006).
- ¹¹ C.J. Joachain, A.N. Chester, S. Martellucci, and D. Batani, *Atoms, Solids, and Plasmas in Super-Intense Laser*, 1st Edition (Springer) 2001.
- ¹² G.S. Voronov and N.B. Delone, “Many-photon ionization of the xenon atom by ruby laser radiation,” *Soviet Physics JETP* **23**, 54 (1966).
- ¹³ A.L. Peratt, “Advances in numerical modeling of astrophysical and space plasmas,” *Astrophysics and Space Science* **242**, 93-163 (1996).
- ¹⁴ N.B. Dahotre and S. Harimkar, *Laser Fabrication and Machining of Materials*, 1st Edition, (Springer) 2007.
- ¹⁵ I. Borgia, L. M.F. Burgio, M. Corsi, R. Fantoni, V. Palleschi, A. Salvetti, M. C. Squarzialupi, and E. Tognoni, “Self-calibrated quantitative elemental analysis by laser-induced plasma spectroscopy: application to pigment analysis,” *Journal of Cultural Heritage* **1**, S281-S286 (2000).
- ¹⁶ O. Samek, D.C.S. Beddows, S.V. Kukhlevsky, M. Liska, H.H. Telle, and J. Young, “Application of laser-induced breakdown spectroscopy to in situ analysis of liquid samples,” *Optical Engineering* **39**, 2248-2262 (2000).
- ¹⁷ H.R. Griem, *Plasma Spectroscopy*, (McGraw-Hill, New York) 1964.
- ¹⁸ P. Singleton, *Bacteria in Biology, Biotechnology and Medicine*, (John Wiley & Sons, Ltd.) 1999.

¹⁹ www.answers.com/topic/bacteria.

²⁰ M. Madigan, J. Martinko and J. Parker, *Brock Biology of Microorganisms*, 9th Edition, (Prentice Hall College Div) 1996.

²¹ K. Talaro, *Foundations in Microbiology*, 6th edition, (McGraw-Hill Science/Engineering/Math) 2006.

²² R. Lins and T. Straatsma, “Computer Simulation of the Rough Lipopolysaccharide Membrane of *Pseudomonas aeruginosa*,” *Biophysical Journal* **81**, 1037-1046 (2001).

²³ C. Lee, Y. Kim, H. Joo and B. Kim, “Structural analysis of lipid A from *Escherichia coli* O157:H7:K using thin-layer chromatography and ion-trap mass spectrometry,” *Journal of Mass Spectrometry* **39**, 514–525 (2004).

²⁴ D. Drewry, J. Lomax, G. Gray and S. Wilkinson, “Studies of lipid A fractions from the lipopolysaccharides of *Pseudomonas aeruginosa* and *Pseudomonas alcaligenes*,” *Biochemical Journal* **133**, 563-572 (1973).

²⁵ M. Asbell and R. Eagon, “Role of multivalent cations in the organization structure, and assembly of the cell wall of *Pseudomonas aeruginosa*,” *Journal of Bacteriology* **92**, 380–387 (1966).

²⁶ H. Ibrahim, S. Higashiguck, Y. Sugimot and T. Aoki, “Role of divalent cations in the novel bactericidal activity of the partially unfolded lysozyme,” *Journal of Agricultural and Food Chemistry* **45**, 89-94 (1997).

²⁷ H. Nikaido and M. Vaara, “Molecular basis of bacterial outer membrane permeability,” *Microbiological Reviews* **49**, 1-32 (1985).

-
- ²⁸ R. Lins and T. Straatsma, “Computer simulation of the rough lipopolysaccharide membrane of *Pseudomonas aeruginosa*,” *Biophysical Journal* **81**, 1037-1046 (2001).
- ²⁹ L. Nollet, *Handbook of Water Analysis*, 2nd Edition, (CRC Press) 2007.
- ³⁰ F.R. Blattner, G. Plunkett III, C.A. Bloch, N.T. Perna, V. Burland, M. Riley, J. Collado-Vides, J.D. Glasner, C.K. Rode, G.F. Mayhew, J. Gregor, N.W. Davis, H.A. Kirkpatrick, M.A. Goeden, D.J. Rose, B. Mau, and Y. Shao, “The complete genome sequence of *Escherichia coli* K-12,” *Science* **277**, 1453-1462 (1997).
- ³¹ K.B. Crossley, K.K. Jefferson, G.L. Archer, and V.G. Fowler, *Staphylococci in Human Disease*, 2nd Edition, (Wiley-Blackwell) 2009.
- ³² R. Ireland, *Clinical Textbook of Dental Hygiene and Therapy*, 1st Edition, (Wiley-Blackwell), 2006.
- ³³ G.F. Hatfull and W.R. Jacobs, *Molecular Genetics Mycobacteria*, (ASM Press) 2000.
- ³⁴ J.F. Hair, W.C. Black, B.J. Babin, and R.E. Anderson, *Multivariate Data Analysis*, 7th Edition, (Prentice Hall) 2009.

CHAPTER 3

Instrumentation and Standard Methods

3.1 Laser System

A huge number of LIBS experimental set-ups have been used which differ from each other according to the collection optics used to collect the emitted radiation coming from the plasma plume. A typical LIBS set-up is shown in Figure 3.1 which consists of:

1. A pulsed laser source which is used to generate the plasma plume.
2. A collection of mirrors and lens in order to direct and focus the laser beam on the target material.
3. An optical fiber cable which is used to collect the light and send it to the spectrometer.
4. A computer to control both the laser and the detector as well as save the resultant spectrum.

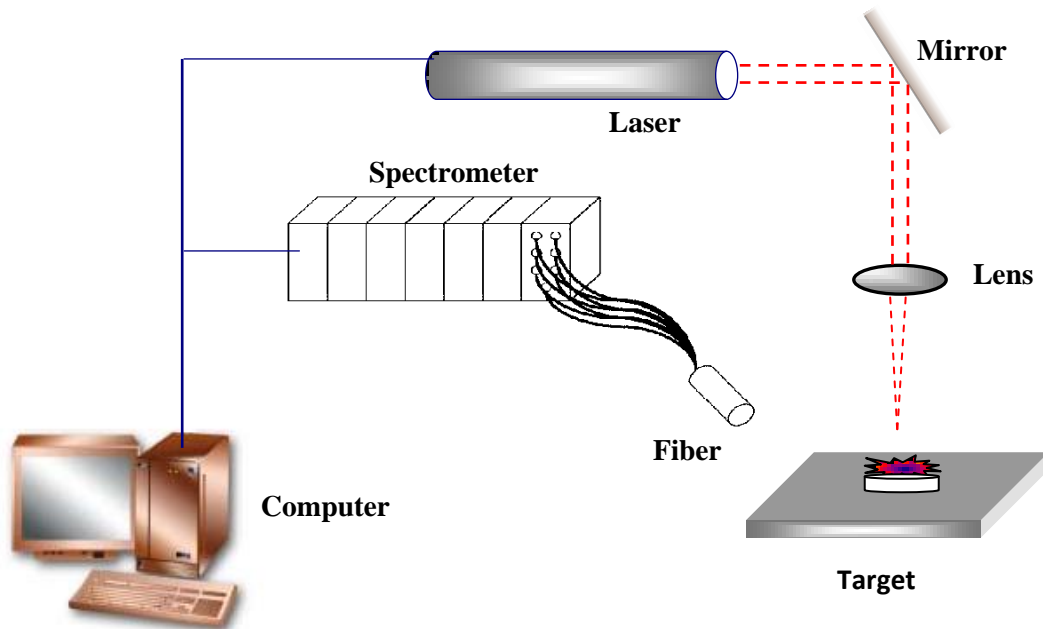


Figure 3.1: Diagram of a typical LIBS set-up.

In our lab we use 10 ns laser pulses from an Nd:YAG laser (Spectra Physics LAB-150-10) as is used for the majority of LIBS experiments. This laser operates at its fundamental wavelength of 1064 nm. This laser is shown in Figure 3.2.



Figure 3.2: High-Power Nanosecond Laser System (Spectra-Physics Lab-150-10).

3. 1.1 Laser Delivery Optics

The output pulse energy of our Nd:YAG laser is 650 mJ/pulse. For LIBS on bacteria the required energy is approximately of the order of 10 mJ/pulse. Therefore, the energy per pulse must be reduced to the desired energy outside of the laser. To do this we make use of the polarization of the laser beam.

Initially, the vertically polarized output beam passes through a half-wave retarder, which can rotate the polarization of the beam to twice the angle between the retarder fast axis and the plane of polarization. Then it enters a polarizing beam splitter, which passes only the vertical polarization while the horizontal one is fed into a beam dump. Therefore small rotations of the half-wave retarder allow very precise control of the pulse energy. This is shown in Figure 3.3, while a picture of the attenuation optics is also shown in Figure 3.4.

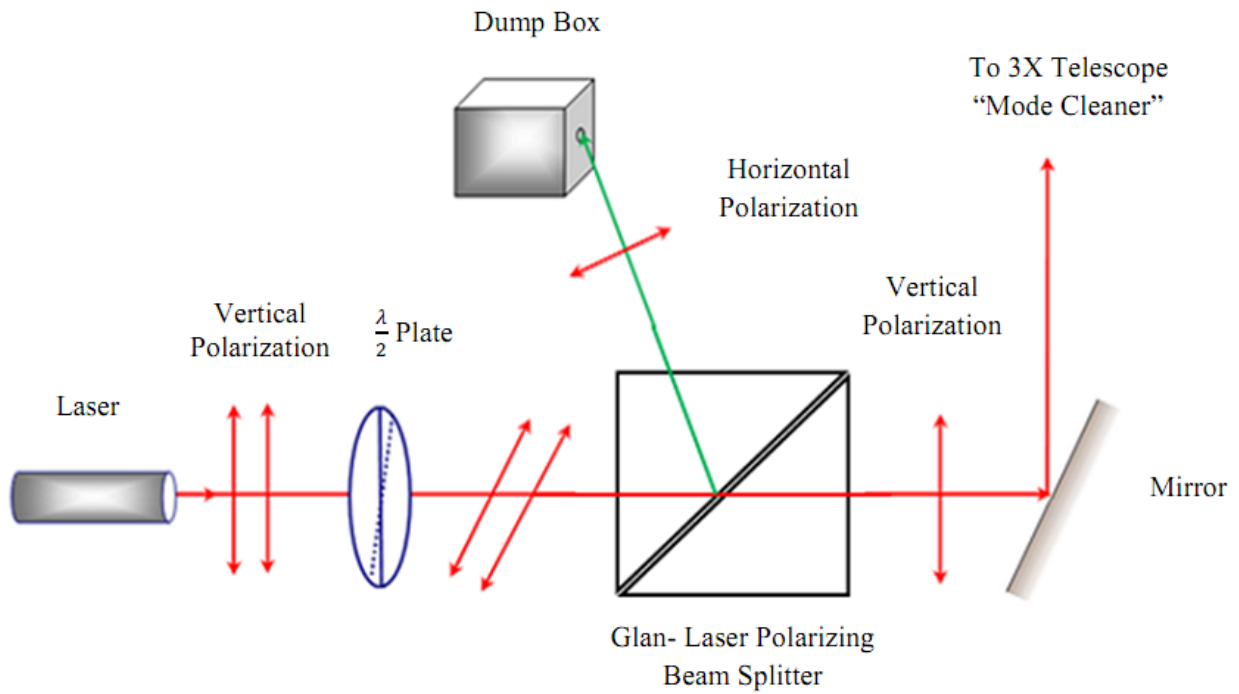


Figure 3.3: A schematic diagram of the energy attenuation optics.

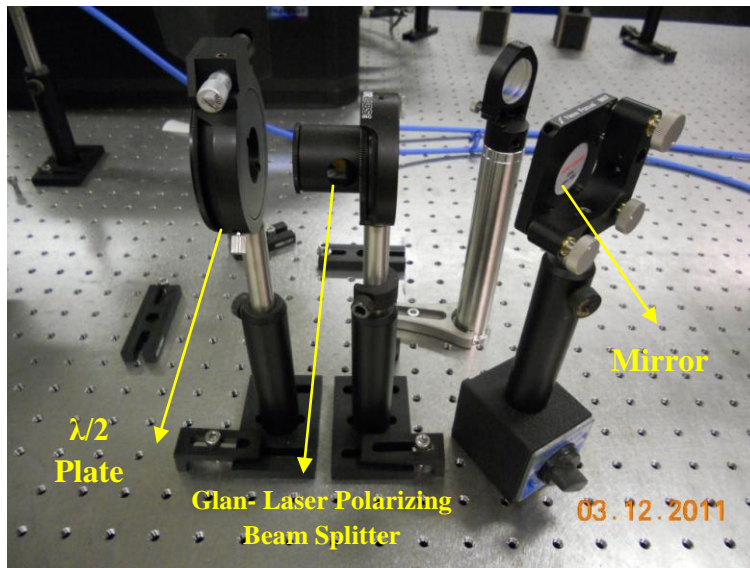


Figure 3.4: A picture of the energy attenuation optics.

After the power attenuation optics, the resultant beam is sent through a spatial “mode cleaner” as illustrated in Figure 3.5. The spatial mode cleaner consisting of a 3X telescope beam

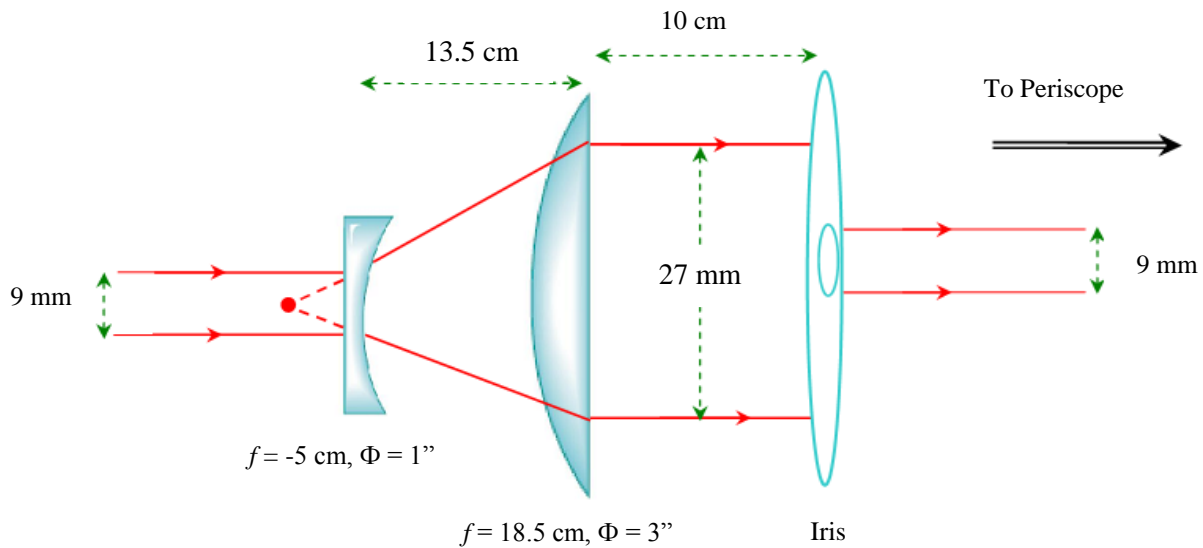


Figure 3.5: A schematic diagram of the telescope.

expander is located 1.3 m after the laser. It is used to expand the beam from its initial diameter of 9 mm to 27 mm. The 3X telescope consists of an AR coated plano-concave lens ($f = -5 \text{ cm}$, $\Phi = 1''$) and uncoated plano-convex lens ($f = 18.5 \text{ cm}$, $\Phi = 3''$). An iris with a 9 mm diameter follows the expanded beam and is used to revert the beam to its initial diameter while only retaining the central, more-Gaussian portion of the beam. A picture of the mode cleaner is shown in Figure 3.6.

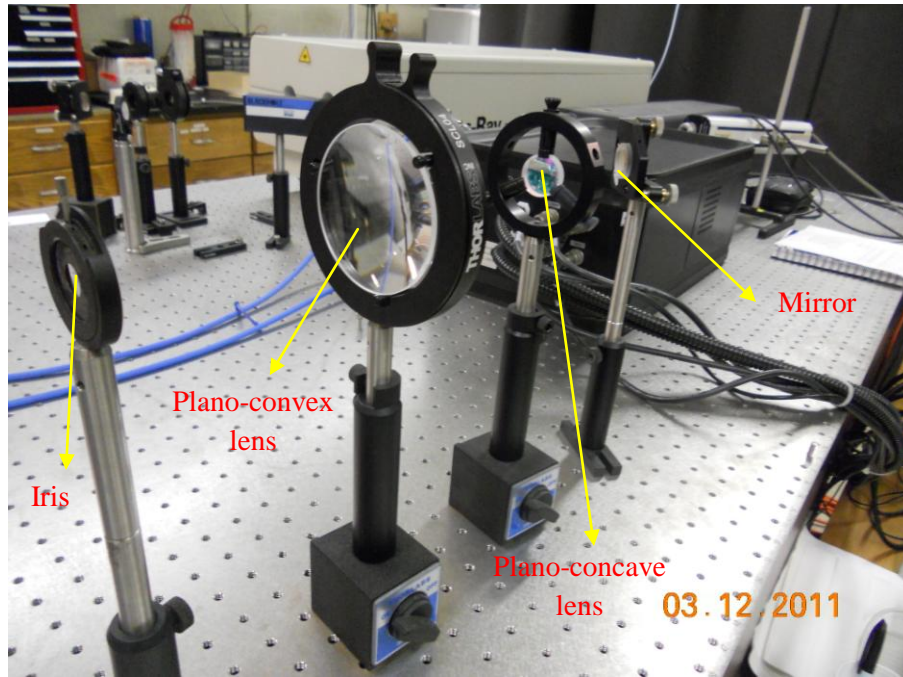


Figure 3.6: A picture diagram of the telescope.

After the mode cleaner, the laser beam enters a periscope for focusing onto the bacterial targets. A helium-neon (He-Ne) laser at 632.8 nm will be used during the experiment as an overlay with the infra-red laser beam for beam visualization which can be achieved by using a beam splitter (50:50 @ 633 nm). After reflection, the two laser beams pass through another beam splitter which allows a CCD camera to image the magnified region on the sample. A high-damage threshold, AR-coated 5X microscope objective with a 40 mm working distance is used to focus both laser beams on the target. As a result, the He-Ne laser gives a visual spot on the target which is related to the location of the ablation. The periscope is shown schematically in Figure 3.7. A picture of the periscope is shown in Figure 3.8.

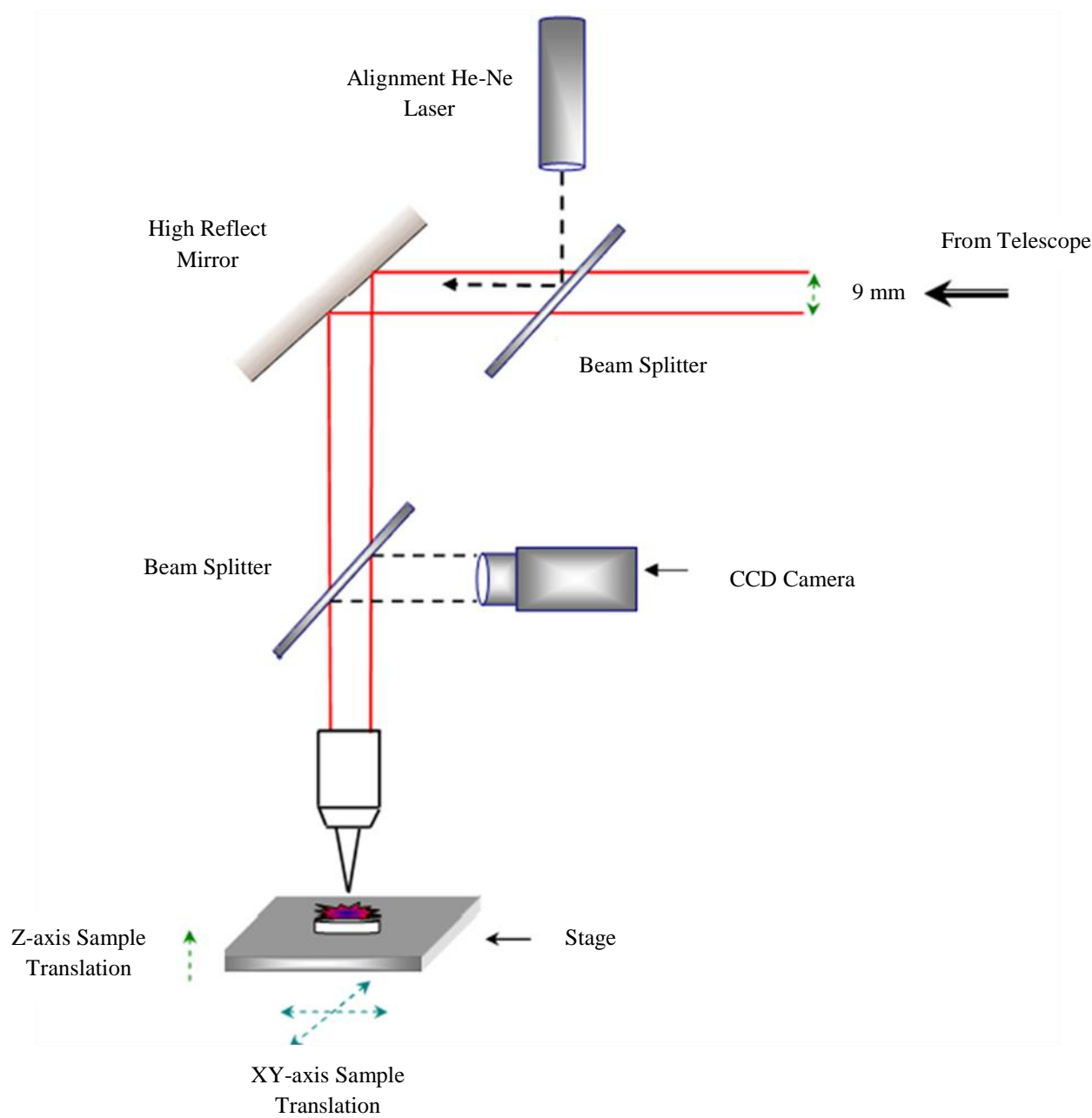


Figure 3.7: The schematic side view of the periscope.

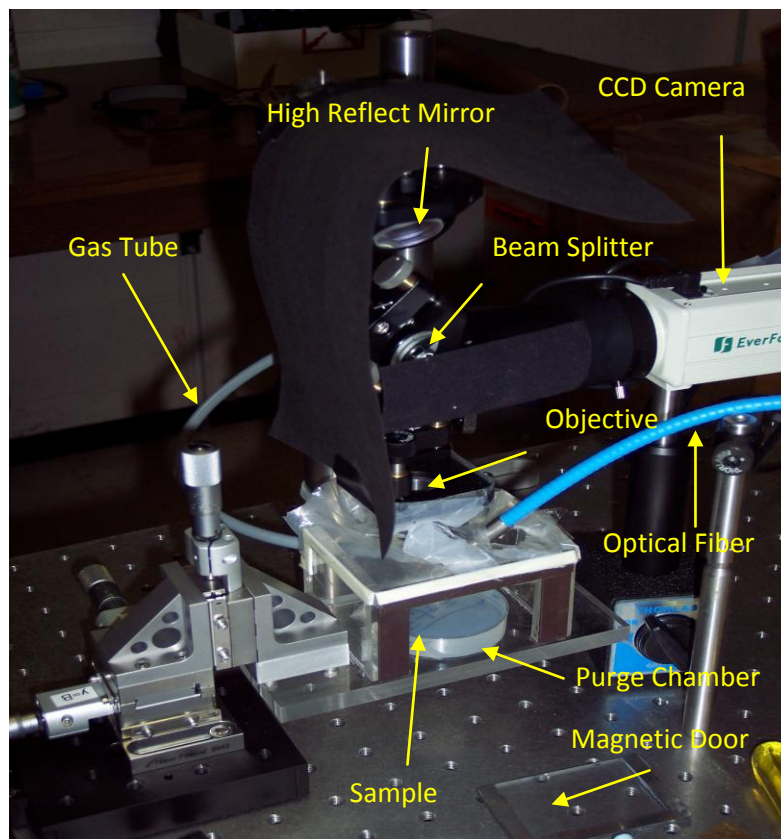


Figure 3.8: A picture side view of the periscope.

A schematic diagram of the sample chamber is shown in Figure 3.9. The chamber was set-up on a stage, which could be translated in the x , y and z directions. The top and the back of the chamber were sealed with a polyethylene sheet in order to permit the movement of the chamber relative to the fixed objective and collecting optical fiber while translating the sample while retaining an argon atmosphere. The chamber can be accessed through a magnetic door, which provided a tight gas seal. In all experiments, a constant flow of 5 standard cubic feet per hour (SCFH) was maintained into the chamber through a small hole in the sheet

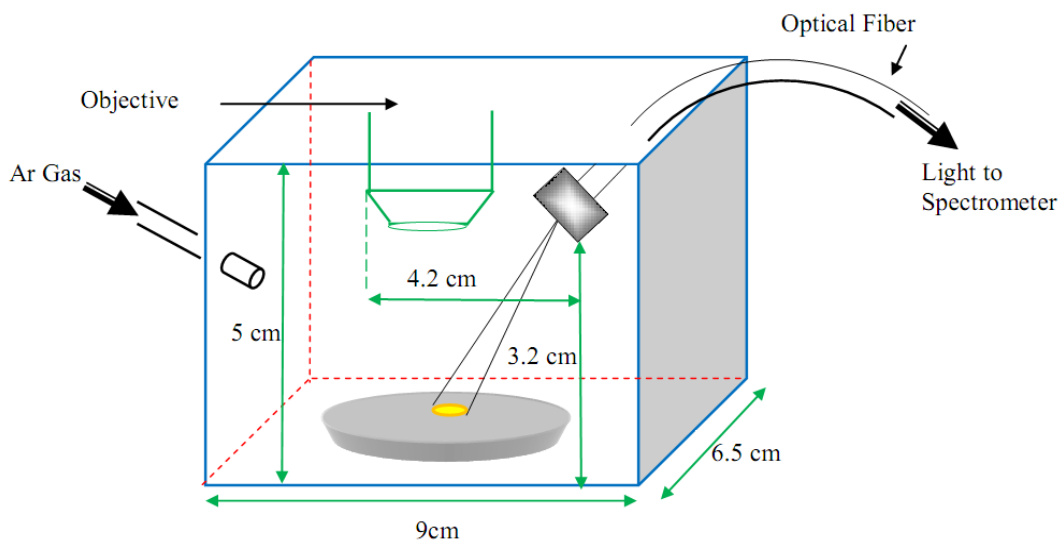


Figure 3.9: A schematic diagram of the purge chamber.

3.1.2 Optical Collection

A 1 m long optical fiber with $600 \mu\text{m}$ core diameter and $\text{N.A.} = 0.22$ was used to collect the optical emission from the microplasma. The fiber was angled at 60° with respect to the sample surface. This fiber was connected to an échelle spectrometer equipped with a 1024×1024 ($24 \mu\text{m} \times 24 \mu\text{m}$ pixel area) ICCD (Intensified Charged Coupled Device) array, which provided us with complete spectral coverage from 200 to 800 nm and with a 0.005 nm resolution in the UV. This échelle spectrometer is an ESA 3000 from LLA Instruments GmbH.

An échelle spectrograph consists of an échelle grating and a prism. The échelle grating is a type of diffraction grating which was first discussed by Harrison in 1949¹ and provides higher dispersion and higher resolution power. It has a low groove density and is optimized for high diffraction orders.²

Figure 3.10 is a schematic representation of an échelle grating. As can be seen, the grooves are widely spaced and have a step-like profile. The light to be dispersed is made to fall

on the grating at right angles to the faces of the grooves. Therefore, interference among the reflected beams (blue lines) can occur. For the interference to be constructive, it is necessary that the path lengths differ by an integral multiple n of the wavelength λ of the incident beam.³

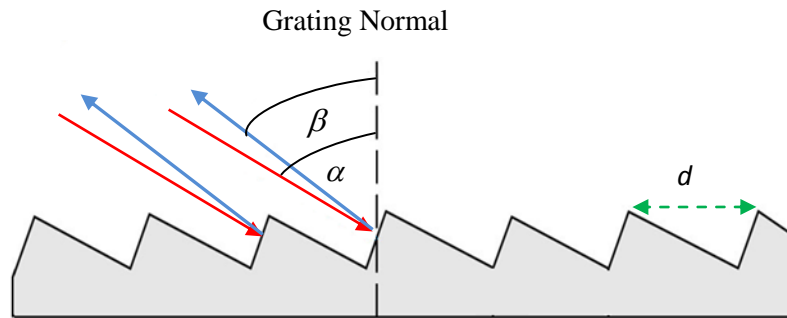


Figure 3.10: The geometry of an échelle grating.

The condition of the constructive interference can be given by the following equation:

$$n \lambda = d(\sin(\alpha) + \sin(\beta)) \quad (3.1)$$

Where α, β are the incident and the reflected angles respectively and d is the groove spacing.

Equation 3.1 suggests that there are several values of λ for a given reflected (diffracted) angle β . Thus, if a first-order line ($n = 1$) of 600 nm is found at β , second-order (300 nm) and third-order (200 nm) lines will also appear at this angle too. Therefore, a series of overlapping spectra will be produced. A second, low-dispersion grating, or a prism as in our case, is used to separate out the overlapping spectra. This can be seen in Figure 3.11.

Overlapping Orders

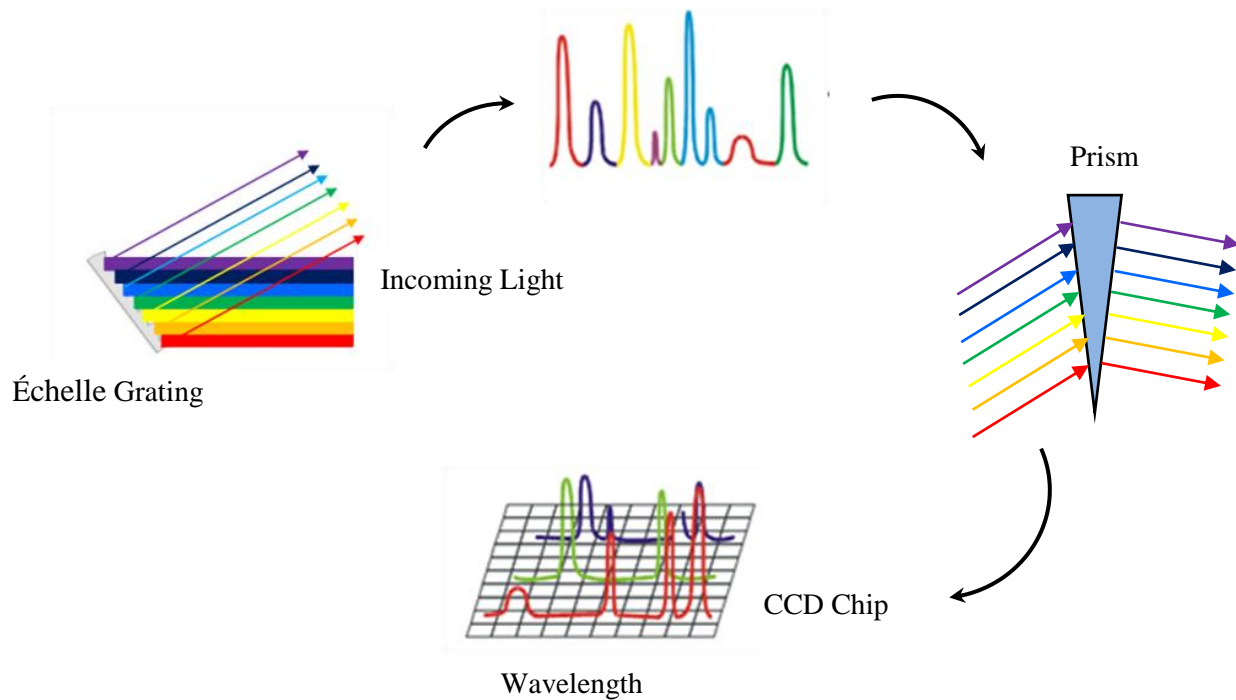


Figure 3.11: Operation principal of an échelle spectrograph.

For the detection of the plasma emissions dispersed in the échelle spectrograph in our LIBS experiments, an Intensified Charged Coupled Device (ICCD) was used. The charged coupled device (CCD) is a device that is used to convert light into electrical charges. The basic structure of a CCD is a shift register by an array of closely spaced potential-well capacitors.⁴ When the light is incident on an array of CCD elements (potential wells), electron-hole pairs will be created due to the absorption of the incident photons and as a result, the potential wells will be filled with electrons.⁵ The quantity of electrons in each well is a measure of the incident light intensity: the brighter the illumination the greater the charge. When the exposure is ended, the charge in each element must be determined. This can be done by transferring the charges to the edge of the CCD device and be picked up by external circuits (read-out circuits). When all elements have been read, the CCD device will be ready for the next exposure.⁶

Our ICCD detector was composed of a CCD coupled to a microchannel plate (MCP) image intensifier to provide time-gated detection of the laser plasma as well as amplification of the optical signal.⁷ For the plasma produced by nanosecond laser pulses, the decay of spectral lines occurs on the microsecond time scale. Therefore, a shutter (i.e. electronic shutter) is necessary to capture the LIBS spectrum at a specific time after the plasma formation. Typical shutters used with array detectors are microchannel plates (MCPs) to provide precise nanosecond control of the shutter opening and closing. These are two-dimensional devices that can be gated on and off very rapidly, on the order of a few nanoseconds for example, to permit or prohibit the passage of light.^{8,5,2} A schematic of the échelle spectrograph is shown in Figure 3.12.

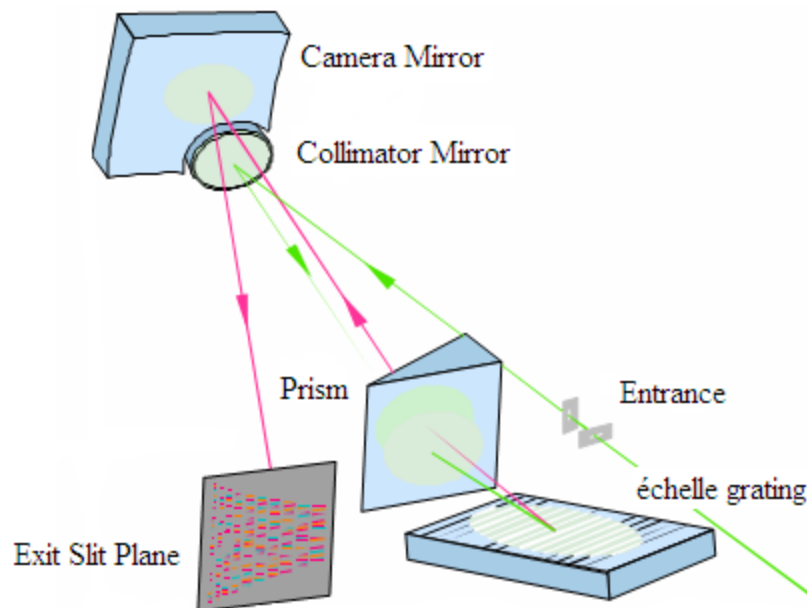


Figure 3.12: Arrangement of the échelle-Spectrograph (ESA 3000).

3.2 Bacterial Culture and Growth

Growth medium (culture) is filled with nutrients that are necessary for the growth of microorganisms such as bacteria. Culture media basically come in solid and liquid form. In the following sections I will talk in brief about the experimental kits that I used for the growing of the bacterial samples that I used in all my studies.

3.2.1 Media Preparation

Trypticase soy agar (TSA) is a rich bacteriological growth medium used for culturing many kinds of microorganisms. TSA medium consists of pancreatic digest of casein, soybean meal, NaCl, dextrose, and dipotassium phosphate.⁹ It is mainly used as an initial growth medium for the purposes of: observing the colonies, developing a pure culture, and for culture storage. TSA medium can be prepared in the following way:

1. 10 g of TSA medium (powder) are suspended in 250 mL of distilled water.
2. Heat with frequent agitation for 1 minute using Bunsen burner to completely dissolve the powder.
3. Autoclave the solution at 121°C for 45 minutes.
4. Place the solution in warm water bath ($T = 45\text{ }^{\circ}\text{C}$) for 15 minutes. Consequently, the solution will be cool enough to handle.
5. Pour carefully into the Petri dishes avoiding bubbles as much as possible.
6. Allow to solidify at room temperature overnight. You may also incubate the plates inside the incubator at $T = 37\text{ }^{\circ}\text{C}$ overnight due to the potential of contamination from human contact or from the surrounding environment.

3.2.2 Liquid Culture

Nutrient broth (NB) is a common laboratory medium that is used for growing most types of bacteria. NB consists of beef extract and peptone. In order to prepare a 50 mL of this medium the following protocol was used:

1. Suspend 8 grams of the medium in 50 mL of distilled water.
2. Mix well and leave to stand until the mixture is uniform.
3. Heat with gentle agitation for one minute, or until complete dissolution.
4. Autoclave the solution at 121°C for 45 minutes.

To grow bacteria in liquid culture such as nutrient broth, a single bacterial colony was transferred to 2 mL of liquid culture. After that, the inoculated tube was put into a 37°C shaking incubator for 24 hours to allow for the growth of bacteria to generate a dense culture. In liquid culture, the medium appears cloudier as the bacteria increase in number by division. Figure 3.13 showed the difference in turbidity, a measure of the cloudiness of liquid culture, between a sterile medium (flask to left) and medium inoculated with *E. coli* the day before (flask on right).



Figure 3.13: Different turbidity due to the growth of bacterial cells.

3.2.3 Inoculating and Dilution on Solid Culture

Solid media, TSA in our case, provide a firm surface on which bacteria can form discrete colonies and they are also used to isolate different bacterial species or to have a pure culture. For all my experiments I used the following protocol for the preparation of bacterial samples:

1. Light a Bunsen burner.
2. Flame the inoculating loop to redness. This procedure acts to sterilize the loop.
3. Let the loop cool a minute. A hot loop will kill the bacteria cells.
4. Insert the sterile inoculation loop into the overnight culture.
5. Streak four to six lines gently across the TSA surface.
6. From one end of the parallel streaks, streak additional four more parallel lines 90° to the original set. Remember to sterilize the loop before and after each use.
7. Turn the plate another 90° and sample some of the bacteria from the second streak.
8. Repeat the previous step and be careful that you do not streak through the first set. See Figure 3.14.
9. Finally, incubate the plate upside down to prevent moisture running onto the TS agar for 24 hours at 37°C .

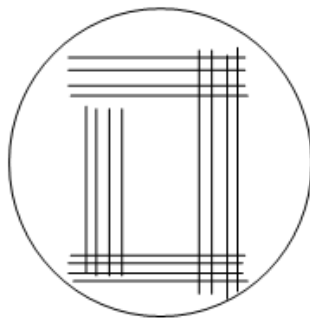


Figure 3.14: Inoculating and employing streak plate techniques to isolate individual bacterial colonies on a solid medium.

For LIBS testing, bacterial cells were harvested by scraping with a sterile wood stick and then transferred to 1.5 mL deionized water. A pellet was collected after centrifuging the liquid at 5000 RPM for 3 minutes at room temperature as shown in Figure 3.15. The supernatant (the bacteria-free liquid above the pellet) was withdrawn and discarded.



Figure 3.15: *E. coli* pellet after centrifugation with the supernatant removed.

3.2.4 Preparation of Bacterial Targets

For almost all LIBS measurements (unless otherwise noted), the bacteria samples were transferred to the surface of a 1.4% bacto agar plate. There are many advantages for using this type of nutrient-free agar as an ablation substrate such as its large area, its moisture which preserves the bacteria in a reasonable state, and most importantly because there is no significant contribution to the bacterial LIBS spectra from elements in the agar. The agar target plates were prepared as follows:

1. An agar powder was mixed with 125 ml of distilled water.

2. The solution was boiled and stirred for 10 minutes on a hot plate at a temperature $T = 300$ °C and a stir speed = 120 rpm. After that, it was poured into a small Petri dish.
3. The top surface of the semi-liquid agar was scraped three times to make it level (assuring a level and uniform agar surface was critical for accurate LIBS results).
4. Finally, the Petri dish was stored in a refrigerator to cool down for at least 30 minutes, after which time the agar was completely solid, with a very flat, level top surface.

Typically agar plates were made one day before the bacteria were deposited on them for LIBS testing.

Ten microliters of a high-density bacterial suspension (pellet) were micropipetted to the surface of the bacto-agar. Bacteria were distributed almost evenly over the surface of an agar plate. This process is shown in Figure 3.16. After approximately thirty minutes, the liquid was absorbed by the agar, leaving a transparent thin film or “bed” of bacteria approximately 0.5 cm^2 in area. Figure 3.17 shows three bacterial pads after ablation.

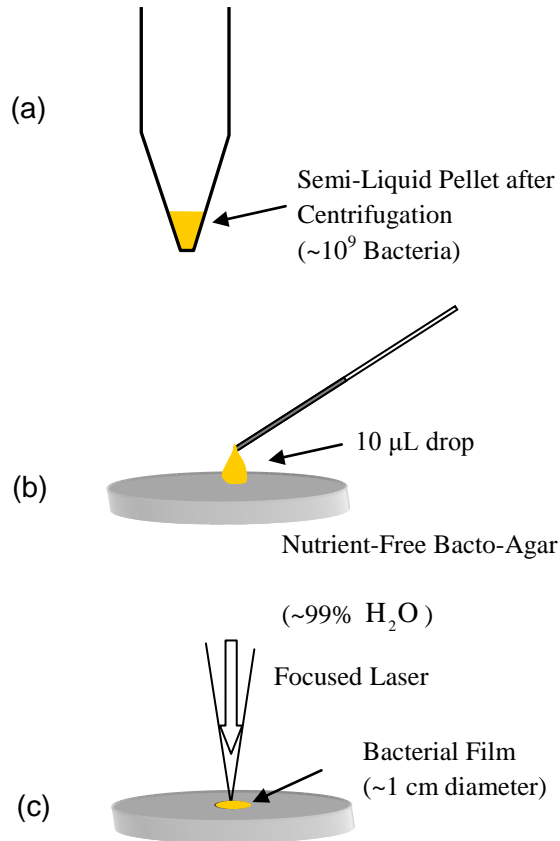


Figure 3.16: The bacterial mounting procedure used in this study. (a) $\sim 10^9$ bacteria were harvested from cultures on solid media and suspended as a semi-liquid pellet by centrifugation. (b) 10 μ L drops were deposited on a nutrient-free bacto-agar substrate. (c) After 30 minutes, the transparent “bed” of bacteria was ablated by a pulsed laser.

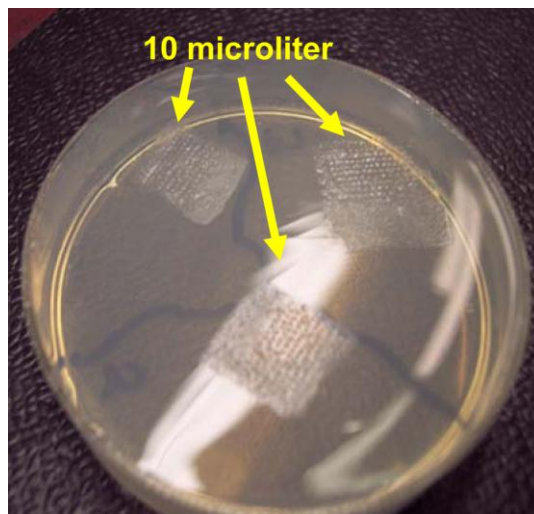


Figure 3.17: Three bacterial pads deposited on the agar surface.

3.3 Experimental Parameters

LIBS spectra were acquired by focusing the Nd:YAG laser pulses onto the bacterial film on the agar plates in an argon environment. Typically, LIBS plasma emission was only collected at a delay time, τ_D , of $2 \mu\text{s}$ after the ablation pulse and with an ICCD gate width (τ_w) of $20 \mu\text{s}$ duration. The symbol τ_w represents the time period over which the light is collected and is determined by the opening of the MCP shutter. Those times (τ_D and τ_w) can be adjusted using the ESAWIN software as shown in Figure 3.18.



Figure 3.18: The control menu of the ESAWIN software which controlled the timing of the laser and spectrometer.

Figure 3.19 shows the timescales of a single laser pulse initiated LIBS plasma (as well as two examples of LIBS plasmas obtained during these regimes), which plots the optical intensity emitted by the plasma as a function of time after the initiation of the laser pulse.⁶ In typical LIBS experiments, we experimentally determine the delay time and the gate width time in order to maximize the emission which comes from the emission lines of interest and also to reduce the contribution that comes from the continuum radiation (described in detail in Chapter 2).

To collect LIBS spectra from bacterial samples, we needed to ensure that the laser beam was well focused on the sample surface. To check this, LIBS spectrum of the bacto-agar was saved and compared with a reference one. In my experiments, five laser pulses were fired in one

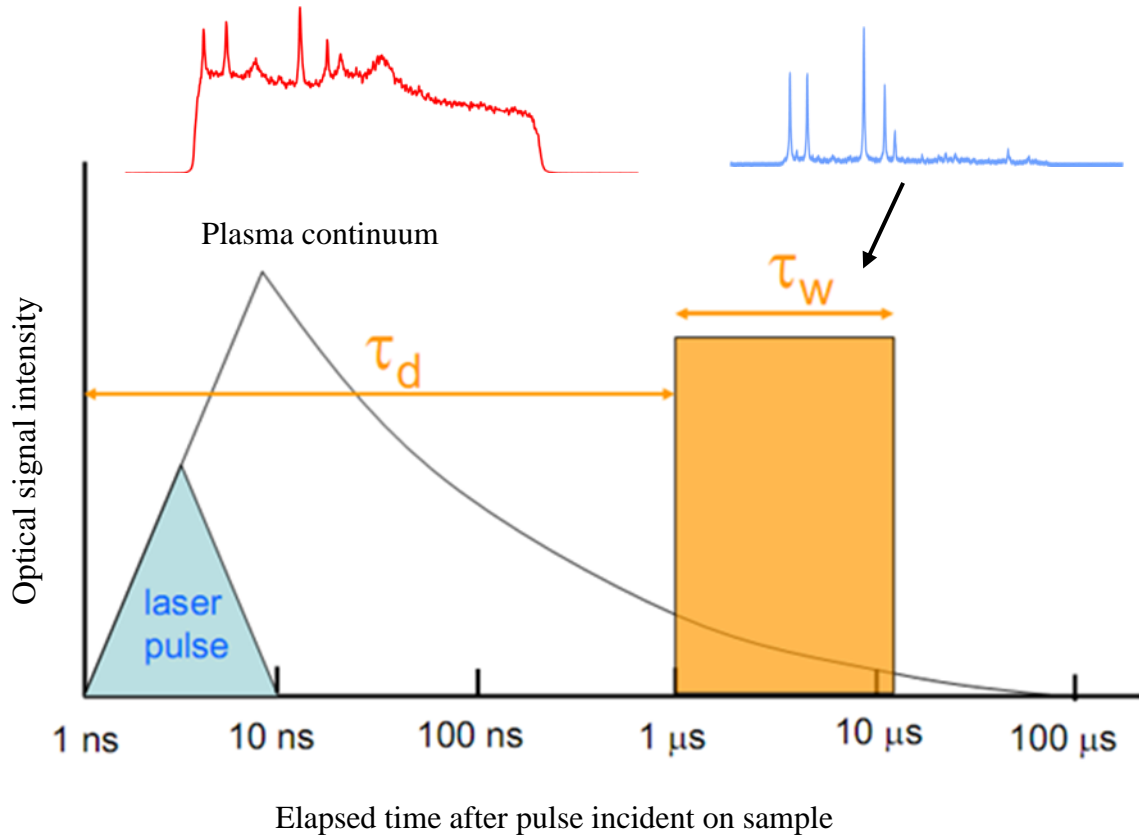


Figure 3.19: Temporal history of LIBS plasma.

location (taking half a second) and emissions were accumulated on the CCD chip camera prior to read out. These five on-chip accumulations (OCA) summed the emission from each plasma which allowed a larger signal to noise, and insured that all the bacteria under the laser were ablated. During this process, the camera was opened for the whole exposure time which is 5 times the gate width. The firing of these five laser shots at one location is called one accumulation. Finally, to obtain one spectrum, five accumulations taken at five different locations were collected and averaged, resulting in a spectrum of 25 averaged laser pulses.

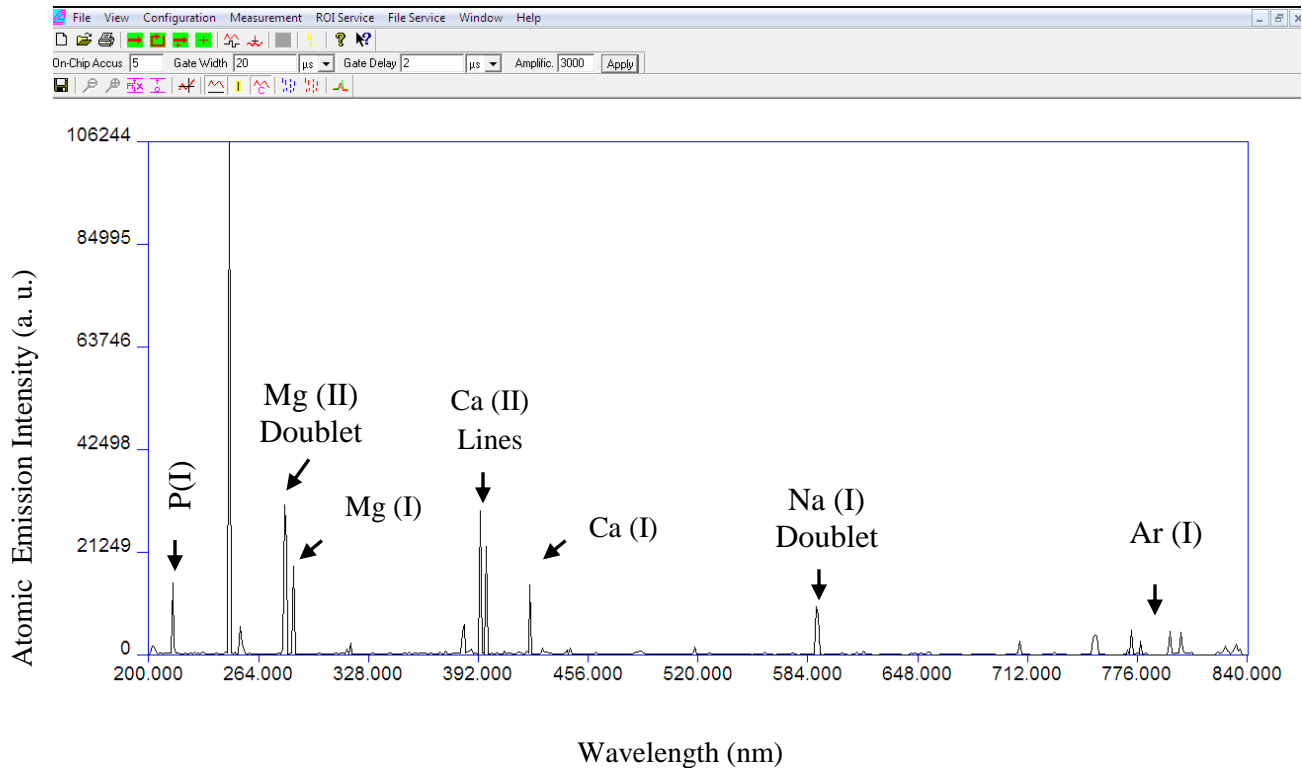


Figure 3.20: A LIBS spectrum of *E. coli* bacteria ablated on agar.

A typical LIBS spectrum from a bacterial sample obtained in our lab is shown in Figure 3.20. The identity of all the relevant emission lines that were observed is given. Note that most of the lines are inorganic metallic elements. This type of spectrum was the “raw data” of our experiment. All atomic emission lines were fully resolved, even though in this magnification this is not obvious (i.e. the Na doublet at 589 nm looks like one peak with this magnification.)

Figure 3.21 shows the CCD camera view of a typical LIBS spectrum. This is the actual raw data that the CCD camera measures, which is then stitched together to form a spectrum like the one in Figure 3.20. In this figure, different diffraction orders are shown with longer wavelengths located at the bottom of the CCD chip. The false-color light ‘spots’ along the different orders correspond to emission from a specific element line i.e. carbon line at 247.857 nm. The spectrum in Figure 3.20 only uses the intensity of the Order 97 peak.

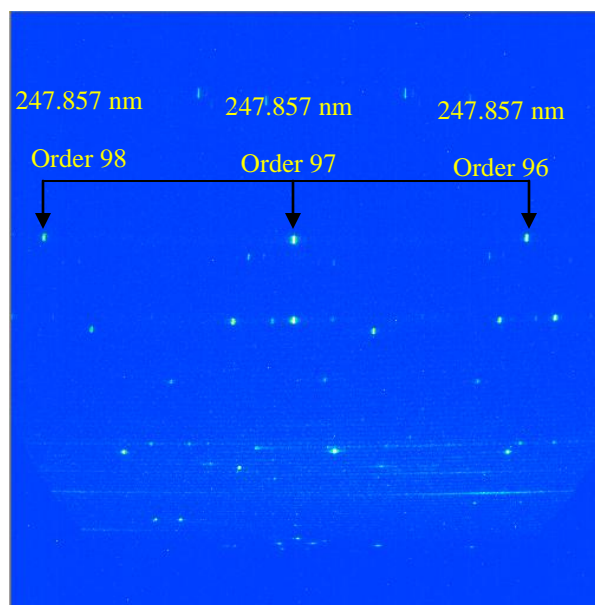


Figure 3.21: Arrangement of orders in the focal plane of an échelle spectrograph.

In our experiments, LIBS spectra were analyzed by measuring the intensity of 13 emission lines from 5 different elements (P, C, Mg, Ca, and Na). The area under each background-subtracted line was determined by the ESAWIN software and is the intensity of that line. To save computing time, only the integrated areas of lines assigned in the so-called “regions of interest” (ROI) were calculated. Only one order is used to calculate a single line intensity in the ROI view. Specifically, the line that falls in the center of the CCD chip was used. Moreover, the intensity of the line in other orders, left and right of the main order, is relatively low if it is compared that of the main line.

Figure 3.22 shows the ROI view of the LIBS spectrum that is shown in Figure 3.19. The line plot in red is the intensity versus X-pixel coordinates for 60 pixels read directly off the CCD chip. The center of the peak as determined from the NIST atomic database is shown as a green vertical line.¹⁰ The text in the upper left hand corner denotes the element of interest whereas the number below each box gives the wavelength in nm of the position in the middle of the window.

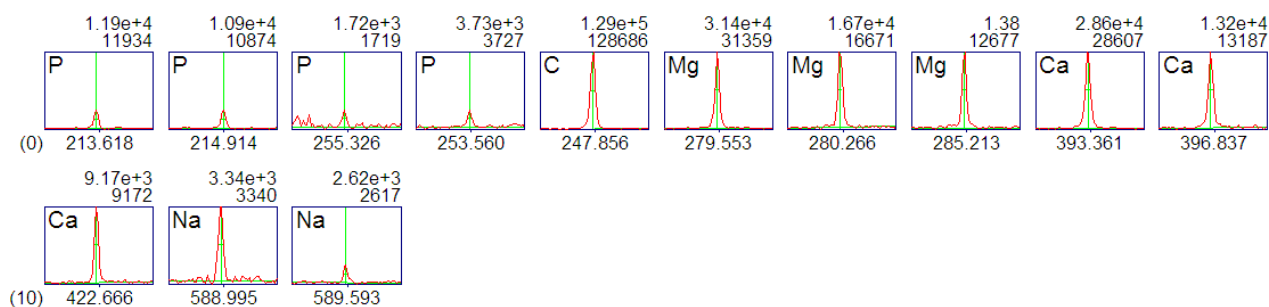


Figure 3.22: The ROI view of the spectrum shown in figure 3.11.

The number above the window is the peak area and the number above this is the ratio of the peak area to certain reference lines (not used in our analysis). After this determination of peak intensity, the intensity of each line was divided by the sum of all 13 line intensities to normalize the spectra for shot-to-shot fluctuations. This was done in a Microsoft Excel sheet which could open and read these saved ESAWIN files. These relative line intensities constituted 13 independent variables which were used for discriminating between the bacteria spectra.

In conclusion, in this chapter I have described the experimental set-up with some details about the instruments used and all of the relevant procedure that were followed. In the following chapters I will present and discuss my results.

REFERENCES

- ¹ G.R. Harrison, “The production of diffraction gratings: II. The design of échelle gratings and spectrographs,” *Journal of the Optical Society of America* **39**, 522-527 (1949).
- ² A.W. Miziolek, V. Palleschi, and I. Schechter, *Laser Induced Breakdown Spectroscopy*, 1st edition, (Cambridge University Press, Cambridge) 2006.
- ³ A. Thorne, U. Litzén, and S. Johansson, *Spectrophysics: Principles and Applications*, 1st edition, (Springer) 1999.
- ⁴ M. Graef, *Introduction to Conventional Transmission Electron Microscopy*, (Cambridge University Press) 2003.
- ⁵ F.T. Yu and X. Yang, I.R. Kenyon, *Introduction to Optical Engineering*, (Cambridge University Press) 1997.
- ⁶ D. Cremers and L. Radziemski, *Handbook of Laser-Induced Breakdown Spectroscopy*, (John Wiley & Sons Ltd.) 2006.
- ⁷ I.R. Kenyon, *The light Fantastic: A Modern Introduction to Classical and Quantum Optics*, 2nd edition, (Oxford University Press, USA) 2011.
- ⁸ J.P. Singh and S.N. Thakur, Eds., *Laser-Induced Breakdown Spectroscopy*, (Elsevier, Amsterdam) 2007.
- ⁹ K. Talaro, *Foundations in Microbiology*, 6th edition, (McGraw-Hill Science/Engineering/Math) 2006.
- ¹⁰ http://physics.nist.gov/PhysRefData/ASD/lines_form.html

CHAPTER 4

The Effect of Sequential Dual-Gas Testing on LIBS-Based Discrimination: Application to Brass Samples and Bacterial Strains

4.1 Introduction

It is well known that time-resolved laser induced breakdown spectroscopy (LIBS) is a powerful tool for elemental analysis.¹ There are many experimental parameters that can affect the laser-induced plasma, and currently the wide variety of experimental configurations that exist in the numerous labs performing LIBS measurements is a limitation to the standardization of the technique.^{2,3} As has been discussed in previous chapters, along with laser wavelength, pulse energy, pulse duration, beam waist and time-resolved gate delay (to name a few), the atmosphere in which the ablation occurs is one of the important experimental parameters that strongly affect the emission characteristics of the plasma.⁴ Several studies have been performed in order to investigate the influence of various buffer gases on the plasma formation. Sdorra and Niemax studied the effect of different ambient gases (argon, neon, helium, nitrogen, and air) in the production of plasma by using a nanosecond Nd:YAG laser on a copper sample.⁵ The results showed that argon produced a higher plasma temperature and a higher electron density compared with densities obtained from other gases under fixed experimental conditions. Kuzuya et al. investigated the affects of laser energy and surrounding atmosphere on the emission characteristics of the produced plasma.⁶ The results showed that the maximum spectral intensity was obtained in argon when the pressure was 200 Torr and at a higher laser energy of 95 mJ.

Wisbrun et al. found that an argon atmosphere was most favorable in terms of higher analyte emission intensity and better reproducibility.⁷ Moreover, Rehse et al. investigated the importance of atmosphere above the surface of laser-ablated pure water samples and concluded that argon produced a higher temperature and electron density in these plasmas (compared to air or dry nitrogen) but the largest effect was on the temporal evolution of the emission from the plasma, particularly from hydrogen atoms and recombining molecular species.⁸

Due to the sensitivity of the plasma emission characteristics on the ambient gas environment, the aim of this experiment was to investigate the effect that sequential testing in two ambient gas environments at atmospheric pressure would have on the ability to identify or discriminate between highly-similar samples of bacteria and less-similar samples of brass based on their LIBS spectra. In both the brass-alloy and the bacterial system, sequential LIBS analysis in argon and helium yielded an enhanced discrimination between highly-similar targets when LIBS emission intensities were analyzed with (DFA). This enhanced discrimination ability was evidenced by an increase in the overall accuracy of identification and an increase in the magnitude of the between-group variances.

4.2 Experimental

Initial experiments were performed on four Cu-Zn brass alloys with different stoichiometries and compositions ablated first in argon, then in helium. The brass samples were chosen as a representative test system to optimize reproducibility due to the simplicity in sample preparation, surface flatness, and high (relative) alloy homogeneity. Subsequently, the

experiment was performed on bacterial samples, with which it was significantly more difficult to produce reproducible measurements.

All LIBS testing was done in a small purge gas box mounted on an x-y translation stage, as illustrated in Chapter 3. Gas was inlet at a volumetric flow rate of approximately $8 \times 10^{-5} \text{ m}^3/\text{s}$ and a slight overpressure was achieved in the intentionally leaky box. Given the small size of the purge box, it took no more than one minute for a new gas to completely displace the old gas in the box. Samples were introduced through a magnetically sealable door. Thus, it took very little time to test a sample in more than one gas.

In the case of bacteria, spectra were acquired in the argon environment at a delay time of $2 \mu\text{s}$ after the ablation pulse with an ICCD gate width of $20 \mu\text{s}$ duration. In helium, the delay time was set to $1 \mu\text{s}$ in order to obtain a better signal-to-noise ratio. In the case of the brass alloys, LIBS spectra were acquired in both gas environments at a delay time of $1 \mu\text{s}$ after the ablation pulse with an ICCD gate width of $20 \mu\text{s}$ duration. All delay times were determined experimentally to yield optimal signal to noise for the specific target and bath gas, while minimizing the broadband background emission. Specifically, the bacterial experimental conditions are the same as those used in all of our previous studies.^{9,10,11,12}

For the bacteria samples, five spectra were averaged at one location and five different locations were analyzed per data point, resulting in a spectrum of 25 averaged laser shots. For the brass samples, five spectra from four different locations were analyzed per data point. Each data point took approximately 20-30 seconds to acquire, mostly limited by ICCD readout speed. Sequential dual-gas testing was performed by preparing the samples as described below, then

acquiring the desired number of spectra sequentially in a single buffer gas. The purge gas box was then flushed with the new gas (which took about one minute), and an equal number of spectra were acquired in the new gas. In this way the purge box only needed to be flushed once per sample. The argon and helium data were analyzed together only later in software, so the order of gas testing was not important. For discrimination of an unknown sample, when repeated measurements would not typically be made, one spectrum would be acquired in one gas (30 seconds) the chamber would be flushed (1 minute), and the second spectrum acquired in the second gas (30 seconds). This process does slow data acquisition, but only by a factor of two, and could be improved by reducing the size of the purge chamber which would decrease the time to displace the old buffer gas with the new one.

The brass alloy samples were chosen to provide a simple, well-behaved test system. Four-brass alloys (McMaster-Carr) were used: alloy 464 (unleaded naval brass) which contains a high zinc content, alloy 360 (free-machining brass), alloy 353 (machinable and formable engravers brass) which contains a lower lead content, and alloy 260 which represents a simple copper-zinc alloy. The compositions of these four alloys as provided by the manufacturer are given in Table 4.1.

Samples were machined to a 2 cm x 2 cm size and the surface was prepared by cleaning with acetone to remove any organic chemical contaminants on the surface. After that, the acetone was rinsed off with methanol. No attempt was made to remove the inorganic contaminants. A single 2 cm x 2 cm sample was used for each alloy.

Table 4.1: The composition of the four brass alloys used in this study.

Alloy DFA #	Name	Alloy Number	Composition
1	Naval Brass	Alloy 464	60% Cu 0.8% Sn 39.2% Zn
2	Ultra-Machinable Brass	Alloy 360	60-63% Cu 2.5-3.7% Pb 35-37% Zn.
3	Machinable and Formable Engravers Brass	Alloy 353	55-60% Cu 0.5-1.5% Al 0.4% Pb 39% Zn
4	Formable Cartridge Brass	Alloy 260	68.5-71.5% Cu 0.07% max Pb 28.5-31.5% Zn

4.3 Results and Discussion

4.3.1 Brass Samples

Typical LIBS emission spectra from one of the brass samples obtained in the ambient atmospheres of argon and helium are shown in Figure 4.1. The spectra are dominated by emission from Cu, Zn, Pb, C, and Al, and they also contain emission from Na and Ca. In the case of argon gas, 4.1(a), the intensity of the spectral lines was much higher than that for helium, 4.1(b). These two spectra were taken with different detector amplification settings to eliminate ICCD bloom and pixel saturation, so the vertical scale is not consistent from 4.1(a) to 4.1(b). The ICCD was set to a much higher amplification (image intensifier voltage) while acquiring spectra in helium than it was while acquiring spectra in argon due to the much stronger emission from the argon plasma. This can be explained by the fact that argon produced a higher plasma temperature and therefore the excitation of analyte atoms was more efficient than that in the case

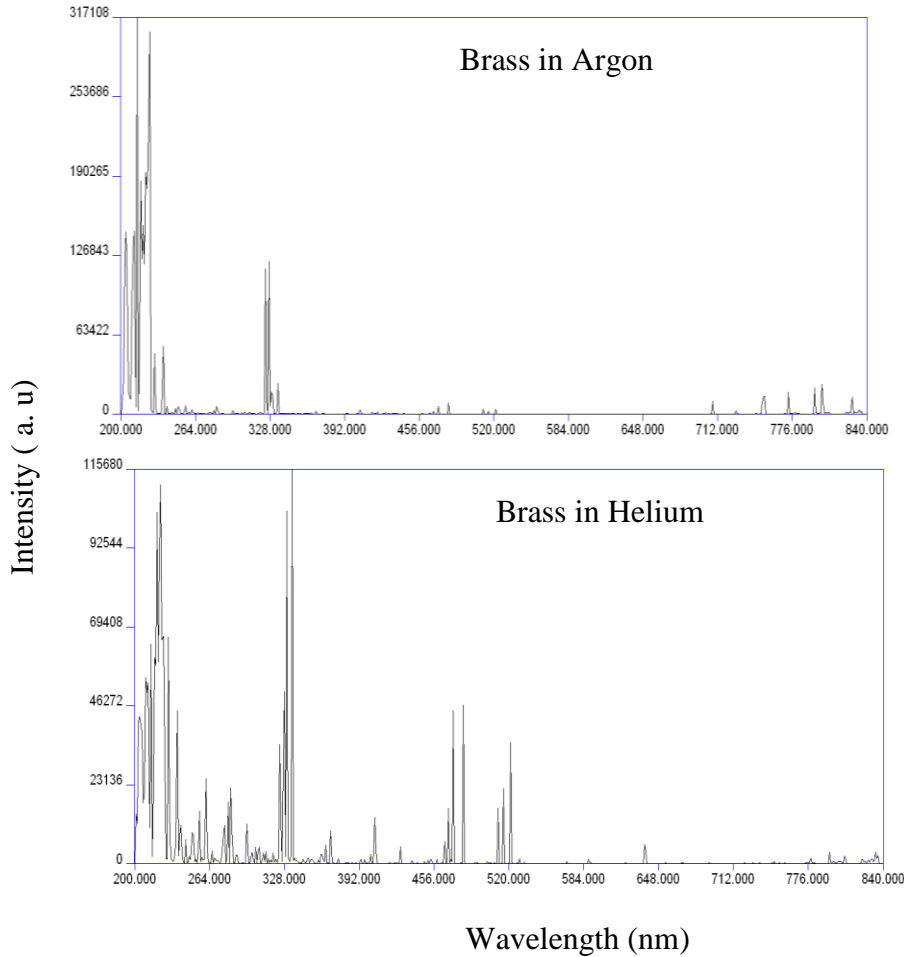


Figure 4.1: LIBS emission spectra for one of the brass samples in (a) an argon environment and (b) a helium environment at atmospheric pressure.

of helium. Moreover, the spatial confinement of the plasma in argon was stronger than that in helium, and this will directly affect the temperature of the produced plasma.

The strongest emission lines observed in both spectra shown in Figure 4.1 are listed in Table 4.2. The intensities of 15 of these emission lines of Cu, Zn, C, Na, Al, Pb, and Ca marked with an asterisk in Table 4.2 were analyzed in every spectrum by ESAWIN by nonlinear least squares fitting of a Lorentzian line shape to the emission curve. These 15 lines were chosen specifically to produce the most effective discrimination between samples. After that, the

Table 4.2: The strongest emission lines observed in brass LIBS plasmas acquired in argon and helium.

Wavelength (nm)	Line Identification
202.547	Zn II
204.380*	Cu II
213.855*	Zn I
217.000*	Pb I
218.177*	Cu I
219.227*	Cu II
221.811	Cu II
223.007	Cu I
247.856*	C I
261.837	Cu I
282.437*	Cu I
283.305*	Pb I
324.755	Cu I
330.258	Zn I
334.502	Zn I
363.957*	Pb I
368.346*	Pb I
393.366*	Ca II
396.152*	Al I
406.265	Cu I
465.112	Cu I
468.014	Zn I
472.215*	Zn I
481.053	Zn I
510.554	Cu I
515.325	Cu I
521.820	Cu I
588.995*	Na I
589.593*	Na I

* Lines used in the DFA.

intensity of each line was divided by the sum of all line intensities in order to normalize for shot-to-shot fluctuations. After this normalization, these relative line intensities constituted 15 independent variables and were then input into the SPSS software which performed the DFA.

In chapter two, we saw how DFA uses a set of independent variables (the emission intensities) from each spectrum (each spectrum is treated as a single data point) to predict the group membership of that particular spectrum in three basic steps. In this analysis, a set of

orthogonal discriminant functions is constructed from the data sets from all the groups. In this step, a canonical correlation analysis produces a set of canonical discriminant functions which are essentially the eigenvectors of the data expressed in a basis that maximizes the difference between groups. For a discrimination between N groups, $N-1$ discriminant functions (DF) are constructed with the first canonical discriminant function (denoted DF1) accounting for more of the variance between groups than the second canonical discriminant function (DF2), which accounts for more of the variance than the third canonical discriminant function (DF3), etc.

When DFA was used to discriminate similar spectra, such as those obtained from bacteria, typically almost all of the variance (upward of 90%) was described by only the first two canonical discriminant functions. Therefore plots are often presented showing only the first two discriminant function scores for each spectrum.

Figure 4.2 shows a DFA plot of all brass samples tested in an argon atmosphere. Each colored object in the plot represents an entire spectrum (there are roughly 50 spectra per category). In this analysis, although three canonical discriminant functions were used to characterize the four groups, most of the discrimination was performed by the first two functions. The DFA analysis showed that 88.6% of the variance between groups was represented by discriminant function one (DF₁) and 10.5% by discriminant function two (DF₂).

Another parameter returned by the SPSS DFA is called the structure matrix, which shows the correlations of each variable with each discriminant function. Typically, identifying the largest absolute correlations between specific emission lines and each discriminant function can help determine which elements play a crucial role in the discrimination provided by that function

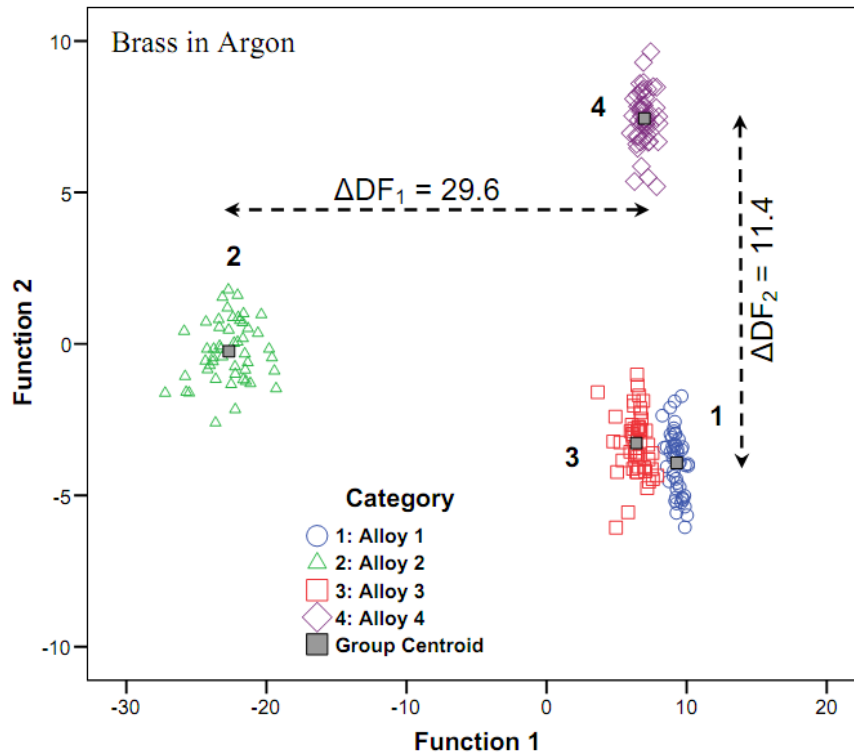


Figure 4.2: A discriminant function analysis plot showing the first two discriminant function scores of LIBS spectra obtained from four brass samples in argon.

(plotted along one axis of the plot). Shown in Table 4.3 is the structure matrix from the analysis of the LIBS spectra from the four brass alloys ablated in argon. The first column identifies the specific emission lines given by the element symbol and the wavelength of the transition, while the other three “function” columns show the absolute correlations between the line and that particular discriminant function. As can be seen, each predictor variable is correlated with each function, but the strongest overall correlation for each variable is indicated with an asterisk. The SPSS program then orders the predictor variables in descending order on the basis of the absolute value of their strongest correlation only, first for DF1, then DF2, etc. For example, in Table 4.3, the zinc line at 213 nm has a correlation of -0.457 with DF1 while the Cu line at 219 nm has a correlation of only $.212$. But the zinc 213 nm line has its strongest correlation (-0.478)

with DF2, therefore it is listed lower on the list than the copper line, because function 2 accounts for less of the overall variance than does function one. This does not indicate that the 213 nm zinc line does not correlate with DF1, it indicates that it correlates most strongly with DF2. Similarly, the copper line at 204 nm has a correlation with DF1 of .133, yet it is listed last in the structure matrix, because it is most strongly correlated (-.596) with DF3, which accounts for less of the variance than DF1 or DF2. The “a” next to the Ca 393 nm line indicates it was determined that the line not used in the analysis most likely due to statistical insignificance. Although included, the sodium lines played very little role in the discrimination, as one would expect.

Table 4.3: The structure matrix for the DFA of four brass alloys ablated in an argon atmosphere

	Function		
	1	2	3
C247.856	-.620*	-.054	-.015
Pb283.305	-.423*	-.089	.029
Pb368.347	-.418*	-.074	-.068
Pb363.957	-.408*	-.062	-.124
Pb217.000	-.362*	-.106	.157
Ca393.366 ^a	-.320*	-.041	-.191
Al396.152	-.319*	-.020	-.234
Na588.995	-.270*	-.028	-.150
Na589.593	-.240*	-.027	-.133
Cu219.227	.212	.528*	.115
Zn213.855	.457	-.478*	.193
Zn472.215	.060	-.356*	-.100
Cu218.177	.182	.293*	.161
Cu282.437	.070	.213*	-.048
Cu204.380	.133	.124	-.596*

From Figure 4.2, it can be seen that there is an obvious difference between group two and the other three brass samples. The structure matrix of this analysis shown in Table 4.3 indicates it was primarily the lead content that was used to construct DF1. This result confirms the fact that alloy 2 contained more lead than the other alloys as shown in Table 4.1. According to this analysis, despite possessing similar spectra, the DFA of samples tested in Ar achieved an overall cross-validation (leave-one-out) classification accuracy of 99.5% (199 out of 200 correct), which indicates the benefit of using LIBS as a technique for the rapid identification of alloys and discrimination between brass samples.

In order to study the effect of helium on our discrimination, the same samples were tested in a helium environment. Figure 4.3 shows the results of the DFA performed on LIBS spectra acquired from the four brass samples. The DFA analysis showed that 91.5% of the variance between groups was represented by DF₁, 6.1% by DF₂, and 2.3% by DF₃. In the leave-one-out analysis, a classification accuracy of 97.0% (194 out of 200 correct) was achieved. In this analysis different correlations between spectral lines were used to construct different discriminant functions. This can be explained by the different relative emission intensities from the various elements (observed in Figure 4.1) due to different plasma temperatures compared to what was observed in the argon environment. The structure matrix of the four samples tested in the helium environment, Table 4.4, shows this difference.

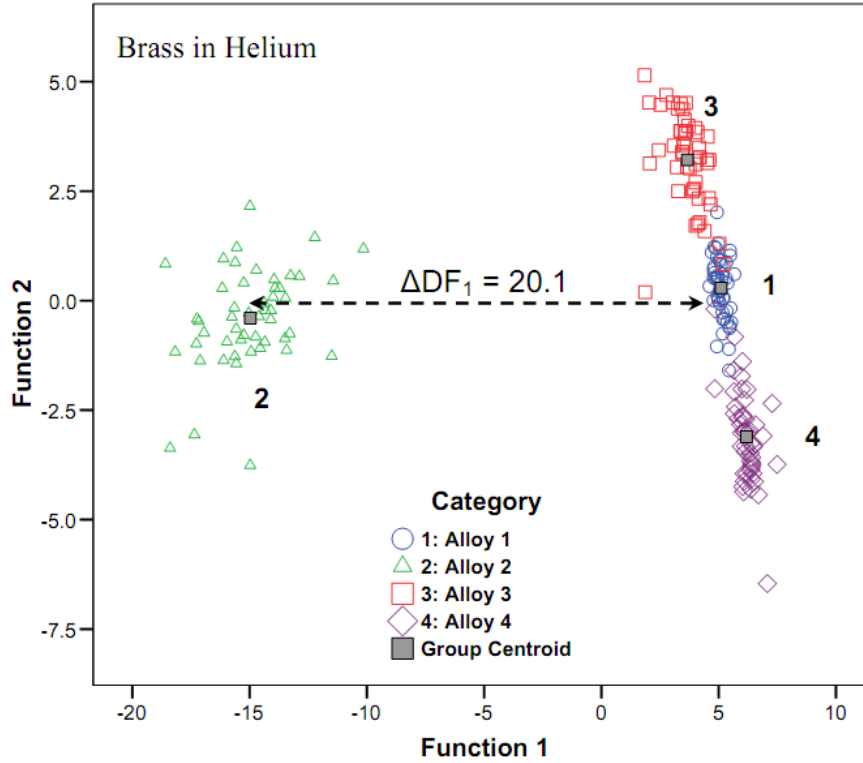


Figure 4.3: A discriminant function analysis plot showing the first two discriminant function scores of LIBS spectra obtained from four brass samples in helium.

Table 4.4: The structure matrix for the DFA of four brass alloys ablated in a helium atmosphere

	Function		
	1	2	3
Pb283.305	-.707*	.170	.383
Ca393.366 ^a	-.686*	-.235	-.031
Pb368.347	-.680*	.035	.250
Pb363.957	-.663*	-.023	.187
Al396.152	-.608*	-.233	-.055
Na588.995	-.540*	-.183	-.085
Pb217.000	-.527*	.130	.318
Na589.593	-.463*	-.162	-.053
Cu204.380	.136*	-.047	.136
Cu282.437	.137	-.250*	.171
Cu218.177	.126	-.192*	.109
C247.856	-.296	-.034	.330*
Zn472.215	.068	.179	-.321*
Cu219.227	.150	-.079	.185*
Zn213.855	.067	.031	-.117*

When the two 15-line spectral fingerprints obtained from the samples tested in both argon and helium were combined to form a single 30-spectral line fingerprint for the alloy, an overall 100% classification accuracy was achieved. DFA plots of the four alloys as shown in Figure 4.4 showed that the distances between the group centroids (center of mass for the distribution of measurements) were increased. This is indicative of an enhancement in the ability to distinguish one alloy from another. For example, the distance between the centroids of alloy one and alloy two was increased by almost 100% over what was observed in helium and by 15% over what was observed in argon. Although alloys 1 and 3 appear unchanged, the distance between the centroids of alloy 1 and alloy 3 increased by over 65% in function 3 (not shown in Figures 4.2 or 4.4) over what was observed in argon. Although DF3 is typically not plotted, it does indeed contribute to discrimination and classification. Also, the scatter of measured data points around

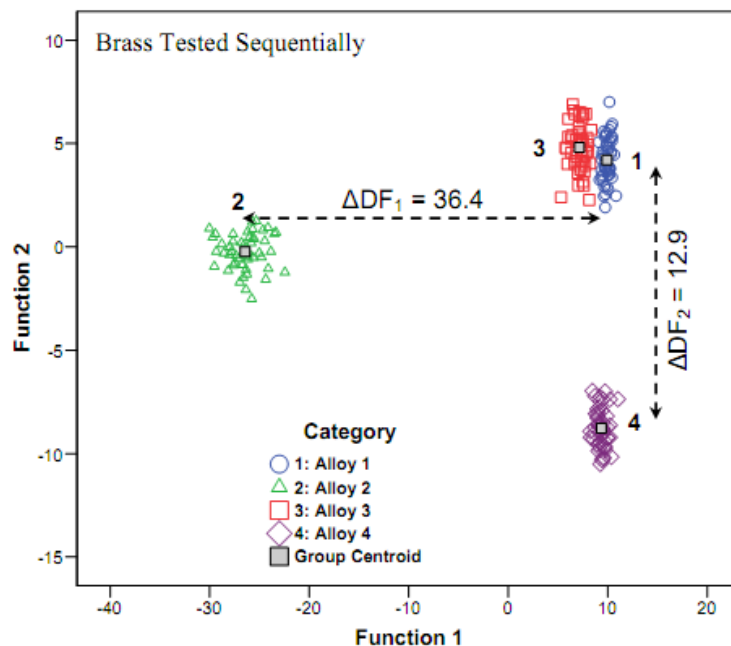


Figure 4.4: A discriminant function analysis plot of brass samples tested in both gases sequentially. This data did not take substantially longer to acquire than that taken in a single gas atmosphere and discrimination is enhanced.

the centroids was reduced. This result showed the benefit of using dual ambient gases in sequence for an enhancement of discrimination between the samples. Because our sample chamber was small, these gases could be quickly cycled in and out in about a minute, adding very little complexity to the analysis for a modest increase in discrimination ability.

An increase in the discrimination of brass (as evidenced by the slight increase in classification accuracy and the increase in the separation of group means) was seen, but was not large due to the ease with which the samples could be discriminated in argon alone due to the differences in the samples.

4.3.2 Bacteria Results

Our previous results using a DFA to identify/discriminate LIBS spectra obtained from bacterial samples showed that bacteria can be efficiently discriminated when tested in air or in argon or helium. However, the highly similar nature of the spectra from different strains of a single species could eventually limit the ability to identify samples in a mixed, contaminated, or low concentration sample. Based on the previous study with the Cu-Zn brass alloys, a similar study was performed to demonstrate an enhanced discrimination between two strains of *Escherichia coli* (a Gram-negative bacterium) and a Gram-positive bacterium when LIBS spectra were sequentially obtained in two different gas environments. The intensities of 13 emission lines from Mg, Ca, P, Na, and C were used in the discriminant function analysis.

Figure 4.5(a) shows the results of the DFA performed on LIBS spectra acquired from *E. coli* HF4714 and *E. coli* C and *Streptococcus mutans* in an argon environment. It is obvious from the plot that the bacterial strains are reproducibly different from each other. The analysis

showed that 82% of the variance in this test was in DF_1 and 18% of the variance was contained in DF_2 . The structure matrix showed that carbon and magnesium were mainly used in DF_1 to discriminate bacteria from each other while phosphorus and calcium were responsible for the discrimination in DF_2 . In this analysis 96.7% (87 out of 90) of all samples were correctly classified.

The same samples were then ablated in a helium atmosphere. Figure 4.5(b) shows a DFA plot for the *E. coli* and *S. mutans* specimens. In this analysis, 61% of the variance between groups was represented by DF_1 and 39% by DF_2 . Of the original grouped cases, 97.8% of all data sets (88 out of 90) were correctly classified. In addition to that, the structure matrix showed sodium and magnesium were responsible for the discrimination in DF_1 while calcium and phosphorus concentrations played a stronger role in the discrimination in DF_2 .

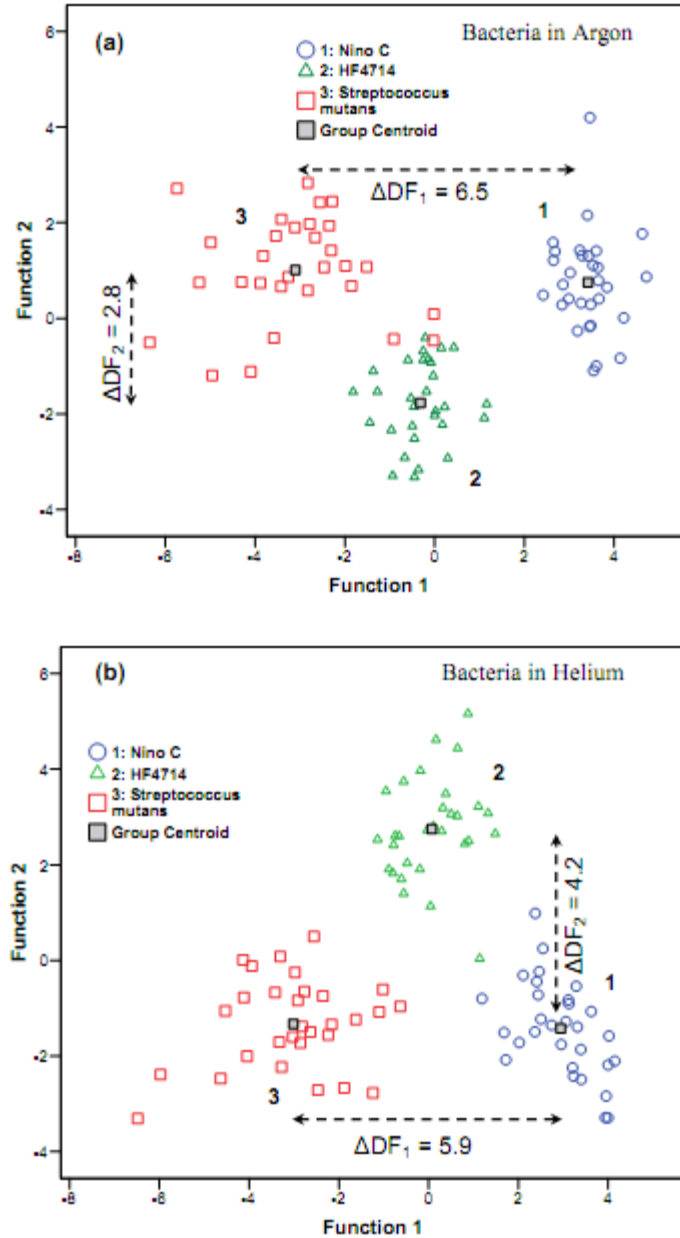


Figure 4.5: (a) A discriminant function analysis plot of LIBS spectra from bacterial specimens of two strains of *E. coli* (Nino C and HF4714) and *Streptococcus mutans* ablated in an argon environment. (b) A DFA of the same three specimens ablated in a helium environment.

When the data from the samples tested sequentially in both gases were combined to create a 26-emission line spectral fingerprint, a 100% classification accuracy (90 out of 90) was achieved. The results of this DFA are shown in Figure 4.6. Compared to testing in either gas singly, the distances between the group centroids in the DFA were increased, and compared to the brass samples, the dual-gas testing procedure had a much more pronounced effect on the separation of the group centroids. For example, the distance in DF1 between the centroids of group one (*E. coli* C) and group three (*Strep. mutans*) was increased by 70% over what was observed in helium and by 56% over what was observed in argon. The distance in DF2 between the centroids of group two and groups one and three increased by 89% over what was observed in argon and 26% over what was observed in helium. As was observed in the brass samples, the scatter of measured data points around the centroids was also reduced.

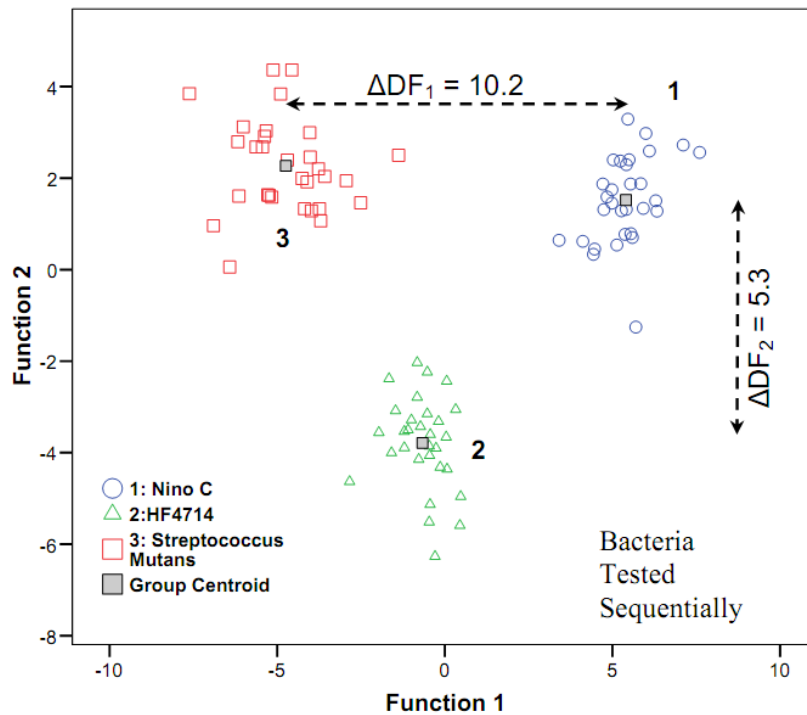


Figure 4.6: A discriminant function analysis plot of three bacterial samples tested sequentially in both argon and helium. Enhanced discrimination relative to testing in either gas individually is observed.

This result demonstrates that the use of sequential dual-gas testing is most appropriate when the specimens are highly similar and difficult to discriminate. In such situations, even small gains in discrimination and classification accuracy may be advantageous. The improvement in classification accuracy involved only a small number of spectra that had previously been incorrectly classified, so future tests are called for where a lower classification accuracy (50% or less) is observed when a single gas is used. Currently, all of our bacterial specimens classify with well over 90% accuracy, typically, so the use of sequential dual-gas testing is not called for.

4.4 Conclusions

The emission characteristics of laser-induced plasmas are strongly influenced by the gaseous environment in which the plasma is created. Noble gases such as argon or helium are often used to improve emission and reproducibility in such plasmas. LIBS spectra from four alloys of brass and three different bacterial specimens were obtained from samples ablated sequentially in argon and then in helium. A small purge box allowed these measurement to be taken in almost the same amount of time that testing in one gas only would require. The highest spectral line intensities were obtained in argon which can be related to the higher plasma temperature.

When emission intensities from spectra acquired sequentially in argon and helium were combined to form new spectral fingerprints, an enhanced DFA discrimination was observed as evidenced by an increase in the distances between the group centroids of all the samples (in both the brass and the bacterial systems) and a reduction of the observed scatter of measured data

points around the group centroids. Most importantly, the absolute accuracy of the identification/discrimination was increased from 99% to 100% in the brass system and 97% to 100% in the bacterial system. As expected, the absolute increase in classification accuracy was smaller for the brass samples, because of the relative ease with which they could be discriminated by either gas alone. The increase in the classification accuracy of the bacterial specimens however was significant, particularly the increase in the separation between group means that was an obvious result.

This result could be useful for future identification or discrimination between several species or strains of bacteria that are highly similar to each other. In systems where large differences exist between samples and discrimination based on the observed LIBS spectrum is relatively easy, this dual-gas technique possesses little advantage over a LIBS analysis in pure argon alone.

4.5 Summary

In summary, Four Cu-Zn brass alloys with different stoichiometries and compositions were analyzed by laser-induced breakdown spectroscopy (LIBS) using nanosecond laser pulses. The intensities of 15 emission lines of copper, zinc, lead, carbon, and aluminum (as well as the environmental contaminants sodium and calcium) were normalized and analyzed with a discriminant function analysis (DFA) to rapidly categorize the samples by alloy. The alloys were tested sequentially in two different noble gases (argon and helium) to enhance discrimination between them. When emission intensities from samples tested sequentially in both gases were combined to form a single 30-spectral-line “fingerprint” of the alloy, an overall

100% correct identification was achieved. This was a modest improvement over using emission intensities acquired in argon gas alone. A similar study was performed to demonstrate an enhanced discrimination between two strains of *Escherichia coli* (a Gram-negative bacterium) and a Gram-positive bacterium. When emission intensities from bacteria sequentially ablated in two different gas environments were combined, the DFA achieved a 100% categorization accuracy. This result showed the benefit of sequentially testing highly-similar samples in two different ambient gases to enhance discrimination between the samples.

REFERENCES

- ¹ C. Pasquini, J. Cortez, L. Silva and F. Gonzaga, "Laser induced breakdown spectroscopy," *Journal of the Brazilian Chemical Society* **18**, 463-512 (2007).
- ² D. Cremers and L. Radziemski, *Handbook of Laser-Induced Breakdown Spectroscopy*, (John Wiley & Sons Ltd.) 2006.
- ³ J.P. Singh and S.N. Thakur, Eds., *Laser-Induced Breakdown Spectroscopy*, (Elsevier, Amsterdam) 2007.
- ⁴ V. Detalle, M. Sabsabi, L. St-Onge, A. Hamel, and R. Héon, "Influence of Er:YAG and Nd:YAG wavelength on laser-induced breakdown spectroscopy measurements under air or helium atmosphere," *Applied Optics* **42**, 5971-5977 (2003).
- ⁵ W. Sdorra and K. Niemax, "Basic investigations for laser microanalysis: III. Application of different buffer gases for laser-produced sample plumes," *Mikrochimica Acta* **107**, 319-327 (1992).
- ⁶ M. Kuzuya, H. Matsumoto, H. Takechi, and O. Mikami, "Effect of laser energy and atmosphere on the emission characteristics of laser-induced plasmas," *Applied Spectroscopy* **47**, 1659-1664 (1993).

- ⁷ R. Wisburn, I. Schechter, R. Niessner, H. Schroder, and K. Kompa, "Detector for trace elemental analysis of solid environmental samples by laser plasma spectroscopy," *Analytical Chemistry* **66**, 2964-2975 (1994).
- ⁸ M. Adamson, A. Padmanabhan, G. J. Godfrey, and S. J. Rehse, "Broadband laser-induced breakdown spectroscopy at a water/gas interface: A study of bath gas-dependent molecular species," *Spectrochimica Acta Part B* **62**, 1348-1360 (2007).
- ⁹ J. Diedrich, S.J. Rehse, and S. Palchadhuri, "*Escherichia coli* identification and strain discrimination using nanosecond laser-induced breakdown spectroscopy," *Applied Physics Letters* **90**, 163901 (2007).
- ¹⁰ J. Diedrich, S.J. Rehse, and S. Palchadhuri, "Pathogenic *Escherichia coli* strain discrimination using laser-induced breakdown spectroscopy," *Journal of Applied Physics* **102**, 014702 (2007).
- ¹¹ S.J. Rehse, J. Diedrich, and S. Palchadhuri, "Identification and discrimination of *Pseudomonas aeruginosa* bacteria grown in blood and bile by laser-induced breakdown spectroscopy," *Spectrochimica Acta Part B* **62**, 1169-1176 (2007).
- ¹² S.J. Rehse, N. Jeyasingham, J. Diedrich, and S. Palchadhuri, "A membrane basis for bacterial identification and discrimination using laser-induced breakdown spectroscopy," *Journal of Applied Physics* **105**, 102034 (2009).

CHAPTER 6

The effect of bacterial environmental and metabolic stresses on a LIBS-based identification of *E. coli* and *S. viridans*

6.1 Introduction

Recent results have shown progress toward realizing the potential of a rapid LIBS point-of-contact diagnostic.^{1,2,3,4} The diagnostic has exhibited excellent sensitivity and specificity, as evidenced by a 100% accuracy in a blind identification trial of four different methicillin-resistant *Staphylococcus aureus* (MRSA) strains and a non-pathogenic *E. coli* strain and has exhibited a low limit of identification (LOI) evidenced by achieving a 100% accuracy in discriminating only 2500 bacterial cells of *Mycobacterium smegmatis* from a genetically modified mutant of the same strain.^{5,6} Work remains to be done, however, to investigate the loss of specificity and the increase in the LOI that may arise due to naturally occurring biodiversity in live (as opposed to freeze-dried or “lyophilized”) bacterial cells, biochemical variations that may arise due to environmental influences during growth, and to develop protocols for sample preparation that will minimize risks to health-care professionals. To this end, in this chapter we discuss the effect on bacterial identification of: (1) intentionally changing the nutrition medium environment during the growth of closely-related *E. coli* strains; (2) killing or inactivating the bacteria by bactericidal UV irradiation and autoclaving prior to LIBS testing; and (3) depriving the bacterial cells of nutrition sources or carbon-sources for extended periods of time (nutrient deprivation or “starvation”) prior to LIBS testing,

representing changes that may occur when bacterial cells are tested on an abiotic or inert surface.

6.2 LIBS Instrumentation

The experimental setup used to perform LIBS on the bacteria specimens has been described in detail in chapter 3.^{6,7} All the LIBS spectra were acquired under the same conditions i.e. $\tau_D = 2 \mu\text{s}$ after the ablation pulse with an integration τ_w of 20 μs duration. Moreover, all the bacteria, with concentration 10^9 bacteria/mL, analyzed in this chapter were mounted again on a 1.4% nutrient-free bacto-agar substrate as a semi-liquid droplet. Specifically, a ten μL micro-pipette was used to withdraw the bacteria-containing liquid and deposit the suspension on the bacto-agar. After approximately thirty minutes, the liquid was absorbed by the agar, leaving a transparent thin. High-resolution optical microscopy was performed on these specimens before and after LIBS testing and a representative micrograph is shown in Figure 6.1. Figure 6.1(a) shows a 5x magnification of the bacterial bed, showing the magnification scale and an approximate size of the laser spot for reference. Figure 6.1(b) shows a 100x magnification with the same scale and laser spot size for reference. Individual *E. coli* bacteria are visible within the laser beam diameter. A conservative estimate of the number of bacterial cells ablated per sampling location based on our initial knowledge of the titer of the semi-liquid pellet, the volume of liquid deposited, the area of the thin film, and the area of the focused laser spot size is approximately 1500.⁶

The LIBS spectra acquired from these bacteria were similar to those reported by us and others for other bacteria,^{1,8,9} being dominated by emission from trace inorganic metals and salts, specifically calcium and magnesium, as well as phosphorus, carbon, and sodium. The absolute emission intensity (integrated area under the curve) for thirteen lines in these five elements was recorded for each spectrum and divided by the sum of all thirteen intensities (the total spectral power) to normalize the data. These thirteen normalized intensities were used for the analysis of all bacterial samples under this study using DFA.^{10,11}

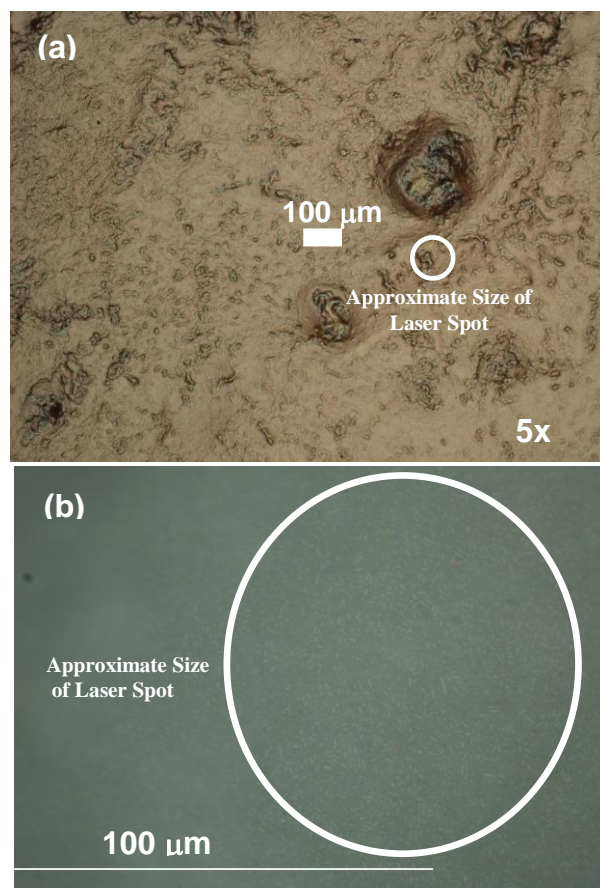


Figure 6.1: Optical micrographs of the bacterial bed mounted on an agar substrate. (a) A 5x magnification of the bacterial bed showing the magnification scale. Some non-uniformities in the bacterial bed can be seen. (b) A 100x magnification with the magnification scale. Individual *E. coli* bacteria are visible within the laser beam diameter.

6.3 Nutrition Medium Environment: Effect on *E. coli* Strain Discrimination

LIBS spectra from three similar strains of non-pathogenic *E. coli* (C, HF4714, and ATCC 25922) were acquired as described earlier. In addition to these three specimens, one specimen of *E. coli* C was cultured on a bile salts-containing nutrient medium (a MacConkey agar with a 0.01% concentration of deoxycholate). Trypticase-soy agar is a basic nutrition medium used for culturing most types of bacteria. It is also used as an initial growth medium for different purposes such as developing pure cultures. Conversely, MacConkey agar is a selective medium which inhibits the growth of Gram-positive bacteria due to the presence of bile salts and crystal violet. Figure 6.2 is a DFA plot showing the first two discriminant function scores of a DFA performed on spectra acquired for the four specimens cultured with these media. Regardless of nutrition medium, the *E. coli* specimens were effectively discriminated from each other on the basis of their DF_1 and DF_2 scores. The specimens of *E. coli* C cultured on the two different media (TSA and MacConkey) were still closely grouped despite possible membrane alteration due to the detergent action of the deoxycholate on the lipid bilayer outer membrane of the *E. coli*.³ In this DFA, 100% of the bacteria were correctly classified by strain, regardless of nutritional environmental conditions. This analysis is therefore suggestive that clinical specimens obtained from infected persons could be identified on the basis of their LIBS spectra independent of the chemical environment present in the host. While this data is promising, extensive blind trials on clinical specimens isolated from patients positively diagnosed via other methods are required to confirm this conclusion.

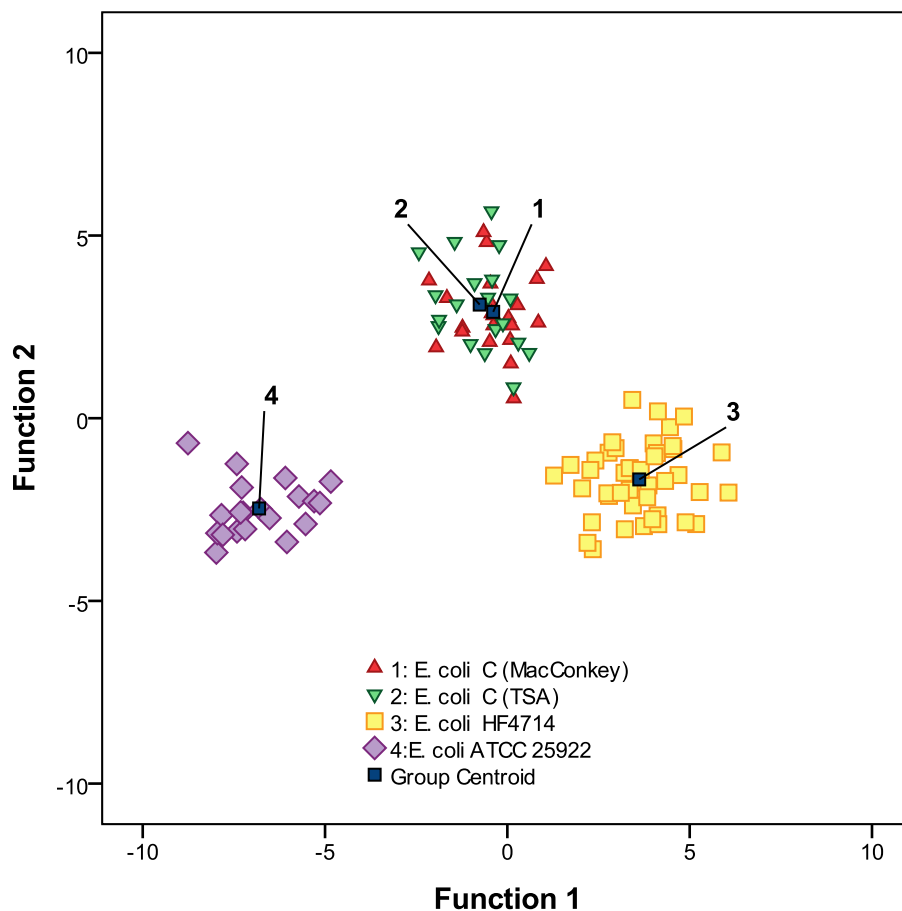


Figure 6.2: A DFA plot of the LIBS spectra from four *E. coli* strains. The C strain was cultured on two different nutrition media, including a bile salts-containing MacConkey agar and a trypticase soy agar medium. These two specimens of *E. coli* C cultured on different media were indistinguishable from each other and were discriminated with 100% accuracy from *E. coli* strain HF4714 and *E. coli* strain ATCC 25922, both of which were cultured on the trypticase soy agar medium.

6.4 LIBS Identification of Live and Dead Bacteria

To study whether the LIBS spectral pattern is dependent upon the bacterial phase of growth, bacteria were prepared in three ways prior to LIBS testing. Live bacteria were harvested while reproducing in log-phase and then tested as described earlier. Autoclaved bacteria were autoclaved in a standard microbiological autoclave to kill the

bacteria prior to mounting on the agar substrate. This is the standard method for rendering a biological specimen completely safe prior to disposal. Specifically, a 1.5 mL tube of *E. coli* C was subjected to high pressure steam at 121 °C for 45 minutes. To assure the total death of bacteria, a small number of these bacteria were picked up on a sterile loop for streaking on a standard TSA plate after autoclaving. No evidence of any bacterial growth was observed after incubation of this TSA plate at 37 °C for 24 hours, indicating death of all the bacterial cells in the autoclaved samples. Autoclaving the bacteria after mounting the cells on the nutrient-free bacto-agar substrate would have resulted in melting of the agar, so this test was not conducted.

UV-irradiated bacteria were mounted on the nutrient free agar as usual, but after absorption of the fluid by the agar, the specimen was irradiated for 20 minutes by 248 nm radiation from a bactericidal lamp. Such lamps are commonly used in microbiology to disinfect surfaces after cleaning. Exposure to this UV light does not technically “kill” the bacteria, but it does destroy their ability to divide, rendering them harmless to the personnel working with them.

In all cases, multiple pads of bacteria were placed on a single agar substrate. In the autoclave test, one pad was used for LIBS testing and one pad was not ablated as a control. In the case of the UV-exposed specimens, four pads were placed on the substrate. Two were exposed to UV light and two were not. One UV-exposed and one unexposed pad were tested with LIBS, leaving two non-LIBS tested pads as a control. All control pads were tested for activity via the standard microbiological method of restreaking and counting the number of colony forming units (CFU) to confirm the inactivation of greater than 99% of the bacteria in the specimen.

Figure 6.3(a) shows the DFA of the LIBS spectra acquired from three specimens of *E. coli* C (“live”, “autoclaved,” and “UV”), one specimen of *E. coli* strain ATCC 25922, and one specimen of *Mycobacterium smegmatis*, a genetically modified strain of an organism commonly used as a surrogate for *M. tuberculosis* utilized by us in previous studies (denoted as strain “TA”). The results of the DFA show that all three *E. coli* C specimens possessed nearly identical LIBS spectra, and were identified 100% of the time as *E. coli* C regardless of whether they were live, dead, or inactivated. All three specimens were indistinguishable and showed excellent discrimination from the closely-related *E. coli* ATCC 25922. The two *E. coli* strains possessed similar LIBS spectra, as evidenced by the similarity in their discriminant function one scores in Figure 6.3(a), compared to the *Mycobacterium* specimens. Despite their similarity, the two *E. coli* strains were well-separated and classifiable with 100% accuracy.

This result is highly suggestive that LIBS testing can provide accurate results on specimens rendered innocuous via commonly available non-chemical anti-microbial procedures. Moreover, not only can this analysis be performed with no significant decrease in accuracy, but no decrease in the intensity of the LIBS signal was observed. Figure 6.3(b) shows the total spectral power (in arbitrary units) for the “live” and UV-inactivated specimens. Also shown is the average of all the data points for each specimen category and the 1σ standard deviation (a measure of total LIBS signal fluctuation). The total spectral powers for both the “live” and “UV” specimens were the same within error and the sample sets exhibited the same scatter. While spectral variations of absolute intensities on the order of 16% to 21% are slightly larger than the <15% that is expected

in reproducible LIBS data, it is not unusual for our LIBS experiments on bacteria where specimen mounting uniformity plays a role.

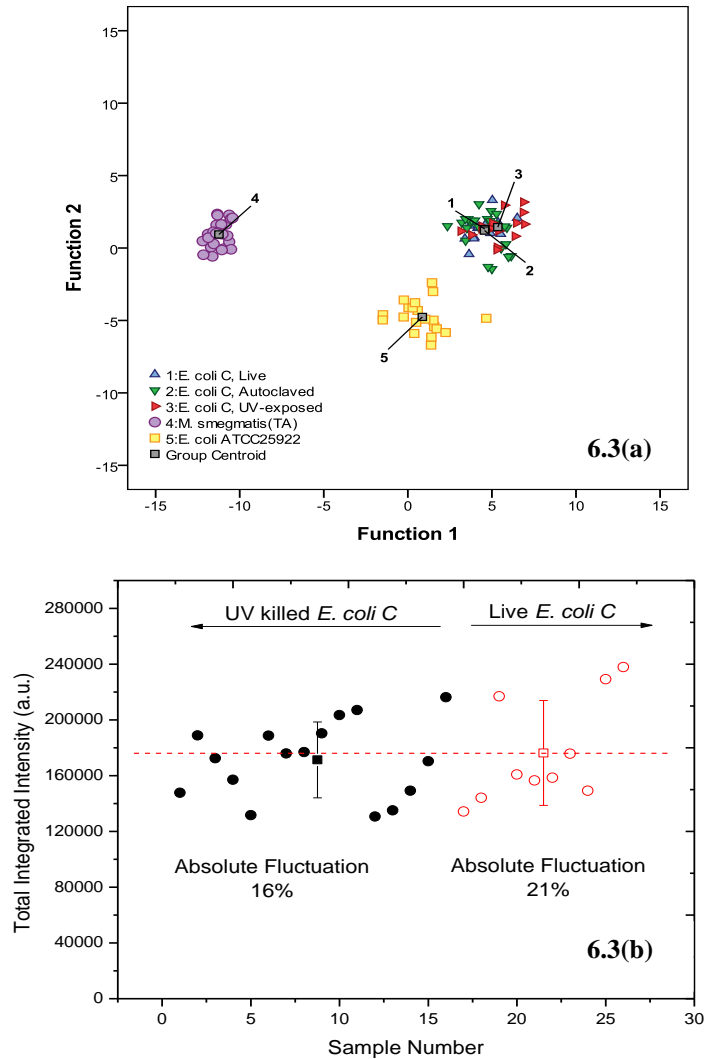


Figure 6.3(a): A DFA of three specimens of *E. coli* strain C, one specimen of *E. coli* strain ATCC 25922, and one specimen of *M. smegmatis*. Group 1 (“live”) was tested while alive. Group 2 (“autoclaved”) was killed by autoclaving prior to testing. Group 3 (“UV”) was inactivated via exposure to 248 nm UV irradiation prior to testing. Figure 6.3(b): The total spectral power (in arbitrary units) of the individual spectra from the live and UV-irradiated specimens. Also shown is the average of all the data points for each specimen category (the square symbol) and the 1 σ standard deviation of the measurements (a measure of total LIBS signal fluctuation). The total spectral powers of the two specimens were the same within error and the sample sets exhibited similar scatter.

The *E. coli* specimens tested in Figure 6.3 were Gram-negative and non-pathogenic. To illustrate the universality of this result, this test was repeated with specimens of Gram-positive bacteria, specifically an avirulent derivative of the pathogen *Streptococcus viridans*. Figure 6.4(a) shows the DFA of the three specimens of *S. viridans* treated with the anti-bacterial methods described above, in addition to one specimen of *E. coli* ATCC 25922, and one specimen of *M. smegmatis*. From the DFA plot, it can be seen easily that all three specimens of *S. viridans* possessed nearly identical LIBS spectra. This result implies that a bacterial sample can be accurately identified whether it is pathogenic or non-pathogenic and regardless of whether it is alive or killed. This suggests the possibility of reducing the biosafety hazard level of the LIBS-based test to biosafety level-1 (BSL-1) by killing or inactivating the bacteria prior to LIBS testing. This will ultimately save time and expense in a clinical diagnostic test. The total spectral powers for the spectra from “live” and UV-inactivated specimens of *S. viridans* were calculated and compared. In Figure 6.4(b), the average of the total spectral power for the two types of specimens, (“live” and “UV”) is the same, as is their scatter about the mean value, indicating again that the LOI of this test was not affected by this treatment of the bacteria. All tests were conducted with no loss of useful signal.

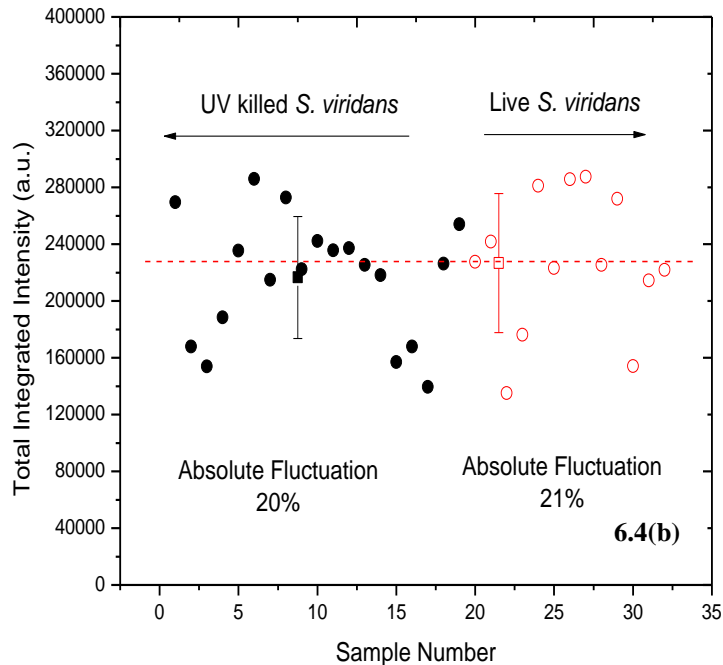
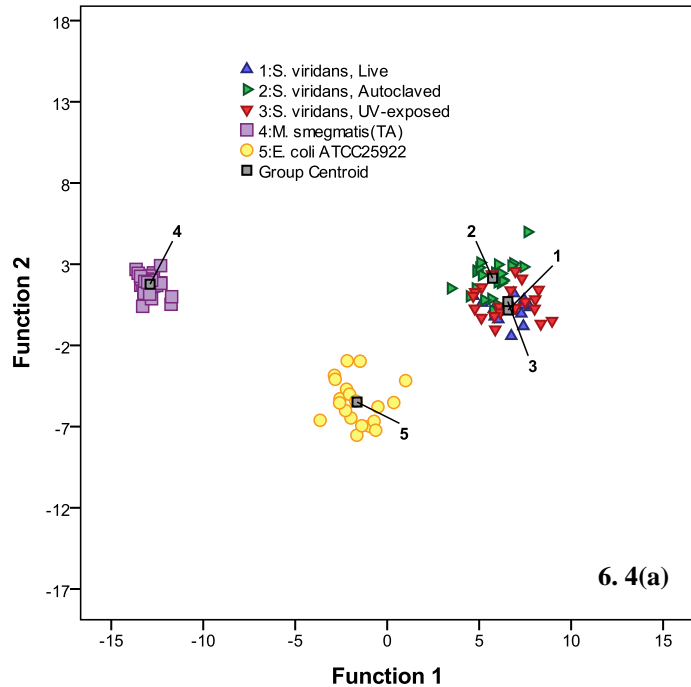


Figure 6.4(a): A DFA of three specimens of *S. viridans*, one specimen of *E. coli* strain ATCC 25922, and one specimen of *M. smegmatis*. Group 1 (“live”) was tested while alive. Group 2 (“autoclaved”) was killed by autoclaving prior to testing. Group 3 (“UV”) was inactivated via exposure to 248 nm UV irradiation prior to testing. Figure 6.4(b): The total spectral power (in arbitrary units) of the individual spectra from the live and UV-irradiated specimens. Also shown is the average of all the data points for each specimen category (the square symbol) and the 1σ standard deviation of the measurements (a measure of total LIBS signal fluctuation). The total spectral powers of the two specimens were the same within error and the sample sets exhibited similar scatter.

6.5 LIBS Identification of Pathogenic and Non-Pathogenic Bacteria under Nutrient Deprivation Conditions

To test the effect that depriving the bacteria of nutrition (“starvation”) had on the bacterial LIBS spectrum, specimens of the non-pathogenic *E. coli* C and the pathogenic *S. viridans* were prepared in the standard manner detailed above, mounted on nutrient-free agar substrates, and placed in a 21° C isolated environment. LIBS spectra were then acquired one day, six days, and nine days after mounting the *S. viridans* specimens. LIBS spectra were acquired one, four, six, and eight days after mounting the *E. coli* C specimens. The bacteria did not die during this starvation trial, but having no external nutrients to consume, they would have initially consumed internal reserves of nutrients then entered a dormant non-reproducing state. In the dormant state, the bacterial cells are metabolically active but cannot be cultured by known laboratory techniques.¹²¹³ All LIBS spectra were analyzed with a DFA. The results are shown in Figure 6.5. 100% of the starved *E. coli* C specimens were classified as *E. coli* C regardless of the time of starvation and 100% of the starved *S. viridans* specimens were correctly classified as *S. viridans*. Therefore, in our experiment we found that the bacteria retained indistinguishable LIBS spectra even after they had entered a metabolically dormant, non-culturable state. In addition, the total spectral power of the bacterial spectra for both *E. coli* C and *S. viridans* did not significantly decrease from the first day to the last day of starvation. Therefore we conclude that the LOI is independent of the time the bacterial specimens have spent in a nutrient-free environment.

For completeness, and in an attempt to “confuse” the DFA, the autoclaved and UV-irradiated specimens from the previous study were included in the analysis shown in Figure 6.5.

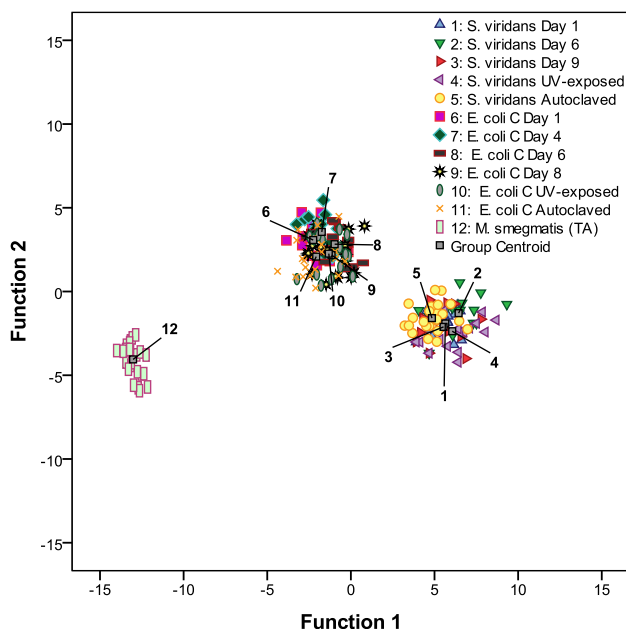


Figure 6.5: A DFA plot of the spectra from many different bacterial specimens: starved *S. viridans* (3 different starvation durations), autoclaved *S. viridans*, UV-irradiated *S. viridans*, starved *E. coli C* (4 different starvation durations), autoclaved *E. coli C*, UV-irradiated *E. coli C*, and *M. smegmatis*. No significant differences were observed between the LIBS spectra of a given species acquired from bacterial specimens that had been deprived of a metabolic source, autoclaved, or exposed to bactericidal UV light. For all three species of bacteria, 100% of the spectra were correctly classified and discriminated from the other species.

In this analysis, no *E. coli C* spectra were identified as anything but *E. coli C* (100%) and no *S. viridans* spectra were identified as anything but *S. viridans* (100%). All the *M. smegmatis* LIBS spectra were correctly classified. The results of this test and the previous two tests are summarized in Table 6.1, which shows the identification accuracies of all three tests described in this paper (nutrition medium test,

autoclaved/UV/live test, and starvation test). Based on Table 6.1, one can see that the LIBS spectra of both *E. coli* C and *S. viridans*, chosen to give a representative cross-section of both Gram-negative and Gram-positive bacteria as well as pathogenic and non-pathogenic bacteria, are not altered by a wide variety of biologically diverse conditions that the bacteria may be exposed to prior to LIBS testing.

Table 6.1: The LIBS classification accuracies of the three tests described in this article.

Nutrition Medium Test		
Specimens	# of Spectra Tested	Accuracy
<i>E. coli</i> C	20	100%
<i>E. coli</i> HF4714	44	100%
<i>E. coli</i> ATCC 25922	20	100%
<i>M. smegmatis</i> (TA)	25	100%
<i>S. viridans</i>	15	100%
Live / UV-irradiation / Autoclave Test		
Specimens	# of Spectra Tested	Accuracy
<i>E. coli</i> C/ UV- exposed	16	100%
<i>E. coli</i> C/ Autoclaved	24	100%
<i>S. viridans</i> / UV- exposed	20	100%
<i>S. viridans</i> / Autoclaved	23	100%
Starvation Test		
Specimens	# of Spectra Tested	Accuracy
<i>E. coli</i> C Day 1	15	100%
<i>E. coli</i> C Day 4	15	100%
<i>E. coli</i> C Day 6	16	100%
<i>E. coli</i> C Day 8	18	100%
<i>S. viridans</i> Day 1	14	100%
<i>S. viridans</i> Day 6	15	100%
<i>S. viridans</i> Day 9	14	100%

6.6 Conclusions

The specificity and sensitivity of a LIBS-based *E. coli* strain identification was not changed by culturing the bacteria on different media prior to LIBS testing. The LIBS-based DFA was also not dependent upon the metabolic activity of the bacteria, whether live, autoclaved, or inactivated by UV exposure. This was demonstrated for a representative species of both Gram-negative and Gram-positive bacteria. In addition, the signal-to-noise of the bacterial LIBS spectra was not reduced, indicating that the LOI of this test was not increased in any statistically significant amount by treatment with these common bactericidal techniques. *E. coli* bacteria that were deprived of nutrition for up to 8 days prior to LIBS testing were still identifiable and were discriminated from the pathogenic Gram-positive *S. viridans* which were deprived of nutrition for up to 9 days with 100% accuracy. In all three of these tests, all LIBS spectra were correctly classified. The signal-to-noise of the bacterial spectra was not decreased in any significant way due to the nutrition deprivation conditions, indicating that this also would not increase the LOI of the LIBS test.

We believe that these results should be fairly universal for many types of bacteria, despite our testing of only two species (one Gram-negative and one Gram-positive). Fundamentally, these processes (particularly UV irradiation, autoclaving, and starvation) do not change the elemental composition of the bacteria on which the classification is based. The most significant change induced by most of our stressors involved the hydration or water content of the cell. However, we do not use lines of hydrogen or oxygen in our analysis, therefore the test is relatively insensitive to hydration. More likely, sample hydration would effect the strength of the plasma emission and the

temperature of the LIBS plasma, which could result in varying emission ratios observed from samples with an otherwise identical composition. This was the motivation for the experiments described herein. Our data lead us to conclude that such hydration-induced plasma-formation differences, if present, did not alter the LIBS plasma enough to significantly disrupt accurate classification.

Lastly it is worth noting that the stressor most likely to truly alter bacterial elemental composition was the composition of the medium in which the bacteria reproduced. That the nutrient medium did not significantly alter the LIBS spectrum is not surprising, as many bacteria can actually only survive within a narrow window of environmental conditions, including temperature, pH, osmotic pressure, and ionic concentration. All nutrient rich media are optimized for bacterial growth, therefore the range of environmental conditions is not as great as supposed. As well, it is likely that the bacteria cannot survive if their elemental composition is significantly altered beyond a narrow range, particularly given the important role that the divalent cations of Ca and Mg play in regulating cell function and membrane porosity. Undoubtedly media could be obtained or created which would significantly alter bacterial elemental concentrations while still encouraging growth. However, because we are attempting to develop a biomedical diagnostic, we are primarily interested in testing bacteria in conditions that they are likely to experience *in vivo*, not in arbitrary or unrealistic chemical environments. This paper has shown that for a variety of bacterial stressors likely to be encountered environmentally or administered intentionally, the LIBS-based diagnostic retains its selectivity and sensitivity.

6.7 Summary

In this chapter we investigated the effect that adverse environmental and metabolic stresses have on a laser-induced breakdown spectroscopy (LIBS) identification of bacterial specimens. Single-pulse LIBS spectra were acquired from a non-pathogenic strain of *Escherichia coli* cultured in two different nutrient media: a trypticase soy agar and a MacConkey agar with a 0.01% concentration of deoxycholate. A chemometric discriminant function analysis showed that the LIBS spectra acquired from bacteria grown in these two media were indistinguishable and easily discriminated from spectra acquired from two other non-pathogenic *E. coli* strains. LIBS spectra were obtained from specimens of a non-pathogenic *E. coli* strain and an avirulent derivative of the pathogen *Streptococcus viridans* in three different metabolic situations: live bacteria reproducing in the log-phase, bacteria inactivated on an abiotic surface by exposure to bactericidal ultraviolet irradiation, and bacteria killed via autoclaving. All bacteria were correctly identified regardless of their metabolic state. This successful identification suggests the possibility of testing specimens that have been rendered safe for handling prior to the LIBS identification. This would greatly enhance personnel safety and lower the cost of a LIBS-based diagnostic test. LIBS spectra were obtained from pathogenic and non-pathogenic bacteria that were deprived of nutrition for a period of time ranging from one day to nine days by deposition on an abiotic surface at room temperature. All specimens were successfully classified by species regardless of the duration of nutrient deprivation.

REFERENCES

-
- ¹ J. Diedrich, S.J. Rehse, and S. Palchaudhuri, “*Escherichia coli* identification and strain discrimination using nanosecond laser-induced breakdown spectroscopy,” *Applied Physics Letters* **90**, 163901-1-3 (2007).
- ² S.J. Rehse, J. Diedrich, and S. Palchaudhuri, “Identification and discrimination of *Pseudomonas aeruginosa* bacteria grown in blood and bile by laser-induced breakdown spectroscopy,” *Spectrochimica Acta Part B* **62**, 1169–1176 (2007).
- ³ S.J. Rehse, N. Jeyasingham, J. Diedrich, and S. Palchaudhuri, “A membrane basis for bacterial identification and discrimination using laser-induced breakdown spectroscopy,” *Journal of Applied Physics* **105**, 102034 (2009).
- ⁴ J. Diedrich, S.J. Rehse, and S. Palchaudhuri, “Pathogenic *Escherichia coli* strain discrimination using laser-induced breakdown spectroscopy,” *Journal of Applied Physics* **102**, 014702 (2007).
- ⁵ R. Multari, D.A. Cremers, J.M. Dupre, and J.E. Gustafson, “The use of laser-induced breakdown spectroscopy for distinguishing between bacterial pathogen species and strains,” *Applied Spectroscopy* **64**, 750-759 (2010).
- ⁶ S.J. Rehse, Q.I. Mohaidat, and S. Palchaudhuri, “Towards the clinical application of laser-induced breakdown spectroscopy for rapid pathogen diagnosis: the effect of mixed cultures and sample dilution on bacterial identification,” *Applied Optics* **49**, C27-C35 (2010).

-
- ⁷ S.J. Rehse and Q.I. Mohaidat, “The Effect of Sequential Dual-Gas Testing on a LIBS-Based Discrimination of Brass and Bacteria,” *Spectrochimica Acta B* **64**, 1020-1027 (2009).
- ⁸ A.C. Samuels, F.C. DeLucia, Jr., K.L. McNesby, and A.W. Miziolek, “Laser-induced breakdown spectroscopy of bacterial spores, molds, pollens, and protein: initial studies of discrimination potential,” *Applied Optics* **42**, 6205-6209 (2003).
- ⁹ S. Morel, M. Leone, P. Adam, and J. Amouroux, “Detection of bacteria by time-resolved laser-induced breakdown spectroscopy,” *Applied Optics* **42**, 6184-6191 (2003).
- ¹⁰ R.G. Brereton, *Applied Chemometrics for Scientists* (Wiley, Chichester, 2007).
- ¹¹ J.F. Hair, W.C. Black, B.J. Babin, and R.E. Anderson, *Multivariate Data Analysis*, 7th Edition, (Prentice Hall) 2009.
- ¹² James D. Oliver, “The Viable but Nonculturable State in Bacteria,” *The Journal of Microbiology* **143**, 93 (2005).
- ¹³ G. Begosian and E.V. Bourneuf, “A matter of bacterial life and death,” *European Molecular Biology Organization Reports* **2**, 770-774 (2001).

CHAPTER 5

The effect of mixed cultures and sample dilution on bacterial identification

5.1 Introduction

The identification of bacteria in clinical samples is critical in certain diseases which can kill within hours of symptoms appearing (i.e. bacterial meningitis), when the administration of antibiotics as early as possible is of the utmost importance.^{1,2} As well, knowledge at time-zero of the particular pathogen causing infection would help to reduce the over-use and abuse of broad spectrum antibiotics that contribute to the growing crisis in antibiotic resistance.

The number of bacteria that may be present in a specimen to be tested via LIBS is dependent on the type of specimen (blood culture, contaminated water, tainted food product, etc.). Even in the case of clinical specimens, the number of bacteria present in an infected patient will vary from one organism to another, and the numbers present in specimens from asymptomatic patients will be different from symptomatic patients. For example, the infectious dose (the number of bacteria required to produce an infection) for intestinal diseases caused by *Shigella* or enterohemorrhagic *E. coli* (EHEC) is approximately 10 organisms.³ In the case of *V. cholerae* (responsible for cholera) it is about one million organisms, while *Campylobacter* infections require several hundred organisms. It is therefore crucial to establish the lowest number of bacteria that can be identified with the LIBS technique. In this chapter we will investigate the effect that reducing the number of bacterial cells has on the LIBS-based identification.

Bacteria may be present in mixed samples under some (but certainly not all) conditions. There are multiple clinical examples of sterile samples (i.e. blood, urine, CSF) where the bacteria causing an infection will be the only bacteria present.⁴ In these situations, concerns about mixing with other bacteria are unfounded. Still, the presence of other biological material (i.e. cells in blood, proteins in urine) may have some effect on the LIBS-based diagnosis. In specimens obtained from stool, sputum, or contaminated food or water, or even specimens contaminated by environmental bacteria, the bacteria causing the infection may be present along with other minority bacteria. In this chapter we will investigate the effect that the presence of a second bacterium has on the LIBS-based identification. Lastly, we will show that a discriminant function analysis of LIBS spectra obtained from multiple genera of clinically relevant bacteria (such as *Escherichia*, *Streptococcus*, and *Staphylococcus*) yielded a discrimination between species that indicates an identification of unknown bacterial samples using a pre-compiled reference library of spectral fingerprints is feasible.

5.2 Experiment

5.2.1 LIBS Experiment

In all LIBS experiments, 1064 nm ten nanosecond laser pulses from an Nd:YAG laser were used to ablate bacteria. Pulse energies were 10 mJ/pulse. Moreover, LIBS spectra were collected in an argon environment at atmospheric pressure. For the data acquisition, initially ten micro-liters of a high-density bacterial suspension (pellet) were micro-pipetted to the surface of the bacto-agar which was kept at room temperature. After that, five laser pulses were fired at every sampling location and the spectra from five different locations were collected and averaged, resulting in a spectrum of 25 averaged laser pulses per bacterial spectrum. Although

data from five sampling locations was used in this study, a signal-to-noise ratio sufficient for effective discrimination was usually achieved after only two locations, indicating that in the future the quantity of bacteria required could be reduced. LIBS spectra were acquired at a delay time of 2 μs after the ablation pulse with an integration gate width of 20 μs duration. LIBS spectra were collected and were analyzed with a discriminant function analysis (DFA) as described in our previous work and in previous chapters.^{5,6,7}

5.2.2 Bacterial Sample Preparation

Multiple species of bacteria were prepared in two separate microbiology facilities in the course of this work. Gram-negative and Gram-positive bacterial species (*Escherichia*, *Streptococcus*, and *Staphylococcus*) were prepared in the manner described in Chapter 3. In addition, two conditional mutant strains of *Mycobacterium smegmatis* bacteria were grown for 24 hours on a 7H9/ADC agar plate containing 5 ng/ml tetracycline and 50 mg/ml hygromycin. These bacterial cells were prepared in the laboratory of Dr. Choong-Min Kang (WSU, Department of Biological Sciences) and are two of the three cell lines routinely prepared in that laboratory which express different wag31 (a protein) alleles (DNA sequences) (wild-type, phosphoablative, or phosphomimetic wag31).⁸ In all cases, bacteria were harvested from the growth plates and suspended in 1.5 ml phosphate-buffered saline (PBS) or deionized water. Finally, bacterial pellets were produced by centrifuging the tubes for 3 minutes at 5000 rev/min at room temperature. The supernatant fluid was withdrawn and discarded. Spectra obtained from bacteria isolated from PBS and water were identical, indicating that any small volumes of residual buffer present after centrifugation were insignificant.

5.2.3 Mixed Samples

Mixtures of known mixing fraction were prepared from suspensions *M. smegmatis* and *E. coli* C (Nino). The mixing of these two particular species would almost certainly never occur in a clinical setting, but the easily observed differences in the LIBS spectra of these two microbes (resulting from the physiological variation between the two, one being a Gram-neutral *Mycobacterium* and one a Gram-negative *Escherichia*) provided an optimal experiment in which to initiate bacterial mixing experiments compared to, for example, the use of a mixture of two highly-similar *E. coli* strains. Morphologically however, the two microbes are fairly similar. Two separate suspensions (one of *M. smegmatis* and one of *E. coli*) were prepared prior to the mixing. A spectrophotometer was used to measure the optical density of the two bacterial suspensions to ensure equal concentrations prior to mixing. The turbidity or optical density of the suspension of bacteria cells was measured at a wavelength of 600 nm (OD_{600}) with the bacteria in their mid-log phase of growth. The measured optical density was 1.83 for both. The fact that the cell size of the *M. smegmatis* and the *E. coli* C cells are very similar (1.5-4 μm in length and 0.3-0.5 μm in width) confirmed the initial numbers of bacteria were the same.⁹

After establishing the initial bacterial concentration, six separate mixtures were prepared with a ratio *M. smegmatis* to *E. coli* C given by $M_{1-x}:C_x$ with $x=0.0, 0.1, 0.2, 0.3, 0.5, 1.0$. Multiple 1.5 mL tubes of these mixtures were prepared, thoroughly agitated via vortex mixing, then centrifuged for 3 minutes at 5000 rev/min. The supernatant was discarded to produce the bacterial pellet. Again, 10 μL of the dense pellet was mounted on the agar surface prior to LIBS testing.

5.3 Results and Discussion

5.3.1 Mixing Experiment

LIBS spectra from pure samples of *M. smegmatis* wild type (WT), *Streptococcus viridans*, and *E. coli* C bacteria were collected. *S. viridans*, a Gram-positive organism, was included in the DFA of the *M. smegmatis*/*E. coli* mixtures to serve as a negative control. No mixing fraction should ever classify as the control. In order to investigate the differences between the bacteria, spectra from the agar substrates on which all the bacteria were ablated, which lacked many of the elements present in the bacteria, were included in the DFA. Figure 5.1 shows the first three discriminant function (DF) scores for these four sets of spectra. A “leave-one-out” (LOO) analysis of this data indicated that 100% of all samples were correctly classified which shows that LIBS spectra obtained from the pure bacterial samples were distinctly different from each other and from the agar substrate as well. In a LOO analysis, a single data point is omitted during the construction of the discriminant functions. DF scores are calculated for the omitted (assumed to be unidentified) point using the new functions and the unknown point is assigned a group classification on the basis of these scores. Therefore rule sets for classification are always created from “known” samples, but the specificity results are always obtained from “unknown” or unidentified samples and all data points are tested as unknown.

A useful output generated by the DFA analysis is the structure matrix table which returns the statistical weights of the elements or the atomic transition lines that comprise the various discriminant function scores. The structure matrix from this analysis indicated that the two 213.618 nm and 214.914 nm phosphorus lines were primarily used in the discrimination between bacterial and agar spectra, while the 396.837 nm calcium line and 285.213 nm magnesium line

were responsible for the discrimination between *E. coli* C and *M. smegmatis* (WT) bacterial spectra.

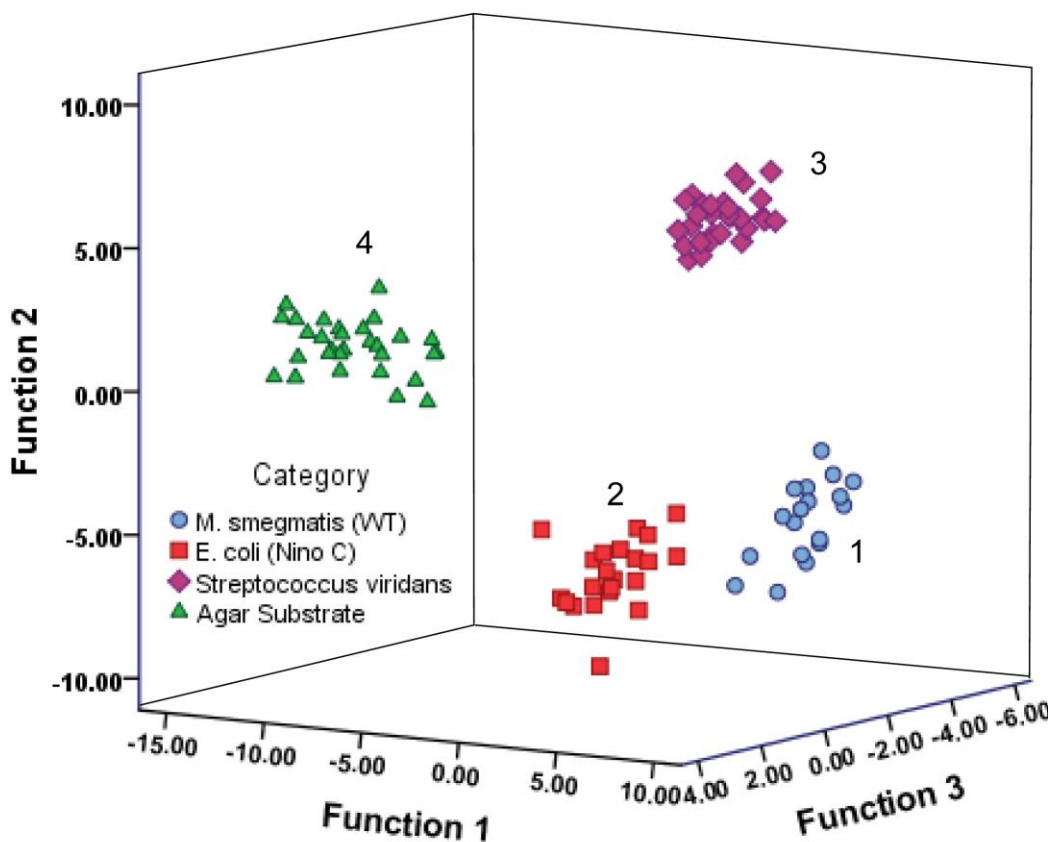


Figure 5.1: The first three discriminant function scores from a DFA of the LIBS spectra from pure samples of three different bacteria: (1) *Mycobacterium smegmatis* (WT), (2) *E. coli* C, and (3) *Streptococcus viridans*, in addition to (4) the agar substrate on which they were ablated.

Figure 5.2 shows a plot of the first two DF scores from a DFA of the LIBS atomic emission spectra from pure samples of *M. smegmatis* (WT) and *E. coli* C, as well as the four mixtures with the mixing fractions described above. As established earlier, the spectrum from a sample of pure *M. smegmatis* (Group 1) was easily differentiable from a spectrum from a sample of pure *E. coli* (Group 6). Spectra from mixtures classified strongly with each other, not with spectra from pure samples, confirming the homogeneity of the mixtures. As the fraction of *E.*

coli in the mixture became progressively higher, the DF1 score of the spectra from the mixtures (indicative of the primary discrimination between the two bacterial types) shifted closer to the DF1 score of pure *E. coli*. Moreover, the DF1 score of the centroid (which is the effective “center of mass” of the distribution of measurements) of the 50% mixture (Group 5) shifted approximately 50% of the way between Group 1 and Group 6. The spectra from the 90% and 80% mixtures were closely grouped with the 100% pure sample spectra. This means that spectra from *M. smegmatis* bacteria could be identified with a high confidence even in the presence of low concentrations of *E. coli*. The previous result is in good agreement with what may occur in some clinical samples in which microbial contamination can exist, but only at minority or trace concentrations. In this setting, clinical microbiologists need to isolate the mixed organisms from each other and grow them in pure culture in order to identify each organism. This process may take several days in order to determine the correct organism. In contrast, our results can be obtained almost instantaneously upon obtaining the mixed sample.

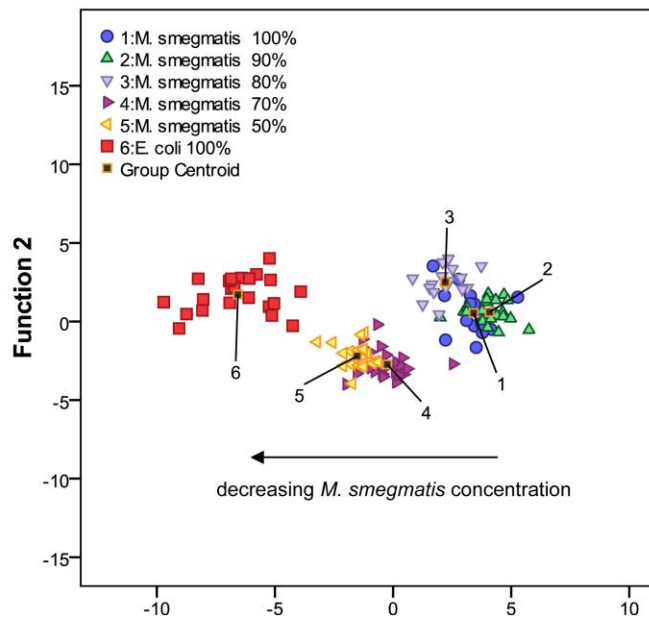


Figure 5.2: DFA plot showing the first two discriminant function scores for the spectra obtained from pure samples of two bacteria, (1) a wild-type strain of *M. smegmatis* (WT) and (6) a strain of *E. coli* (C) and four mixtures of those two bacteria at various mixing fraction (2-5).

In order to determine the accuracy of the identification of the mixed samples, a DFA of the LIBS spectra from the two pure samples, the four mixed samples, and the pure *S. viridans* was performed. The DFA also performed a LOO classification on these spectra, which evaluated the selectivity of the experiment by calculating the misclassification percentage of each group. This is known as the resubstitution estimate and the corresponding results are shown in Table 1.

Table 5.1: Classification results from the discriminant function analysis of *M. smegmatis*/*E. coli* mixed samples.

Category	# of Spectra	Classification Results		
		<i>M. smegmatis</i>	<i>E. coli</i>	<i>S. viridans</i>
100% <i>M. smegmatis</i> , 0% <i>E. coli</i>	21	100%	0%	0%
90% <i>M. smegmatis</i> , 10% <i>E. coli</i>	20	100%	0%	0%
80% <i>M. smegmatis</i> , 20% <i>E. coli</i>	16	100%	0%	0%
70% <i>M. smegmatis</i> , 30% <i>E. coli</i>	21	76%	34%	0%
50% <i>M. smegmatis</i> , 50% <i>E. coli</i>	19	47%	53%	0%
0% <i>M. smegmatis</i> , 100% <i>E. coli</i>	25	0%	100%	0%

The spectra obtained from the control samples of *S. viridans* bacteria were completely distinct from any other samples and no mixtures classified as the control. This test was repeated with additional species of bacteria, and the mixtures only ever classified with the species that comprised the mixture. The 90% and 80% mixtures classified 100% of the time with the majority species, indicating the strong likelihood that spectra from mixtures with only trace amounts or small minority fractions of contaminant bacteria will be easily identifiable as belonging to the majority species. These experiments will need to be reproduced with a greater number of specimens to statistically determine whether this identification accuracy is truly 100%

or whether it is somewhat lower. The identification accuracy dropped quickly for mixing fractions below 80%, achieving the anticipated 50% level for 50:50 mixtures. Because the DFA must assign the spectrum to one of the two “pure” groups, it is not surprising that the classification accuracy tracked the mixing fraction as the concentration of the majority species was decreased.

5.4 Sample Dilution

To study the effect of cell number on the LIBS-based identification of a bacterial target, three different bacterial concentrations of the wild-type (WT) strain of *M. smegmatis* were prepared. The first concentration was the standard undiluted concentration, which was 4.7×10^8 bacteria/ml. This concentration was calculated in the standard microbiological way based on the bacterial growth curve. For the second concentration, 10 μ L of the bacterial suspension was added to 10 μ L PBS, while the third concentration was achieved by adding 10 μ L of the bacterial suspension to 20 μ L PBS. In order to insure the homogeneity of the mixture, all samples were agitated with a vortex mixer. 10 μ L from each concentration was then mounted on the agar surface.

5.4.1 Dilution Experiment

Figure 5.3 shows the first two DF scores for a DFA performed on spectra obtained from the three different concentrations of *M. smegmatis* (WT), a similar mutant called *M. smegmatis* (TE), and *S. viridans*. In this analysis, the group centroids of all concentrations of the *M. smegmatis* (WT) were closely grouped together. This indicates that the LIBS spectra for all concentrations of *M. smegmatis* (WT) were the same, regardless of the number of bacterial cells present. This was not unexpected, as the spectra were always normalized by the total spectral

power, and therefore should be independent of the number of cells. The centroid location of Group 4, *M. smegmatis* (TE), was well-separated from that of Groups 1-3, *M. smegmatis* (WT), but possessed a similar DF1 score. This confirmed the fact that *M. smegmatis* (TE) is highly-similar to *M. smegmatis* (WT) and possessed a highly-similar LIBS spectrum, but both were completely distinct from the *S. viridans* (a Gram-positive bacterium) spectrum. 100% of all *M. smegmatis* (TE) spectra were correctly classified regardless of concentration. This is a significant result for a clinical diagnostic, as some clinical tests are dependent on the pathogen concentration or the absolute number of pathogens present. The LIBS-based chemometric identification is independent of these factors. Also, as we attempt to extend this diagnostic to clinical applications, a reference library of LIBS spectral fingerprints from important organisms will be constructed, most likely using well-characterized strains and samples with a high-number of cells to provide excellent signal-to-noise.

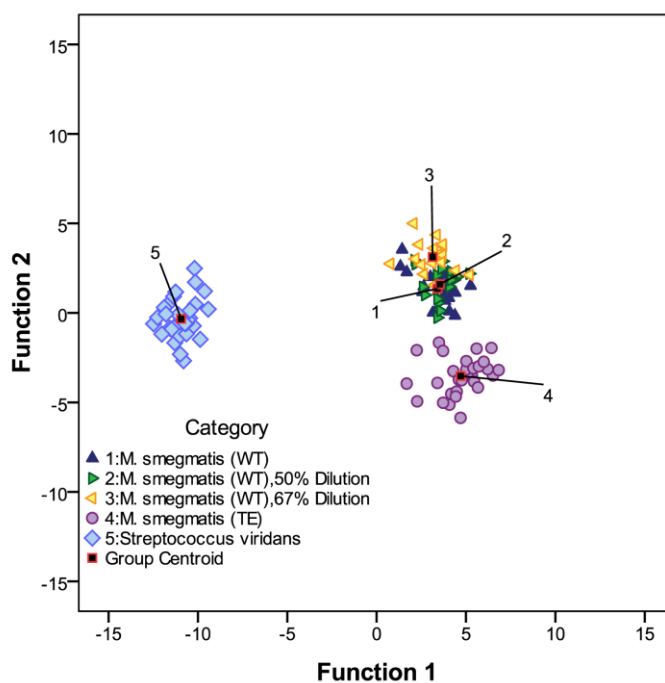


Figure 5.3: A DFA plot showing the first two DF scores for three different concentrations of *M. smegmatis* (WT) (1-3), a highly similar mutant called *M. smegmatis* (TE) (4), and the Gram-positive *S. viridans* (5). The ability to identify and differentiate the *M. smegmatis* (WT) samples was independent of sample concentration.

It is important to prove that the LIBS spectra obtained from clinical specimens, which will contain much lower numbers of bacteria, classify 100% of the time with the reference library spectra obtained from samples with much higher numbers.

Using the known initial titer of our liquid bacterial suspension, the volume of suspension mounted on the agar, the area of the mounted bacterial pad, and the area of our ablation craters we calculated the number of bacteria ablated in any given sampling location. This number was approximately 1500 cells for our normal “undiluted” samples. Because five sampling locations were averaged together to make one LIBS spectrum, our initial calculations showed that we were identifying approximately 7500 bacteria with every LIBS spectrum. All spectra from the two dilutions were 100% correctly identified, indicating that 3750 and 2500 bacteria were also identifiable. These estimates of the bacterial number have at least a 10% uncertainty.

Figure 5.4 shows a typical LIBS spectrum obtained from the lowest concentration tested in the dilution study. Approximately 2500 bacterial cells total were ablated to obtain this spectrum, which is dominated by emission from C, Mg, and Ca, and to a lesser extent emission from P and Na. The signal-to-noise of these emission lines was still completely adequate for identification purposes, as was shown in Figure 5.3, and the background was small. The LIBS spectrum was acquired at the same experimental parameters as given before. These results are encouraging, as the required number of bacterial cells is lower than the infectious dose for many (not all) diseases as described earlier.

The limiting factor in the number of cells that can be identified was the emission intensities of the phosphorus lines at 253.560 and 255.326 nm which eventually decreased below the background intensity. However, our optical detection efficiency can be improved by constructing a new light collection optical system. As mentioned before we used only an optical

fiber with a 600 μm core mounted ~ 2 cm away from the plasma to collect the emission. The percentage of total emission that is collected with this arrangement is less than 1%. The use of short focal length large diameter dual parabolic reflectors would increase the amount of collected light by a factor of 1000 based on calculations which assume a purge chamber similar to what we use now and commercially available parabolic reflectors. We also intend to explore the use of dual-pulse nanosecond LIBS which could conservatively yield a factor of two increase in emission intensity, although this has not yet been demonstrated in bacterial systems. A second ns-Nd:YAG laser exists in our lab for this purpose. With these improvements we intend to lower the minimum number of bacterial cells to around ten.

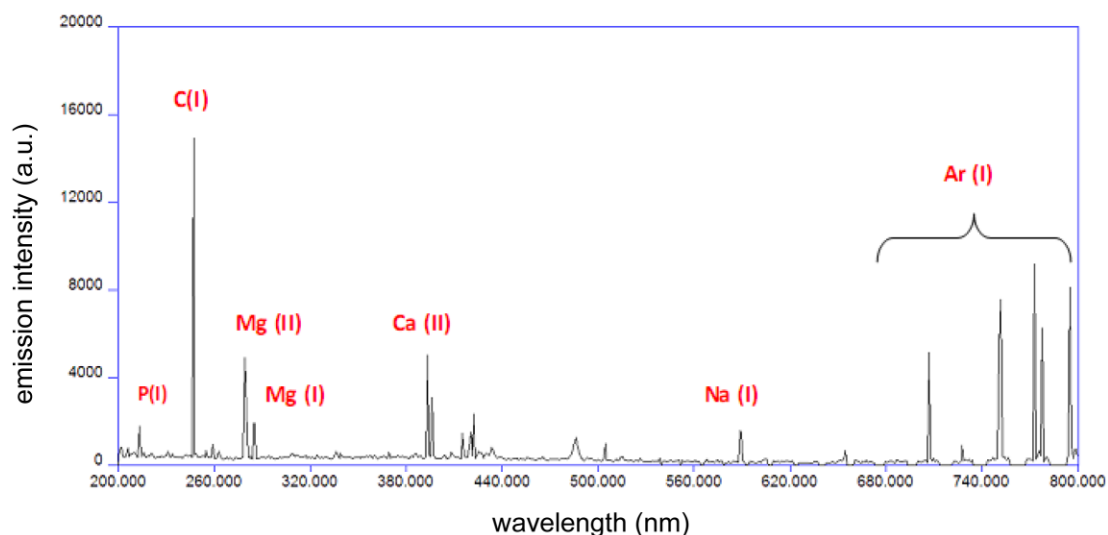


Figure 5.4: A typical LIBS spectrum from the lowest concentration of *M. smegmatis* (WT) tested in this study. The sample was ablated in argon and the emission lines are identified. A total of approximately 2500 bacteria were ablated to create this spectrum.

The total spectral power measured from the various concentrations was linearly dependent on the number of bacterial cells ablated. This is shown in Figure 5.5. The total

spectral powers from all spectra from a given concentration were averaged and the standard deviation is shown as the uncertainty. A linear fit to this data ($R^2=0.953$) shows the expected linear dependence of the LIBS signal intensity with bacterial cell number. Based on this result, it is possible we may be able to correlate the bacterial number with the measured total spectral power in future experiments. This could have relevance as a rapid check of bacterial resistance since many fast-growing bacterial species double their number every 15-20 minutes and since the LIBS total spectral power can easily resolve a doubling of the bacterial number. An experiment could be designed where a clinical bacterial sample is obtained and half is tested via LIBS and half is exposed to a rich nutrient medium in the presence of an antibiotic. Twenty minutes later another LIBS spectrum could be obtained from the sample growing with the nutrient medium.

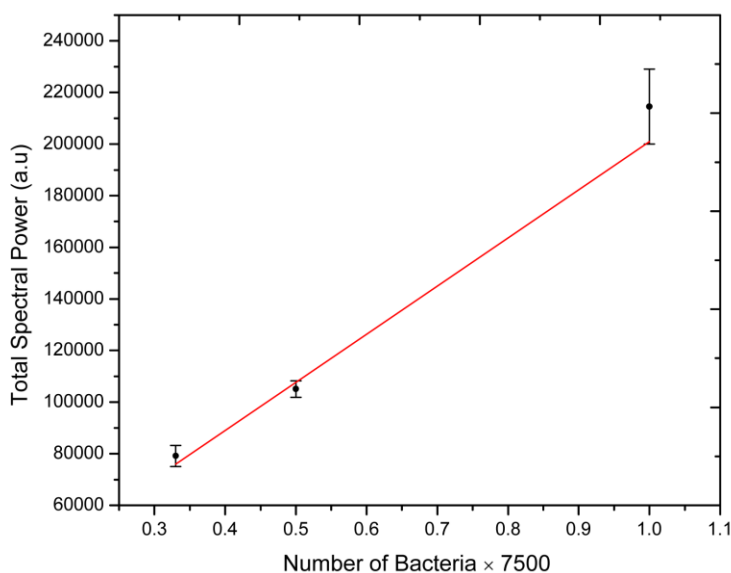


Figure 5.5: The total spectral power associated with each of the five elements observed in the LIBS spectrum of *M. smegmatis* (WT) ablated in argon as a function of bacterial cell number. A linear dependence was observed.

Antibiotic-sensitive bacteria should show no increase or a decrease in LIBS total spectral power as the cells are unable to divide. Antibiotic-resistant bacteria on the other hand should multiply exponentially, and a corresponding increase in LIBS total spectral power from the first test should be observed. This process is traditionally done in a similar method, but with a “culture-and-count” confirmation of bacterial growth. This method can take from 24-72 hours to determine the presence of antibiotic resistant strains.

5.5 Bacterial Discrimination and Library

Four strains of *E. coli* (enterohemorrhagic *E. coli* O157:H7, C (Nino), HF4714, and HfrK12), two conditional mutants of *Mycobacterium smegmatis* (WT and TA), two *Staphylococcus* species (*aureus* and *saprophyticus*), and two *Streptococcus* species (*viridans* and *mutans*) were ablated as described above and the spectra were analyzed together using a DFA. The first two DF scores of this analysis are shown in Figure 5.6.

In this analysis, 79.0% of the variance between the groups was described by function 1, 12.2% by function 2, 3.6% by function 3, 2.5% by function 4, and the rest of the variance, 2.7%, was described by the remaining discriminant functions. Only the first two DF scores are plotted in Figure 6, which contain most of the variance, yet a statistically significant amount of variation is contained in the rest of the functions which are not shown. In this analysis, 92.3% of all the original grouped cases were correctly classified in a LOO. All errors of identification occurred only between spectra belonging to the same genus or species, as is shown by the highlighted cells in Table 5.2.

The results of this LIBS-based diagnostic applied to a variety of bacteria are indicative that the technique is not merely basing an identification/discrimination on random differences in the spectra. The fact that spectra are closely grouped by genus (*Staphylococcus* and *Streptococcus*), and are even more closely grouped by genus and species (*E. coli* and *M. smegmatis*) demonstrate that the technique is identifying the true microbiological diversity of these organisms. It is important to point out that because $N-1$ discriminant functions are always constructed when N groups are classified, as additional bacteria are added to the reference library of existing LIBS spectral fingerprints, the phase space of the DFA correspondingly increases. In this way, concerns about an “overcrowding” of discrimination space (and subsequent loss of selectivity) as additional bacteria are added to the reference library may be unfounded. Lastly, it is very important to note that as this diagnostic is extended toward clinical applications, patient case histories will play an extremely important role in the determination of which potential candidate bacteria are included in a reference library against which an unknown pathogen will be tested. In most circumstances, knowledge of the case history will preclude all but a few suspect pathogens. Therefore a DFA comparing an unknown pathogen against a reference library composed of all known pathogens will almost certainly not occur. This clinical fact reduces concerns about the ultimate selectivity of the technique based on the overcrowding of discrimination space.

5.6 Conclusions / Summary

Nanosecond laser-induced breakdown spectroscopy followed by a discriminant function analysis clearly showed the discrimination between several bacterial species, with a close grouping based on specimen genus, species, and strain observed. The issues of sample dilution

and sample mixing (important questions that must be addressed as the LIBS technology moves toward the goal of clinical diagnoses) have been investigated.

We have characterized the effect that the presence of a second bacterial species in the ablated specimen had on the identification of the majority species. It was shown that in a mixture of two bacteria, accurate identification was possible down to a 80:20 mixing ratio, with a subsequent loss of selectivity observed at lower mixing fractions. At no time were spectra from mixed samples classified as anything other than one of the two bacteria comprising the mixture.

Bacterial specimens were diluted by a factor of two and three to determine the effect that reducing the number of bacterial cells in the LIBS plasma would have on the bacterial identification. All dilutions of a bacterial suspension classified 100% of the time with the most dense “control” concentration, even when compared to a closely-related mutant of the same species. It was shown that for the lowest dilution, approximately 2500 bacteria were required for the accurate identification of the bacteria. This number can be reduced in the future (perhaps by a factor of 1000) with the construction of a better light collection system. In addition, a linear dependence of the total spectral power as a function of cell number was determined.

Lastly, high selectivity was obtained during the construction of a LIBS spectral library composed of 10 bacterial specimens from four genera representative of bacteria that may be encountered in a clinical setting.

REFERENCES

-
- ¹ J.H. Stein, *Internal Medicine*, 5th ed. (Mosby, 1998).
- ² A.L. Smith, "Central nervous System," in *Mechanisms of Microbial Disease*, 3rd Ed. M. Schaechter, N.C. Engleberg, B.I. Eisenstein, and G. Medoff, eds. (ASM Press, 1999), pp. 535-548.
- ³ D. Mara and N.J. Horan, *Handbook of Water and Wastewater Microbiology*, 1st ed. (Wiley, Academic Press, 2003).
- ⁴ Dr. H. Salimnia (University Health Center/Detroit Receiving Hospital), private communication.
- ⁵ S.J. Rehse, J. Diedrich, and S. Palchadhuri, "Identification and discrimination of *Pseudomonas aeruginosa* bacteria grown in blood and bile by laser-induced breakdown spectroscopy," *Spectrochim. Acta B* **62**, 1169-1176 (2007).
- ⁶ S.J. Rehse and Q.I. Mohaidat, "The effect of sequential dual-gas testing on a LIBS-based discrimination of brass and bacteria," *Spectrochim. Acta B* **64**, 1020-1027 (2009).
- ⁷ J. Diedrich, S.J. Rehse, and S. Palchadhuri, "Pathogenic *Escherichia coli* strain discrimination using laser-induced breakdown spectroscopy," *J. Appl. Phys.* **102**, 014702 1-8 (2007).
- ⁸ C.M. Kang, S. Nyayapathy, J.Y. Lee, J.W. Suh, and R.N. Husson, "Wag31, a homologue of the cell division protein DivIVA, regulates growth, morphology and polar cell wall synthesis in mycobacteria," *Microbiology* **154**, 725-735 (2008).
- ⁹ R.K. Poole, *Advances in Microbial Physiology*, Volume 55 (Academic Press, 2009).

CHAPTER 7

Toward The Identification of Bacteria In Clinical Samples

7.1 Introduction

As we know, doctors order urine tests for their patients (most often women) to make sure that the kidneys and other organs are functioning well or when the patient may have an infection in his/her kidneys or bladder. Upon successful diagnosis, conducted with traditional culturing techniques and taking at least 24 hours, the patient will be treated with the proper antibiotic.

Staphylococcus epidermidis is a Gram-positive bacterium cocci commonly found in the natural skin flora that sometimes causes human illness.¹ Infection caused by *S. epidermidis* is usually associated with medical devices, such as indwelling catheters since it has the ability to form biofilms which will grow on those devices.² Hall and Snitzer investigated urinary tract infections in children that may be caused by *S. epidermidis*. In their study, they concluded that the presence of *S. epidermidis* bacteria in the urine culture should not be automatically considered a contaminant, especially when the clinical findings are compatible with urinary tract infection.³

In chapter 5, we proved that LIBS has the capability of identifying bacteria in mixed samples, specifically discriminating between *M. smegmatis* and *E. coli* C. At that time we chose the previous mentioned samples for the proof-of-principle. Moreover, in that study we studied several mixture samples including 50:50 mixtures.⁴ But in real-world situations where the LIBS-based identification is desperately needed, the pathogen that may cause the infection will be the

majority species in any specimen of urine, blood, etc. Therefore, the ability to identify a species in a 1:1 mixture with another species is most likely not necessary.

To this end, in this chapter I used LIBS to identify bacteria (*S. epidermidis*) in bio-fluids such as urine to investigate if the presence of proteins, salts, and other bio-chemicals in the sterile urine will interfere with the spectral identification. The effect of mixing bacterial samples was quantified by creating mixtures of known titer. I mixed specimens of distinct bacteria, *E. coli* ATCC 25922 and *Enterobacter cloacae* ATCC 13047 in a 10:1, 100:1, and 1000:1 ratio to simulate real clinical situations. This was done to create samples that as faithfully as possible simulated the properties of actual clinically-occurring cases.⁵ Finally, *E. coli C* bacteria will be deposited on micro-membrane filter with 0.45 µm pore size and LIBS testing will be conducted directly on the filter in order to test the ability of LIBS for the detection of bacteria in quickly filtered samples.

7.2 Experiment

7.2.1 Bacterial Sample Preparation

E. coli C samples were prepared in our lab in the manner described in Chapter 3. While *S. epidermidis*, *E. coli* ATCC 25922, and *Enterobacter cloacae* ATCC 13047 were prepared in the clinical microbiology lab at the Detroit receiving hospital by Dr. Robert Mitchell. In the case of *E. coli C*, bacteria were harvested from the growth plates and suspended in 1.5 ml deionized water. After that, the tubes were centrifuged and the supernatant was discarded in order to produce the bacterial pellets. Two separate suspensions of *E. coli* ATCC 25922 and *Enterobacter cloacae* ATCC 13047 were prepared prior to mixing, again using deionized water. To be a reasonable test, the two suspensions must have the same bacterial concentration. To do

this, the turbidity or the optical density of each suspension was measured using a spectrophotometer at 600 nm (OD_{600}). In this device light is scattered as it passes through a bacterial suspension and the amount of scatter is proportional to the number of bacteria in the suspension. The measured optical density was 0.78 for both. The measurements were conducted in the laboratory of Dr. Takeshi Sakamoto (WSU, Department of Physics and Astronomy).

Finally, samples of *S. epidermidis* were collected from the growth plates in identical ways and then suspended in de-ionized water and sterile urine. Typically, in a 1.5 mL tubes. After that samples of both were collected without washing to perform the LIBS experiment.

7.2.2 LIBS Experiment

The experimental setup used to perform LIBS on the bacteria samples is the same setup that used in our previous studies.^{4,6,7} LIBS spectra were acquired in an argon environment at atmospheric pressure at a delay time of 2 μ s after the ablation pulse, with an ICCD intensifier gate width of 20 μ s duration. Specifically, 10 μ L of pellet were transferred to 1.4% nutrient free bacto-agar. For the identification of bacteria in mixture samples and in sterile urine, five laser pulses were used to collect the spectra at one location and five accumulations at five different locations were collected and averaged, resulting in a spectrum of 25 averaged laser pulses.

For the testing of bacteria on the micro-filter as shown in Figure 7.1 (more details on the filter preparation are given below), four laser pulses were used to collect the spectra at one location and four accumulations at four different locations were collected and averaged, resulting in a spectrum of 16 averaged laser pulses. In Figure 7.1, the diameter of the membrane filter is approximately 13 mm. Moreover, almost the whole area was covered with bacteria in order to save as many LIBS spectra as we can for the DFA analysis. Nevertheless, one LIBS spectrum

will be enough for future discrimination due to the robustness of the LIBS spectrum for a particular bacterial sample. The selection of the previous parameters was based on the homogeneity of the bacterial sample and to eliminate any possible contribution from the brass mounting square, the yellow metal piece that appears in Figure 7.1, due to the thinness (150 μm) of the membrane filter.



Figure 7.1: *E. coli C* bacteria were deposited on a membrane filter with 0.45 μm pore size. The filter was mounted on a brass sample which can be fitted easily inside the chamber. Details of the filter study are provided below.

7.3 The Identification of *S. epidermidis* Bacteria in A Sterile Urine Suspension

LIBS spectra from *E. coli C*, *S. viridans*, and *S. epidermidis* bacterial specimens that were suspended in water were acquired as described earlier. In addition to these three specimens, LIBS spectra were also collected for *S. epidermidis* bacteria that were suspended in sterile urine. Generally, normal urine consists of 96% water and 4% solutes. Organic solutes include urea, ammonia, creatinine, and uric acid. Inorganic solutes include sodium chloride, potassium sulfate, magnesium, and phosphorus.

Figure 7.2 is a DFA plot showing the first two discriminant function scores of a DFA performed on spectra acquired for the three specimens mentioned above. From this graph, it can be seen easily that the LIBS spectral fingerprint from urine-exposed bacteria (3-Red) was identical to water-exposed bacteria (2-Green), and a DFA correctly classified 100% of the urine-exposed bacteria as being consistent with *S. epidermidis*.

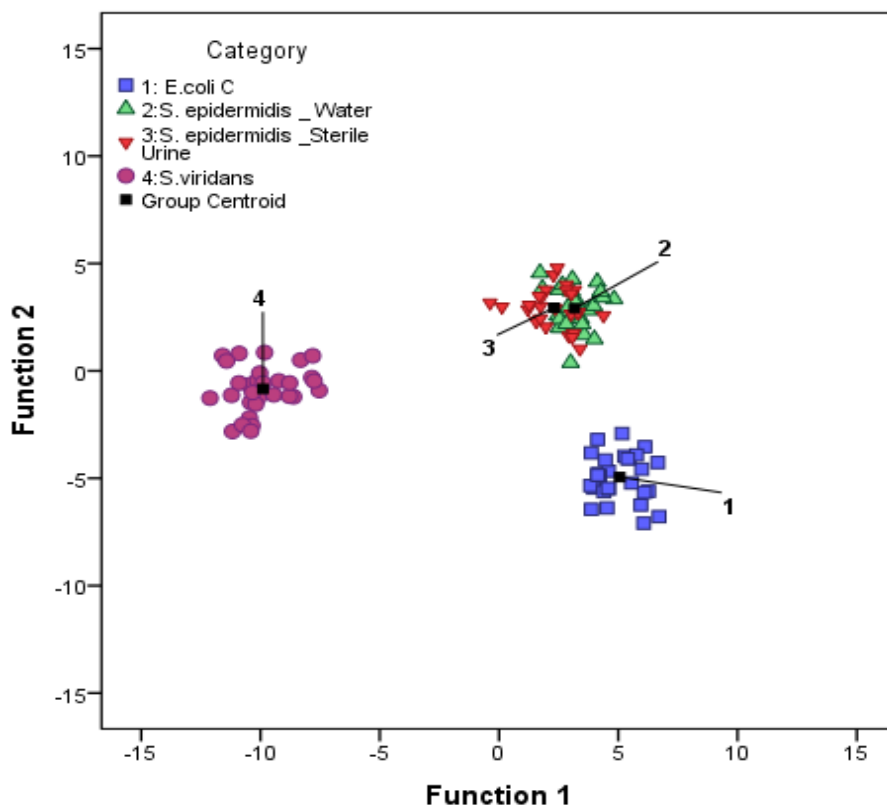


Figure 7.2: A DFA plot of the LIBS spectra from *E. coli C*, *S. epidermidis* harvested from both urine and water, and *S. viridans*. The two *S. epidermidis* samples were identical to each other and were discriminated with 100% accuracy from *S. viridans* bacteria.

To verify our results, LIBS spectra from *S. epidermidis* samples were compared to the LIBS spectra obtained from two other bacterial species within the same genus, specifically *S. aureus* and *S. saprophyticus*. For the DFA analysis, LIBS data of *S. epidermidis* harvested from

urine were entered as unclassified cases (each case represents a whole spectrum). This means that the identity of each unclassified spectrum was unknown and then the SPSS software was asked to assign those cases to the most similar group. In our analysis, all the LIBS spectra of *S. epidermidis* harvested from urine were identical to those that were collected from water and also were distinguishable, 100% classified, from the other two *Staphylococci* species. The results of the DFA are shown in Figure 7.3.

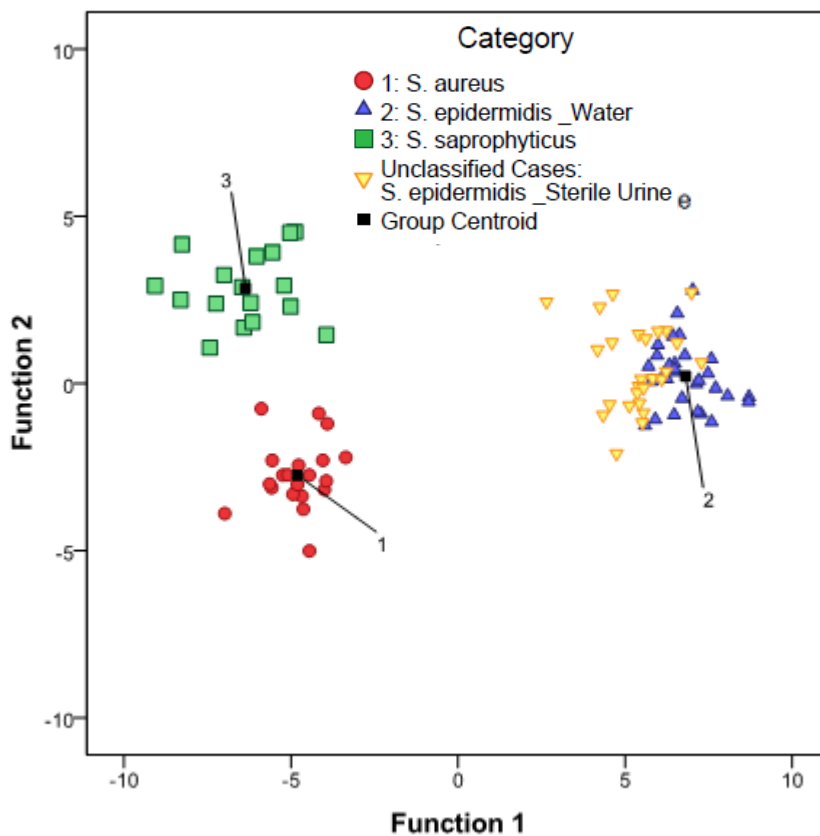


Figure 7.3: A DFA plot of the LIBS spectra from *S. epidermidis* harvested from a urine sample and water, *S. aureus* and *S. saprophyticus*. The two *S. epidermidis* samples were identical to each other and were discriminated with 100% accuracy from other two *Staphylococci* samples.

7.4 Identification of Bacteria in Mixed Clinical Samples

Figure 7.4 shows a plot of the first two DF scores from a DFA of the LIBS spectra from pure samples of *M. smegmatis*, *E. coli* ATCC 25922, and *Enterobacter cloacae* ATCC 13047, as well as the three mixtures with the mixing fractions mentioned in section 7.1. As can be seen from the DFA plot, the LIBS spectral fingerprint of the *Enterobacter cloacae* ATCC 13047 (Group 1) bacterium was easily distinguishable from a spectrum obtained from a sample of pure *E. coli* ATCC 25922 (Group 5). Spectra from the three mixtures (2-4) were classified as the

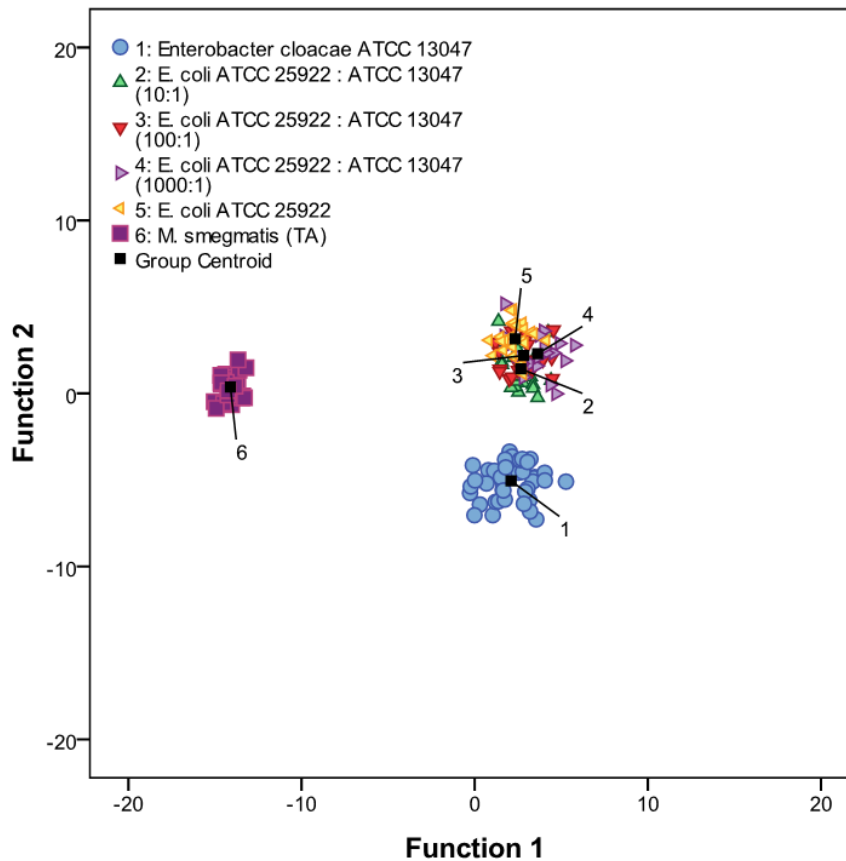


Figure 7.4: DFA plot showing the first two discriminant function scores for the spectra obtained from pure samples of two bacteria, (1) *Enterobacter cloacae* ATCC 13047, (5) a strain of *E. coli* ATCC 25922, (6) *M. smegmatis* and three mixtures of ATCC 25922 and ATCC 13047 at various mixing fraction (2-4).

same spectra of *E. coli* ATCC 25922 with 100 % accuracy. The previous results confirm the fact that the bacterial concentration of *E. coli* ATCC 25922 was the dominant in all the mixture samples.

In this analysis, notice that the DF2 score of the centroid (which is the effective “center of mass” of the distribution of measurements) of the *M. smegmatis* samples was zero. On the other hand, the rest of the samples (pure and mixtures) possessed almost the same DF1 score. The interpretation of this is that the discrimination between the LIBS spectra from *E. coli* ATCC 25922 and *Enterobacter cloacae* ATCC 13047 and their mixtures was based on the difference between their DF2 scores. In addition to that, there is a slight shift downward in the centroid of the 10:1 or 90%:10% mixture (downward toward the DFA space of the minor component) as expected.

This previous results suggest that spectra from *E. coli* ATCC 25922 bacteria could be identified with a high accuracy even in the presence of low concentrations of *Enterobacter cloacae* ATCC 13047, a common clinical contaminant. The previous result is in good agreement with what we discussed back in chapter 5. In that chapter, we mentioned that in clinical samples and in the case of mixtures the infection will most likely be caused by the microbe that has the higher concentration.

7.5 The Detection of Bacteria on a Membrane Filtration Method

In this section I investigated the capability of using LIBS for the identification of bacteria on a different substrate, specifically on a Millipore membrane filter with pore size 0.45µm. For all the experiments conducted before, bacteria were deposited on a 1.4% nutrient free bacto-agar substrate. As we know, not only does the agar substrate keep the bacteria hydrated for many

hours, which allow us to save the LIBS spectra easily, but it did not contribute directly or indirectly to the LIBS spectra of the bacteria. But preparing the agar substrate requires boiling and cooling which definitely slows down the process of bacterial identification. These agar substrates are also not robust, being subject to dehydration from evaporation, which changed their size and shape. Therefore, based on what I have previously discussed, and in order to ease the process of identification, it was decided to try a new substrate. With this substrate, we needed to wait approximately 10 minutes from depositing the bacteria on its surface until start testing or sample. Moreover, a filter is a substrate which can be incorporated easily into a flowing liquid system.

Figure 7.5 shows a typical LIBS spectrum obtained from the blank cellulose membrane filter. As we can see from the figure, the spectrum lacked many of the elements the present in the bacteria such as P, Mg, and Ca at the same time it is dominated by emission from C and a small amount of Na.

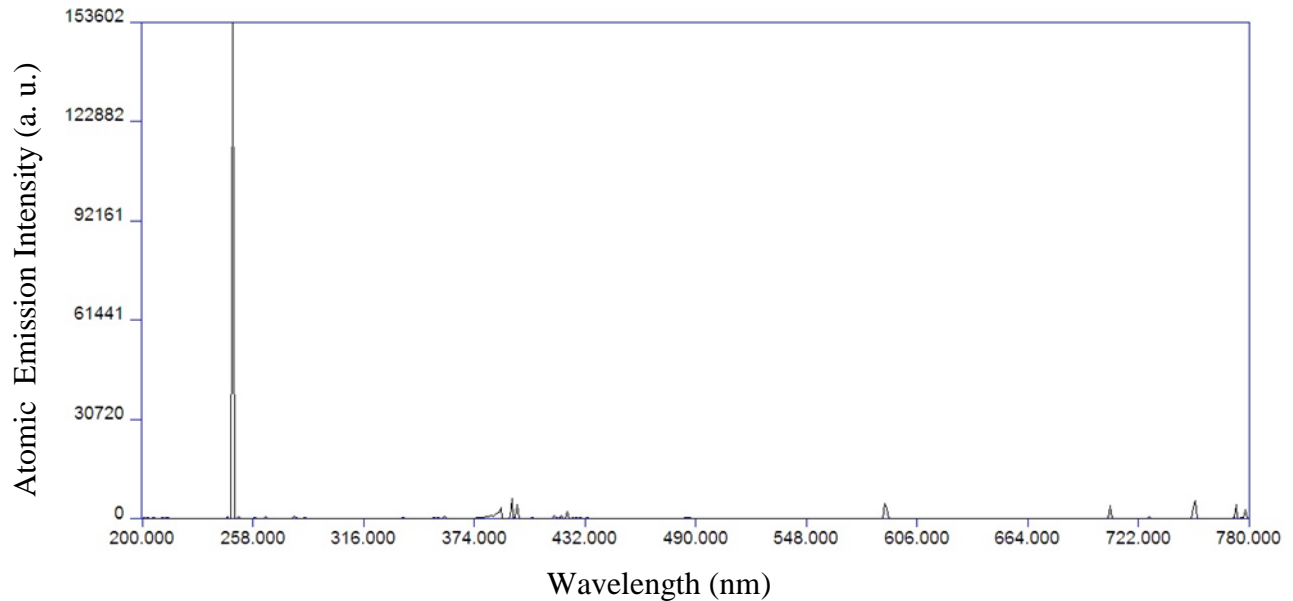


Figure 7.5: A typical LIBS spectrum from the Millipore cellulose membrane filter in this study. The sample was ablated in argon and the emission lines are identified.

E. coli C bacteria were deposited on the membrane filter discussed above. Figure 7.6 shows a typical LIBS spectrum of these bacteria. This spectrum is dominated by emission from C, Mg, and Ca, and to a lesser extent emission from P and Na. It was acquired at the canonical experimental parameters given before except that I changed the value of the MCP image intensifier. Specifically, it was set to be 2600-2800 and in the case of the agar substrate the value was set to be 3000. The reason for decreasing the value of the amplification was the over flow of the atomic line intensities for some elements such as Ca.

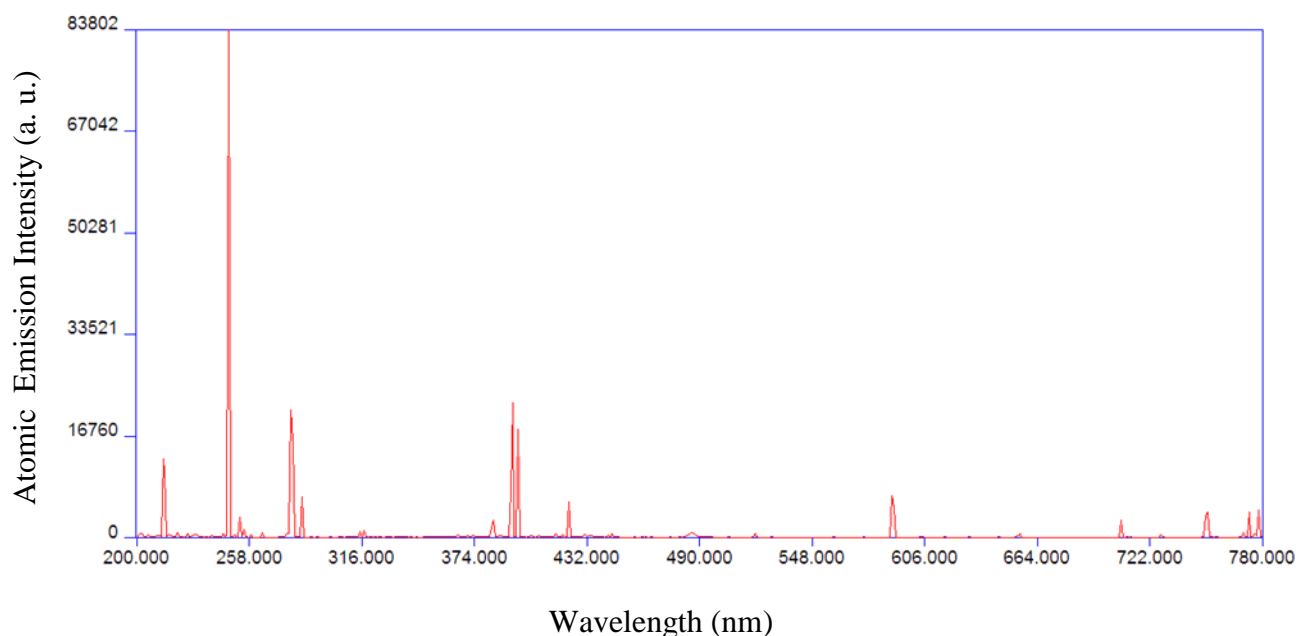


Figure 7.6: A typical LIBS spectrum from *E. coli* bacteria ablated on the cellulose membrane filter in an argon atmosphere.

It can be seen easily that the LIBS spectrum of the *E. coli* bacteria is distinguishable from that of the blank membrane filter. This results support our initial assumption about the possibility of bacterial identification on this substrate. However the contribution of the filter to the spectrum needed to be investigated.

Figure 7.7 shows a DFA plot for two *E. coli* strains: C and ATCC 25922, *M. smegmatis* (TA type), and the membrane filter. LIBS spectra for both ATCC 25922 and *M. smegmatis* bacteria were acquired from testing on agar while *E. coli* C bacteria were tested on the membrane filter. In this analysis, all group memberships were predicated correctly with 100% accuracy.

What is immediately obvious is that while the two *E. coli* strains were distinguishable from each other, whatever contributions came from the membrane filter were small compared to the differences between the actual species. If this were not true, we would have expected the two agar-tested specimens (1 and 2) to group closely together while the membrane-tested bacteria (3) would have been separate or grouped closely with the spectra from the filter alone. This was not the case.

There were two reasons behind using different *E. coli* strains in this test. Firstly, to test whether *E. coli* strain C would group closely to any other *E. coli* sample. It doesn't make sense to compare C with itself (but tested on agar) because of the additional carbon concentration from the membrane filter that would occur. Secondly, the same sample will have two slightly different fingerprints due to the testing on two different substrates (slightly different ablation/evaporation plasma conditions). Finally, I added the LIBS spectra of *M. smegmatis* bacteria to the DFA to prove that not only is the spectral fingerprint of *E. coli* C close to another *E. coli* strain regardless of substrate, but is still easily distinguishable from other types of bacteria which belong to a different genus.

Successful discrimination between several bacterial samples tested on the membrane filter may be achieved since the filter lacks those divalent cations that exist in the bacterial

membrane. Those cations are responsible for the stabilization of the entire bacterial membrane structure.^{8,9,10}

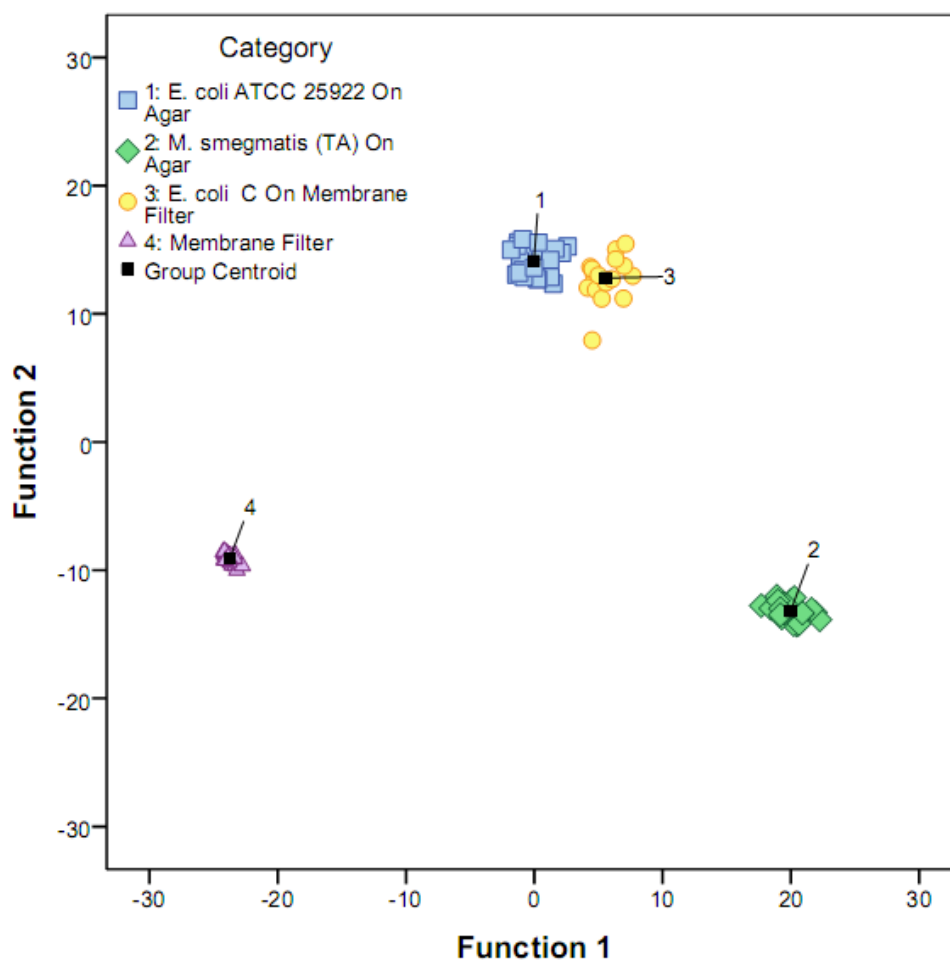


Figure 7.7: DFA plot showing the first two discriminant function scores for the spectra obtained from, (1) *E. coli* ATCC 25922 ablated on agar, (2) *M. smegmatis* (TA) ablated on agar, (3) *E. coli* C ablated on the membrane filter, and (4) the membrane filter.

7.6 Summary

In this chapter I showed that the LIBS fingerprint of *S. epidermidis* harvested from urine is identical to that obtained from de-ionized water. This result may suggest that the proteins, salts, and other bio-chemicals present in fluids do not interfere with the spectral identification.

Moreover, we again proved that the identification of bacteria in mixed cultures is possible, using more clinically relevant microbes. Specifically, I found that the presence of microorganisms in low concentration will not affect our ability to identify the dominant organism which is responsible for the infection. Finally, I also found that a LIBS-based identification of bacteria on a Millipore membrane filter is possible regardless of the high concentration of the carbon element due to the cellulose of the filter.

REFERENCES

-
- ¹ V.A. Fischetti, R.P. Novick, J.J. Ferretti, D.A. Portnoy, and J.I. Rood, *Gram-Positive Pathogens*, 2nd Edition, (ASM Press) 2006.
- ² N. De and M. Godlove, "Prevalence of *S. aureus* and *S. epidermidis* among patients with indwelling catheters and their antibiogram using some commonly used antibiotics," *Journal of American Science* **6**, 515-520 (2010).
- ³ E. David and A.J.A. Snitzer, "*Staphylococcus epidermidis* as a cause of urinary tract infections in children," *The Journal of Pediatrics* **124**, 437-438 (1993).
- ⁴ S.J. Rehse, Q.I. Mohaidat, and S. Palchaudhuri, "Towards the clinical application of laser-induced breakdown spectroscopy for rapid pathogen diagnosis: the effect of mixed cultures and sample dilution on bacterial identification," *Applied Optics* **49**, C27-C35 (2010).
- ⁵ H. Salimnia and R. Mitchell, private communication.
- ⁶ S.J. Rehse and Q.I. Mohaidat, "The effect of sequential dual-gas testing on a LIBS-based discrimination of brass and bacteria," *Spectrochimica Acta B* **64**, 1020-1027 (2009).
- ⁷ Q.I. Mohaidat, S. Palchaudhuri, and S.J. Rehse, "The effect of bacterial environmental and metabolic stresses on a laser-induced breakdown spectroscopy (LIBS) based identification of *Escherichia coli* and *Streptococcus viridans*," *Applied Spectroscopy* **65**, 386-392 (2011).
- ⁸ H. Ibrahim, S. Higashiguck, Y. Sugimot and T. Aoki, "Role of divalent cations in the novel bactericidal activity of the partially unfolded lysozyme," *Journal of Agricultural and Food Chemistry* **45**, 89-94 (1997).

⁹ H. Nikaido and M. Vaara, "Molecular basis of bacterial outer membrane permeability," *Microbiological Reviews* **49**, 1-32 (1985).

¹⁰ R. Lins and T. Straatsma, "Computer simulation of the rough lipopolysaccharide membrane of *Pseudomonas aeruginosa*," *Biophysical Journal* **81**, 1037-1046 (2001).

CHAPTER 8

Conclusions and Future Work

The results presented in this thesis indicate that the LIBS technique may be considered a promising technology for biomedical applications because of its speed, minimum sample preparation, and ruggedness. Several critical experiments have been conducted over the course of three years. We proved that LIBS has the ability to identify bacteria in mixture samples, specifically we have successfully identified the target bacteria when present in up to a 80:20 mixture ratio. This result is really encouraging since the mixture percentage in clinical samples is less than that regardless of the low number of bacteria.

We were also able to show that identifying 2500 bacteria is possible but this number is still far from our target. Our target is making LIBS an applicable technique for clinical applications where the identification of a low number of bacteria, i.e. 100, is desperately needed. We mentioned previously that the total percentage of the collected light from our LIBS plasmas is less than 1%. Improving this percentage may lower our limit of detection. This can be done by using a parabolic mirror which can increase the amount of the collected light by a factor of 1000.

We found that the LIBS spectrum of *E. coli* C grown in two different nutrition media (TSA and MacConkey agar) are indistinguishable from each other. In addition to that, LIBS spectra of *S. epidermidis* harvested from urine are the same as that obtained from bacteria in DI-water.

For all the results mentioned above, it seems that bacterial separation and concentration are the most important missions that may prevent or retard LIBS from competing with other

technologies that I mentioned in Chapter 1 and from being a powerful tool for medical applications. In real situations such as blood or urine samples, bacteria don't exist in pure culture. Therefore, suppose we have a blood sample that is infected with some type of microorganism and we need to use LIBS to identify this microorganism. To do this, we need initially to separate the bacteria from other contents that exist in our sample. As we know, blood is composed of plasma, red and white cells, and platelets. After the separation, the second challenging step is to concentrate the collected bacteria under the laser for further testing. Successfully identifying bacteria in blood and urine will make LIBS one of the leaders among a variety of different technologies.

One suggested way to overcome the separation and concentration problem is to use microfluidic devices that may or may not be integrated with optical trapping. Using optical trapping techniques (similar to the optical tweezers) use forces of laser radiation pressure (typically on the order of piconewtons) to trap small objects. This has been particularly successful in a variety of biological systems in recent years. With regards to the separation of bacteria in blood samples, it has been shown (by colleagues at Translume, Inc. in Ann Arbor, MI) that large cells, such as blood cells, cannot pass through the optical trap, while the smaller (bacteria-sized) platelets can. This proof-of-concept demonstrates that bacteria could simply and automatically be isolated in a flowing blood sample. Subsequent concentration of the sample (as described above) will follow this isolation.

If we proceed with the previous way, i.e. a microfluidic device, a library of LIBS spectral fingerprints for the most important pathogens will be constructed. In hospitals, the number of species of bacteria that need be identified on a daily basis is not that large. Therefore we will

begin construction of the library with the most significant and medically relevant pathogens.

Table 8.1 shows some of those pathogens.

Table 8.1: A list of some bacteria which need to be analyzed by LIBS.

<i>Enterohemorrhagic E. coli</i>	<i>Staphylococcus aureus</i>
<i>Pseudomonas aeruginosa</i>	<i>Staphylococcus epidermidis</i>
<i>Salmonella enterica</i>	<i>Streptococcus viridans</i>
<i>Klebsiella pneumoniae</i>	<i>Streptococcus pneumoniae</i>
<i>Staphylococcus saprophyticus</i>	

From the microbiology point of view, several experiments need to be conducted such as the effect of bacteriophage infection on the LIBS spectrum of pathogenic and nonpathogenic bacteria. In my case, I tried to investigate the effect of bacteriophage induction on the LIBS spectrum of EHEC. This bacterium is pathogenic due to the toxin it produces. The gene for toxin production is present in a dormant lysogenic phage (the phage DNA actually integrates into the host chromosome). However, at a later time, the integrated genome can be excised and begin to be actively transcribed producing virus particles that eventually burst the cell. My preliminary results, not included in my thesis, showed the fingerprint of LIBS spectrum is independent of the presence or absence of the bacteriophage in host microorganism (EHEC in our case). These results need to be confirmed by taking the LIBS spectrum of the phage itself as a control. Moreover, in my experiment I couldn't confirm or disprove the presence of the phage inside the bacterium cell and this confirmation is critical. Therefore more investigations into this novel application are required. One way to activate the lysogenic process is by irradiating the infected cells with UV light.

Biofilm is a collection of microorganisms that adhere to environmental surfaces (e.g., the plaque on our teeth.) It is primarily composed of microbial cell and an extra-cellular polymeric substance (EPS). EPS may account for 50% to 90% of the total organic carbon of the biofilm and it is primarily composed of polysaccharides which allows it to resist host defenses and aids in antibiotic resistance development. In our lab, I compared the LIBS spectrum from EHEC in a biofilm to free-living (planktonic) EHEC. Our preliminary results showed that there is an increase in carbon and a decrease in magnesium for EHEC grown in the biofilm state compared to the planktonic state. The increase in the carbon concentration may be due to the EPS which is mainly composed of carbon. Unfortunately, I couldn't understand or explain the decrease in the Mg concentration. Moreover, again I couldn't confirm if the bacteria really existed in either the biofilm or the planktonic state before or after testing. In order to create the planktonic state, the bacterial culture was incubated in a water bath at 37 °C for 24 hours with shaking.

Another thought to improve our ability for the identification of bacteria is by integrating the vibrational-molecular information obtained from Raman spectroscopy with the atomic one obtained from LIBS. Upon a successful combination of results, a highly unique and robust identification of the bacteria may be achieved which will broaden the impact of both modalities in many areas - especially in the hospitals.

Finally, our preliminary experiments showed encouraging results in the discrimination between different types of bacteria at the strain level and in the ability to identify bacteria in mixtures and urine samples. At this point, significant support or investment is desperately needed to push LIBS toward clinical applications. This is a really a difficult mission, since it

requires a sample handling and preparation system in order to develop highly-reproducible testing protocols and procedures.

ABSTRACT**LASER-INDUCED BREAKDOWN SPECTROSCOPY (LIBS): AN
INNOVATIVE TOOL FOR STUDYING BACTERIA**

by

QASSEM I. MOHAIDAT**August 2011****Advisor:** Dr. Steven J. Rehse**Major:** Physics**Degree:** Doctor of Philosophy

Laser-induced breakdown spectroscopy (LIBS) has gained a reputation as a flexible and convenient technique for rapidly determining the elemental composition of samples with minimal or no sample preparation. In this dissertation, I will describe the benefits of using LIBS for the rapid discrimination and identification of bacteria (both pathogenic and non-pathogenic) based on the relative concentration of trace inorganic elements such as Mg, P, Ca, and Na. The speed, portability, and robustness of the technique suggest that LIBS may be applicable as a rapid point-of-care medical diagnostic technology.

LIBS spectra of multiple genera of bacteria such as *Escherichia*, *Streptococcus*, *Mycobacterium*, and *Staphylococcus* were acquired and successfully analyzed using a computerized discriminant function analysis (DFA). It was shown that a LIBS-based bacterial identification might be insensitive to a wide range of biological changes that could occur in the bacterial cell due to a variety of environmental stresses that the cell may encounter.

The effect of reducing the number of bacterial cells on the LIBS-based classification was also studied. These results showed that with 2500 bacteria, the identification of bacterial specimens was still possible. Importantly, it was shown that bacteria in mixed samples (more than one type of bacteria being present) were identifiable. The dominant or majority component of a two-component mixture was reliably identified as long as it comprised 70% of the mixture or more.

Finally, to simulate a clinical specimen in a precursor to actual clinical tests, *Staphylococcus epidermidis* bacteria were collected from urine samples (to simulate a urinary tract infection specimen) and were tested via LIBS without washing. The analysis showed that these bacteria possessed exactly the same spectral fingerprint as control bacteria obtained from sterile deionized water, resulting in a 100% correct classification. This indicates that the presence of other trace background biochemicals from clinical fluids will not adversely disrupt a LIBS-based identification of bacteria.

AUTOBIOGRAPHICAL STATEMENT

Education

- Wayne State University, Detroit, MI: Doctor of Philosophy (Expected Graduation: August 2011).

Thesis: Laser-Induced Breakdown Spectroscopy (LIBS): An Innovative Tool For Studying Bacteria

Wayne State University, Detroit, MI: M.S. Physics (Graduation: December 2010)

- Yarmouk University, Jordan: B.S. Physics (Graduation: June 1998)

Awards

- Daniel R. Gustafson Graduate Student Outstanding Teaching award, Wayne State University (Department of Physics and Astronomy) 2007.
- First Place Award, Graduate Research Day: Wayne State University (Department of Physics and Astronomy), 2010.

Selected Publications

- S.J. Rehse and Q.I. Mohaidat, "The effect of sequential dual-gas testing on a LIBS-based discrimination of brass and bacteria," *Spectrochimica Acta B* **64**, 1020-1027 (2009).
- S.J. Rehse, Q.I. Mohaidat, and S. Palchadhuri, "Towards the clinical application of laser-induced breakdown spectroscopy for rapid pathogen diagnosis: the effect of mixed cultures and sample dilution on bacterial identification," *Appl. Opt.* **49**, C27-C35 (2010).
- Q. Mohaidat, S. Palchadhuri, and S.J. Rehse, "The effect of bacterial environmental and metabolic stresses on a LIBS-based identification of *Escherichia coli* and *Streptococcus viridans*," *Appl. Spect.* **65**, 386-392 (2011).
- K. Hamasha, Q. Mohaidat, S.J. Rehse, and S. Palchadhuri, "Rapid discrimination of four *Escherichia coli* strains using visible wavelength Raman spectroscopy," in submission (2011).